UNCLASSIFIED

| AD NUMBER | |
|---|---|
| **ADB805296** | |
| CLASSIFICATION CHANGES | |
| TO: | **unclassified** |
| FROM: | **restricted** |
| LIMITATION CHANGES | |
| TO: **Approved for public release; distribution is unlimited.** | |
| FROM: **Distribution authorized to DoD only; Administrative/Operational Use; FEB 1945. Other requests shall be referred to National Aeronautics and Space Administration, Washington, DC. Pre-dates formal DoD distribution statements. Treat as DoD only.** | |
| AUTHORITY | |
| **NACA list dtd 28 Sep 1945; NASA TR Server website** | |

THIS PAGE IS UNCLASSIFIED

# NATIONAL ADVISORY COMMITTEE FOR AERONAUTICS

## TECHNICAL NOTE

No. 957

## THE STRENGTH OF SEMIELLIPTICAL CYLINDERS SUBJECTED TO COMBINED LOADINGS

By E. E. Sechler and J. L. Frederick
California Institute of Technology

Washington
February 1945

CLASSIFIED DOCUMENT

This document contains classified information affecting the National Defense of the United States within the meaning of the Espionage Act, USC 50:31 and 32. Its transmission or the revelation of its contents in any manner to an unauthorized person is prohibited by law. Information so classified may be imparted only to persons in the military and naval Services of the United States, appropriate civilian officers and employees of the Federal Government who have a legitimate interest therein, and to United States citizens of known loyalty and discretion who of necessity must be informed thereof.

NASA Technical Library
3 1176 01433 2747



NATIONAL ADVISORY COMMITTEE FOR AERONAUTICS

TECHNICAL NOTE NO. 957

# THE STRENGTH OF SEMIELLIPTICAL CYLINDERS SUBJECTED TO COMBINED LOADINGS

By E. E. Sechler and J. L. Frederick

## SUMMARY

The present report covers tests made on elliptical cylinders with a center support which were subjected to various simple and combined loadings. The tests yielded a series of interaction curves for combined loadings on such cylinders which should be useful in wing nose section analysis.

## INTRODUCTION

The primary object of this research project was the determination of design criteria for the nose sections of airplane wings. Since the nose portions of most wing sections can be approximated fairly closely by portions of ellipses, it was decided to use unstiffened elliptical cylinders for test specimens in this research. These cylinders were designed in such a way that the boundary restraints of the sheet simulated the boundary restraints present in the sheet covering of an actual wing nose section.

The physical parameters tested were:

1. The degree of ellipticity $\epsilon$ - that is, the ratio of the semimajor to the semiminor axis of the ellipse

2. The length of the cylinder $L$, usually expressed as a suitable dimensionless parameter

3. The thickness of the sheet covering $t$, usually expressed as a suitable dimensionless parameter

The loading conditions to which the cylinders were subjected were as follows:

1. Pure torsion

2. Pure bending

3. Bending plus torsion

4. Bending plus vertical shear

In all cases, the bending moments and the shears were applied in the plane of the minor axis of the section.

This investigation, conducted in the Structures Laboratory of the Guggenheim Aeronautical Laboratory of the California Institute of Technology, was sponsored by and conducted with the financial assistance of the National Advisory Committee for Aeronautics.

## SYMBOLS

$A$ area enclosed by cylindrical shell (Cylinder cross-sectional area), square inches

$A_s$ cross-sectional area of sheet making up cylinder but neglecting cover plates, square inches

$a$ semimajor axis of elliptical part of specimen (Also used as radius of circular cylinders), inches

$b$ semiminor axis of elliptical part of specimen, inches

$E$ modulus of elasticity of material (Taken as $10.3 \times 10^6$ psi throughout report)

$F$ shear load at buckling which, acting at lever arm $l$, causes bending moment $m_b = Fl$, pounds

$I_c$ moment of inertia of cover plates about specimen neutral axis, inches$^4$

$I_s$ moment of inertia of sheet covering of specimens about specimen neutral axis, inches$^4$

$I_t = I_s + I_c$ total moment of inertia of specimen, inches$^4$

$K$ a nondimensional bending stress defined as $K = \frac{b\rho_o}{Et}$

$L$ length of cylindrical specimens between end supports, inches

$l$ lever arm for applied shear load, inches

$M$ bending moment carried by sheet only (excluding that carried by cover plates), inch-pounds $\left(M = m \frac{I_s}{I_t}\right)$

$m$ bending moment applied to specimen, inch-pounds

$M_b$ bending moment carried by sheet only at buckling, inch pounds $\left(M_b = m_b \frac{I_s}{I_t}\right)$

$m_b$ bending moment applied to specimen at buckling, inch-pounds

$M_t$ torsional moment carried by sheet only, inch-pounds (Assuming that the contribution of cover sheets is negligible, $M_t = m_t$.)

$m_t$ applied torsional moment, inch-pounds

$m_{t_b}$ applied torsional moment at buckling, inch-pounds

$m_{t_u}$ applied torsional moment at specimen failure, inch-pounds

$M_u$ bending moment carried by sheet only at failure, inch-pounds $\left(M_u = m_u \frac{I_s}{I_t}\right)$

$m_u$ applied bending moment at specimen failure, inch-pounds

$t$ thickness of sheet covering, inches

$\epsilon$ degree of ellipticity of elliptical part of specimen - that is, ratio of semimajor to semiminor axis of ellipse $(\epsilon = a/b)$

$\rho_o$ maximum radius of curvature of elliptical part of specimen, inches

$\sigma_b$ maximum bending stress at buckling corresponding to $M_b$, psi

$\sigma_b'$ maximum bending stress corresponding to moment supported by a cylindrical specimen immediately after buckling takes place, psi

$\sigma_{b_o}$ maximum bending stress at buckling due to pure bending - that is, no other applied loads, psi

$\sigma_u$ maximum bending stress at failure of specimen, psi

$\sigma_{uts}$ ultimate tensile strength of material, psi

$\sigma_y$ yield stress of material (0.2-percent offset), psi

$\tau$ torsional shearing stress, psi

$\tau_b$ torsional shearing stress corresponding to $m_{t_b}$, psi

$\tau_{b_o}$ torsional shearing stress corresponding to $m_{t_b}$ for pure torsion, psi

$\tau_{s_b}$ direct average shearing stress at buckling corresponding to F, psi

$\tau_u$ torsional shearing stress corresponding to $m_{t_u}$, psi

$\tau_{u_o}$ torsional shearing stress corresponding to $m_{t_u}$ for case of pure torsion, psi

## EXPERIMENTAL TECHNIQUE

### Material and Material Tests

Since it is a very commonly used aircraft structural material, 24S-T aluminum alloy was chosen for the purposes of the experimental investigation. This material was obtained in nominal sheet thicknesses ranging from 0.010 to 0.040 inch. Despite the relatively large deviations from the nominal dimensions of the sheet supplied during the course of the research program, the individual sheets themselves were reasonably uniform.

Random samples were selected from the various shipments of material in an effort to obtain representative properties of the actual material used in the construction of the test specimens. The testing of these samples was limited to that of tension only* since the most important property desired was that of the modulus of elasticity E, which was assumed to be the same in tension and compression.

These material tests were conducted in a standard Riehle testing machine having a maximum rated capacity of 3000 pounds. Strain measurements were made by means of Huggenberger type extensometers having a magnification of approximately 300 times. Typical tensile stress-strain curves are presented in figure 1 and a complete summary of test results is given in table I, from which figure 2 has been plotted. The scatter of experimental points in figure 2 may be attributed to variations in the material itself and to the limitations imposed upon the attainable accuracy by the experimental procedure used.

Inspection of figure 2 indicates that the modulus of elasticity E is substantially independent of the direction of loading relative to the sheet grain, and has an average value of $10.3 \times 10^6$ psi. The ultimate tensile stress $\sigma_{uts}$ is slightly less across the grain than with the grain; while the difference in the defined yield stress ($\sigma_y \sim 0.2$ percent offset in the initial gage length) is more marked. The average values and variations of tensile properties with grain direction are in agreement with previously published results. (See references 1 and 2.) While of general interest, these variations are of secondary importance to the basic research project, since buckling of the test cylinders occurs at stresses considerably below the defined yield point.

## Test Specimens

The specimens consisted of two semielliptical (or semicircular) segments of sheet supported and clamped at the ends of the minor axis of the ellipse, thus simulating two wing nose sections mounted to a common spar and tested as a unit. (See fig. 3a.) It was at first thought possible to use a Wagner spar as a means of providing the required beam

*Approximate compression properties may be obtained if desired by use of table I-1 of reference 1.

support and to subtract the effect of this spar in order to determine the net-load-carrying properties of the curved sheet alone. After several tests had been completed under different loading conditions, it was decided that the presence of a spar having relatively large bending and shear rigidities made it very difficult to obtain accurate and reliable results of the net strength of the sheet covering.

It was therefore decided to replace the Wagner type spar by the system of vertical spacer blocks illustrated in figure 3b. The spacer blocks were joined by a series of loose links in such a manner that relative motion in all directions was possible. This completely eliminated the difficulty of shear rigidities and reduced the problem of the bending rigidity to a minimum. In order to prevent buckling of the sheet covering between spacer blocks, cover plates were placed above and below the junctions of the two semielliptical sections of sheet. The thickness of these cover plates was so chosen that they would have a slightly higher buckling load than that of the curved sheets. It can be readily seen that this means of support would contribute only negligibly to the shear and torsional strength of the specimen, and would carry a definite, calculable amount of bending moment.

At the ends of the specimen were 1-inch-thick steel plates having the cross section of the desired ellipticity, with the addition of a 2-inch rectangular center section to which was attached the above-mentioned support and cover plate system. These end plates served a twofold purpose: namely,

1. They held the ends of the sheet covering to the correct contour.

2. They provided a convenient means of attaching the specimen to the testing machines.

With regard to the first item, the sheet was firmly held to the end plates by 1/4-inch bolts which screwed into tapped holes, spaced 1 inch apart around the circumference of the specimen. For specimens where the failing stresses were quite high, steel bands having the shape of the end plates were placed between the bolt heads and the sheet to distribute the clamping loads of the bolts and to prevent interbolt buckling. A photograph of the assembled specimens is shown in figure 3c.

In the actual assembly of the specimens, considerable care was taken to avoid soft spots or wrinkles in the sheet covering and to insure that each specimen was as accurately formed as possible. There were several unavoidable instances when compliance with the above conditions was not obtained and, therefore, the validity and the consistency of the results of such tests were critically considered and the test results discarded when that was deemed advisable.

All the specimens tested had a depth (equal to twice the length of the semiminor axis) of approximately 6 inches, the degree of ellipticity being obtained by variations in the length of the semimajor axis. The ellipticities were 1.0, 2.0, and 3.0; while the length of the specimens ranged from 1.0 inch to 34.0 inches. These variations, in conjunction with the three nominal sheet thicknesses tested, 0.010, 0.016, and 0.020 inch, reduced the program to a systematic investigation of the effect of the geometry of the test specimens on the load-carrying abilities of the specimens.

## Test Apparatus and Testing Procedure

Because of the various loading conditions decided upon for investigation, it was necessary to use several different testing machines during the course of the experimental program. Each of these machines will be discussed separately in conjunction with the description of the loading conditions for which they were used.

The greater part of the pure torsion test program was conducted on a standard Olsen torsion-testing machine (see fig. 4) having a maximum rated capacity of 50,000 inch-pounds. As shown in this figure, a detachable loading jig consisting of a length of H-beam and a section of steel shafting was used to transmit the torsional moment from the jaws of the testing machine to the end plates of the test specimen. During the majority of these tests, angular deflection measurements were taken over a portion of the length of the specimen, and were used to obtain a check of the buckling load determined from visual observations, since the point of buckling was marked by a change in the slope of the load-deflection curve.

The remainder of the pure torsion, all the pure bending, and all the bending-plus-torsion tests were carried out in the bending-torsion machine shown in figure 5. In the cases of the pure torsion and bending-plus-torsion tests made in

this machine, angular deflection measurements were taken as before. In conjunction with the pure bending and bending-plus-torsion tests, extensometer readings were taken on both the tension and compression sides of each test specimen in order to obtain the stress distribution in the specimen, both before and after buckling of the sheet covering had taken place.

The requirements of testing with a wide range of ratios of bending moments to vertical shear forces in the bending-plus-shear tests necessitated a special testing machine. This machine is shown in figure 6 and the working parts consist of a fixed face plate, shown to the right in this figure, and a movable face plate, to which is attached the head of the loading arm. The specimen to be tested was placed between and bolted to this pair of face plates. In order to eliminate any tare loads from acting on the specimen during the testing operation, the loading arm and the movable face plate unit were counterweighted through a knife-edge lever system, which was so designed as to be independent of the amount of deflection of the loading arm. Thus, the loading arm was made floating with respect to the specimen. Portions of this counterweight system may be seen in the figure. The variation of the bending-to-shear ratio was accomplished merely by shifting the point of load application along the length of the central loading arm. During the bending-plus-vertical shear tests, extensometers were again mounted to the specimens in order to obtain an experimental value of the stresses in the specimen.

Sheet thicknesses were measured on a thickness gage reading to ±0.0002 inch. These measurements were made at several points on the individual sheets used in each specimen, and since the variations were small for any one sheet, the average sheet thickness was recorded for the purpose of subsequent calculations. In some of the earlier tests, the sheet thickness that was used was the nominal thickness and, while this can have no marked effect on the validity of the results presented, it can be noticed in the tabular data and therefore has been mentioned.

## EXPERIMENTAL RESULTS

In all discussions which follow, the cylinders referred to as semielliptical or semicircular were those having a fixed support, such as is shown in figure 3, at the ends of

the minor axis. Cylinders referred to as circular or elliptical are sheet structures with no support other than that applied at the ends of the specimen.

## Pure Torsion of Semicircular Cylinders

Since the problem of the strength of circular cylinders under pure torsion has been extensively covered both theoretically and experimentally (see references 3 and 4), it was decided to test first the semicircular and semielliptical cylinder in pure torsion. As in the case of the circular cylinders, the buckling load of the semicircular cylinders was very close to the utlimate load of the specimen. This is shown in table II, where it can be seen that the value of the torsional moment causing failure $m_{t_u}$ is seldom more than a few percent higher than the torsional moment causing buckling $m_{t_b}$.

In order to express the torsional loads in terms of shearing stress, use has been made of the usual equation of torsional shearing stress in a thin-walled cylinder: namely,

$$\tau = \frac{m_t}{2At} \tag{1}$$

This equation is valid up to the point of buckling and, after buckling, gives a fictitious average shearing stress which, at failure, is analogous to the modulus of rupture in beams. Using equation (1), values for $\tau_b$ and $\tau_u$ have been calculated and are shown in table II.

In reference 3, Donnell derives a theoretical expression for the ultimate strength of short and moderately long cylinders of radius "a" and fixed ends subjected to a pure torsional moment. This equation is

$$\frac{\tau_u L^2}{Et^2} = 5.06 + \sqrt{9.42 + 1.88\left(\frac{L^2}{2ta}\right)^{1.5}} \tag{2}$$

A plot of this curve is shown as the short dashed line in figure 7.

A curve faired through the experimental points for circular cylinders (360° of unsupported skin) is also shown in

figure 7 as the long dashed curve, indicating that the experimental values are somewhat less than those predicted theoretically.

Using the same parameters for the semicircular cylinders (180° of unsupported skin) the data from table II have been plotted in figure 7. A study of this figure brings out the following points:

1. For the longer specimens ($L^2/2ta \doteq 10,000$) the ultimate strength of the semicircular cylinders is approximately twice that of the circular cylinders.

2. For the shorter cylinders ($L^2/2ta \doteq 10$) the semicircular cylinders have an ultimate strength which is only about 10 percent greater than that of the circular cylinders.

3. That equation (2) could be used for designing semicircular cylinders and would be conservative for all specimens in which $L^2/2ta$ was greater than 300 and would not become excessively nonconservative down to a value of $L^2/2ta = 100$. A little later a more exact empirical equation will be given for the case of the semicircular cylinders.

The large increase in the ultimate strength of the longer semicircular cylinders over that of the circular cylinders is explainable by a consideration of the buckle pattern of the two types of specimen. For moderately long specimens, the number of circumferential buckles is small (of the order of 2 in 360°); hence the added restraint due to support at 0° and 180° is quite effective in delaying the buckling. However, as the length decreases, the number of waves increases, so that the presence of the added restraint begins to lose its effectiveness. For the lower limit of the experimental data under discussion, the number of circumferential buckles was of the order of 16 so that any restraint would have an effect on only a small percentage of the area going into the wave state. It is therefore probable that for very short specimens, the experimental curves for the circular and semicircular cylinders would join since the effect of the restraint would become negligible.

## Pure Torsion of Semielliptical Cylinders

Considering now the semielliptical cylinders, it is immediately obvious that conditions are quite different from

what they are in the semicircular cylinders. The radius of curvature on the circumference of a semielliptical specimen varies between a maximum value at the ends of the minor axis to a minimum value at the ends of the major axis, the magnitude of these limits depending on the ellipticity and the depth of the cross section. Thus, it may be expected that the specimen would first buckle in the regions of maximum radius of curvature, and, under further increase in load, these buckles would extend diagonally towards the nose. At the same time, as each section of the circumference reached its critical load, depending on the local radius of curvature, new shear buckles would appear and propagate slowly. Owing to the fact that the minimum radius of curvature is located at the nose of the specimen, this nose portion would resist buckling in such a manner as to act as a stiffener. Consequently, a diagonal tension field would be formed in the remaining portions of the specimen. Under further increase of the applied load, the combined forces due to the induced tension field and the direct torsional loading would soon reach a magnitude sufficient to cause the collapse of the relatively stiff nose and therefore bring about the complete collapse of the cylinder.

Thus, it is seen that for semielliptical cylinders the buckling and ultimate loads are two separate and distinct points in the loading history and that the difference in the values of these two critical loads should increase with increasing ellipticity. It is apparent that this second statement must be true when the relative values of the maximum and minimum radii of curvature as a function of the ellipticity ratio are considered. Similar conclusions were reached by Lundquist and Burke in reference 5. Visual observations confirmed the above-mentioned conclusions as to buckle history, and the data given for these cylinders in tables III and IV show that the difference between the buckling and failure torsional moments increases as the ellipticity ratio increases.

In plotting these data, the same parameters were tried as were used in figure 7: namely, $\tau L^2/Et^2$ against $L^2/2ta$; where $a$ is the semimajor axis of the ellipse. As can be seen from figures 8 and 9, these parameters were satisfactory and the experimental points had comparatively little scatter from a mean curve drawn through them. The solid lines in these figures correspond to equations (3) and (4). The curves of figures 7, 8, and 9 were then collected in figures 10 and 11.

Figure 10 gives the torsional buckling strength of semi-elliptical cylinders as a function of the dimensions of the cylinder and the ellipticity ratio. It is seen here that, as the ellipticity ratio increases, the buckling strength decreases, other items being kept equal. This is in line with the previous physical discussion since the cylinders with the larger ellipticities have a larger maximum radius of curvature and would thus buckle at lower loads than cylinders with smaller ellipticity ratios.

Figure 11, which gives the value of the ultimate load on such specimens, indicates that the cylinders with the larger ellipticities have somewhat better maximum-torsional-moment-carrying abilities. This is due to the fact that the section near the end of the major axis, having a small radius of curvature, acts as a stiffener, and that the larger the ellipticity, the greater the moment which can be developed before this effective stiffener collapses.

A cross plot of figures 10 and 11 led to empirical equations for the buckling and ultimate loads of such semielliptical and semicircular cylinders as follows:

1. For the buckling strength

$$\frac{\tau_b L^2}{Et^2} = 1.60 + \sqrt{14.80 + 1.13\left(\frac{L^2 \epsilon^{1/3}}{2t\rho_o}\right)^{1.6}} \tag{3}$$

or

$$\frac{\tau_b L^2}{Et^2} = 1.60 + \sqrt{14.80 + 1.13\left(\frac{L^2}{2ta\epsilon^{2/3}}\right)^{1.6}} \tag{3a}$$

2. For the ultimate strength

$$\frac{\tau_u L^2}{Et^2} = 1.60 + \sqrt{14.80 + 1.13\left(\frac{L^2 \epsilon^{1/3}}{2ta}\right)^{1.6}} \tag{4}$$

in which $a$ is the semimajor axis and $\rho_o$ is the maximum radius of curvature of the cross section. It can be shown that, for an ellipse,

$$\rho_o = \epsilon a$$

The foregoing equations are plotted in figures 12 and 13 with the experimental points and show good agreement and a reasonable amount of scatter. Thus, equations (3) and (4) and figures 12 and 13 can be considered to be design equations and design curves for semicircular and semielliptical cylinders subjected to a pure torsional moment.

On comparing the present results with those of reference 5 on complete elliptical cylinders, two important differences are noted. For the same sheet thickness and length, an elliptical cylinder buckles at a lower stress than a circular cylinder of radius $\rho_0$; while for semicylinders a higher stress is reached. The reason for this lies in the fact that it was impossible to construct the elliptical cylinders without a slight looseness of the skin at the ends of the minor axis (cf., p. 2 of reference 5), thus introducing a rather large effect of initial irregularities into the buckling-test results. This was not the case in the semielliptical cylinders, since the construction technique used eliminated this difficulty. With regard to the ultimate strengths, the chief difference lies in the presence of the multiplicative $\epsilon^{1/3}$ factor in the parameter for the semielliptical cylinders. An attempt to detect the presence of this same term in the results of reference 5 was unsuccessful, because of the narrow range of ellipticities tested coupled with the usual amount of experimental scatter.

## Pure Bending of Semicircular Cylinders

The next series of specimens was made up of semicircular and semielliptical cylinders subjected to pure bending moments. The bending moment was applied in the plane of the minor axis of the cylinder.

As in the case of pure torsion, it is necessary to define the critical loads of pure bending in terms of suitable stresses. To accomplish this, use has been made of the normal beam equation,

$$\sigma = \frac{Mb}{I_b} \tag{5}$$

The values of stress given by this equation should represent the true stress in the specimens tested up to the point of buckling. Beyond this point, the stresses given are of a fictitious nature, owing to the fact that the neutral axis

of the test specimens will shift toward the tension side of the specimens as the buckle deformations increase on the compression side. Extensometers mounted to the specimens during the testing procedure were used to check equation (5). In figure 14 are plotted sample curves of the experimentally determined stresses on the tension and the compression sides, prior to buckling, as a function of the applied bending moment. For comparison, stress values calculated from equation (5) are included. It can be seen that a linear and symmetrical stress distribution exists before buckling takes place for each of the three examples shown and that the agreement between the actual and calculated stresses is quite good. The fact that the calculated stresses are lower for each of the three cases plotted is merely a result of the selection of the examples and is not typical of the test data when considered as a whole, as can be seen in the upper curve of figure 15, where a comparative summary has been made. The scatter of the data about the line for unity in this figure can be attributed to the inherent difficulties in making stress measurements on curved, thin-walled sections by means of mechanical extensometers. The experimentally determined values of the bending stresses, after buckling has taken place, substantiate the shift in the neutral axis; however, the influence of the local buckle deformations is so great on these readings that they have little practical significance.

The first series of tests consisted of semicircular cylinders of various sheet thicknesses and lengths subjected to pure bending moments applied in the plane of the vertical spacer blocks (the plane of the minor axis for $\epsilon = 1.0$). Prior to the specimens reaching their critical load, the skin covering remained unbuckled; however, at this point in the loading history, the compression side of the specimens would suddenly buckle into a large number of characteristic elliptical and diamond-shape patterns, all directed inward. Although this buckling phenomenon was quite violent at times, the applied bending loads had little tendency to drop off at this point. If the loads were increased, the buckle deformations would increase rapidly both in magnitude and scope, indicating that the sheet covering had already reached its ultimate stress and that the load was being supported by the cover-plate system alone. This conclusion appears to be well substantiated by the fact that the maximum load reached (at cover-plate failure) was independent of the geometric variables of the sheet covering and was solely a function of the cover plate thickness. For this reason, it has been assumed,

in the discussion that follows, that the buckling load was also the maximum load that could be carried by the semicircular shell.

The results of this series of tests on semicircular cylinders are presented in table VI and figure 16. The results have been correlated by using a reduced bending stress K, in which

$$K = \frac{\sigma_b a}{Et} = \frac{\sigma_b \rho_o}{Et} \tag{6}$$

This nondimensional stress coefficient is analogous to that used in reference 6 for axial compression stresses.

A study of figure 16 indicates that the reduced bending stress coefficient K gives a satisfactory parameter for plotting the data for a generalized curve for semicircular cylinders under pure bending. The scatter of the experimental points is not only reasonably small but is random in nature.

The oscillatory nature of the curve in figure 16 was at first questioned, but a study of reference 6 indicated that such a length effect might be expected. Reference 6 contains a linearized theory on the length effect of cylinders under axial compression, and the final results show a length effect that is qualitatively similar to that shown in figure 16. The necessary condition for such an effect was that the number of buckles in the complete circumference of the specimen must remain independent of the length of the cylinder. A careful check of the data on the number of buckles at buckling of the semicircular specimens showed that they varied only from 8 to 10 in range of $L/\rho_o$'s from 0.33 to 11.30 and $\rho_o/t$'s from 147 to 313, and that the variation was random in nature. On this basis, it is thought that the shape of the curve in figure 16 is at least tentatively justified.

In comparing the failing stress of semicircular cylinders under pure bending with the failing stress in circular cylinders under the same loading condition (see reference 7 and p. 466 of reference 8) it is found that the value of K is much smaller for the semicircular cylinders than it is for the full circular cylinders for the same value of $\rho_o/t$. Part of this difference is explainable by the fact that, for

the full cylinders, any seams in the cylinders were placed on the neutral axis of the specimen; while, in the case of the semicircular cylinders, the seams were located in regions of maximum tension and compression stress.

In an effort to determine experimentally the effect of seam location it was decided to construct and test a series of of circular cylinders in pure bending under conditions similar to those of the semicircular cylinders. These specimens consisted of circular end plates approximately 6 inches in diameter, to which were attached the thin sheet covering in exactly the same manner as previously described. The seam or seams were formed by lapping the edges of the sheet and fastening them together by means of two rows of closely spaced, carefully fitted machine screws. These screws were not tightened excessively, in order to keep the deformations of the sheet covering across the seam to a minimum. To obtain the complete effect of the seams, four arrangements were selected:

1. One seam located on the neutral axis

2. One seam located on the tension side

3. One seam located on the compression side

4. Two seams located on the tension and compression sides

All these specimens were tested in the testing machine shown in figure 5, and the results are presented in table V and figure 17. The reduced buckling stress shown for the circular specimens with the single seam on the neutral axis, when compared to the similar specimens of reference 7, shows rather good agreement. With the seam on the tension side, a small reduction in stress is obtained; while, for the single seam on the compression side, the buckling stress is lowered still further. For the specimens with seams on both top and bottom, the reduction in stress is greater than the sum of the second and third configuration. All these buckling stresses are considerably lower than the value given by the classical theory and show clearly the influence of discontinuities in the specimen.

The dotted curve in figure 17 indicates the load carried by those specimens immediately after buckling and shows that all specimens tend to fall on the same curve. This

last phenomenon is explained by the recent work of Kármán and Tsien (reference 9) on the nonlinear buckling problem. In this paper, it was shown that there exist two buckling equilibrium points, one of which is closely given by the classical linearized theory, the other by the nonlinear theory. This latter equilibrium point was shown to exist at a much lower stress than the former point, and buckling could occur at stresses anywhere between these two limits, depending on initial imperfections and eccentricities in the shell and on the presence of external disturbances such as vibrations. Generally, buckling would be characterized by a sudden jump in the applied load to the value corresponding to the lower equilibrium point. This dotted curve then corresponds to the lower equilibrium point of full circular cylinders under bending.

The lower curve of figure 17 gives the values for the semicircular cylinders tested, and it can be seen that the K value for these specimens is still lower than the minimum point for the circular cylinders. The buckling of these semicircular cylinders was characterized by the fact that the applied load had little tendency to jump at the buckling load. This would imply that the specimens had buckled at a stress corresponding to the lowest possible equilibrium stress and never exceeded this value at any previous time in their loading history. The cause of such a conditions existing is undoubtedly the fact that the presence of the support system, including the cover plates, introduced small but sufficient amounts of initial eccentricity and irregularity into the sheet covering to cause failure to occur at the minimum point. This can be understood when it is considered that the cover plates were necessarily located at the most highly stressed point on the circumference of the specimen.

In view of the foregoing discussion, it is thought that figure 16 gives a satisfactory design curve for semicircular cylinders subjected to pure bending. The values obtained, while considerably lower than those obtained for full circular cylinders, probably will give a better approximation to the actual case of the nose section of a wing and therefore should be used for nose-section design where applicable.

## Pure Bending of Semielliptical Cylinders

During the testing of the semielliptical cylinders subjected to pure bending loads, several experimental observations were made which will be discussed before presenting

the quantitative results. These specimens, upon reaching their buckling load, deformed into a type of wave pattern in the large radius of curvature regions that was entirely different from that of the semicircular cylinders. The buckles that appeared were definitely of the characteristic flat-plate type for both ellipticities tested. These large shallow circular or elliptical buckles covered the major portion of the compression sides of the curved sheet covering and were different from the flat-plate type only in that they were all directed inward. In a manner similar to that described under the pure torsion tests, the small radius nose portions of the specimen behaved as if they were stiffeners, and actually formed the lower boundaries for the buckle pattern. The formation of the buckles was characterized by the facts that the buckling was not of a particularly violent nature and that there was no noticeable decrease in the load-carrying ability at the point of buckling.

As the load was increased beyond the buckling load, these same buckles increased in amplitude and scope until they approached quite close to the boundaries formed by the plates, the cover-plate system, and the nose of the section. Upon further application of load, these buckles created much smaller induced buckles, particularly in the four corners of the affected region. In no case, however, did the nose portion fail first since the point of collapse was always dictated by the strength of the cover plates. This is as would be expected, since the loading was pure bending and increasing the amount of material in the cover plates would have the same effect as increasing the size of the spar caps in a wing. The data obtained are therefore directly applicable to wing nose section design.

The results of this series of tests are given in table VII and table VIII, and these data have been combined with the test results in table VI on semicircular cylinders to give the curve shown in figure 18. This curve shows considerable scatter, but retesting and rechecking points indicated that the scatter was random and was inherent in the specimens. For that reason, the suggested design curve shown in the figure is placed near the lower limit of the points rather than through the mean of the experimental points tested.

This suggested design curve can be represented by the equation

$$\frac{\sigma_b}{E}\left(\frac{a}{t}\right)^{1.5} = 1.70 + 0.15\left(\frac{a}{L}\right)^{1.5} \tag{7}$$

or

$$\frac{\sigma_b}{E}\left(\frac{\rho_o}{\epsilon t}\right)^{1.5} = 1.70 + 0.15\left(\frac{\rho_o}{L\epsilon}\right)^{1.5} \tag{8}$$

This can be written as

$$\frac{\sigma_b}{E} = 1.70\left(\frac{t}{a}\right)^{1.5} + 0.15\left(\frac{t}{L}\right)^{1.5} \tag{9}$$

or

$$\frac{\sigma_b}{E} = 1.70\left(\frac{\epsilon t}{\rho_o}\right)^{1.5} + 0.15\left(\frac{t}{L}\right)^{1.5} \tag{10}$$

Equation (9) is plotted in figure 19.

There is some indication that the number of buckles in the buckle pattern of the specimens accounted in part for the wide scattering in figure 18. Further theoretical study may justify this presumption, but until more data are available it is thought that equation (9) or (10) will give a sufficiently conservative value of the critical buckling stress of semicircular or semielliptical cylinders under the action of pure bending.

## Bending-Plus-Torsion Tests

The bending-plus-torsion tests were made on the machine illustrated in figure 5. The loading was so arranged that a constant ratio of bending moment to torsional moment was applied to the specimen up to the failing point. Buckling was noted both visually and with the aid of stress-strain measurements taken in the specimen during loading. The bending and shearing stresses were calculated from the equations

$$\sigma = \frac{mb}{I_t} = \frac{Mb}{I_s} \tag{11}$$

and

$$\tau = \frac{m_t}{3At} \tag{12}$$

Subscripts b and u in the tables correspond to buckling and ultimate stresses, respectively. The values for $\sigma_{b_o}$, $\tau_{b_o}$, and $\tau_{u_o}$ were taken from figures 18, 10, and 11, respectively.

The test data for these specimens are tabulated in tables IX, X, and XI for ellipticity ratios of 1.0, 2.0, and 3.0, respectively. These data have been plotted in figures 30 to 35, in which figures each ellipticity is considered separately. A study of these figures led to the conclusion that single curves would satisfactorily represent the relationships between $\sigma_b/\sigma_{b_o}$ and $M_b/m_{t_b}$, $\tau_b/\tau_{b_o}$ and $M_b/m_{t_b}$, and $\tau_u/\tau_{u_o}$ and $M_u/m_{t_u}$ and that the introduction of the ellipticity ratio into the ultimate bending-stress ratio gave one curve for all ellipticities of the form $\sigma_u/\epsilon\sigma_{b_o}$ as a function of $M_u/m_{t_u}$. It was necessary to use the ratio of the ultimate compressive stress to the buckling compression stress (with no torsion) since, as was discussed under Pure Bending, the failure bending stress for pure bending was solely a function of the size of the cover plates, corresponding to the size of the spar caps in a normal wing.

The combined curves are shown in figures 36 to 39, and it can be seen that, although considerable scatter is present, a consistent trend of the stress ratios with a variation in the $M/m_t$ ratios is indicated. For the values of $\sigma_{b_o}$ in tables IX, X, and XI, the mean curve of figure 18 was used throughout. For the ultimate values, design curves have been indicated which approximate to the lower limits of the experimental data.

If these suggested design curves are cross-plotted, plotting $\frac{1}{\epsilon}\frac{\sigma_u}{\sigma_{b_o}}$ as a function of $\frac{\tau_u}{\tau_{u_o}}$ for constant values of $M_u/m_{t_u}$, it is found that a curve expressed by the following equation is obtained:

$$\frac{1}{\epsilon}\frac{\sigma_u}{\sigma_{b_o}} + \left(\frac{\tau_u}{\tau_{u_o}}\right)^2 = 1 \tag{13}$$

This equation will give conservative results for all values of $M_u/m_{t_u}$ and therefore can be used for design purposes.

A cross plot of the buckling curves (figs. 26 and 27) indicates that a similar equation will give a satisfactory first approximation with considerable scatter (as indicated in figs. 26 and 27). Thus,

$$\frac{\sigma_b}{\sigma_{b_u}} + \left(\frac{\tau_b}{\tau_{b_o}}\right)^2 = 1 \tag{14}$$

The buckling and failure wave patterns of these specimens depended largely upon the $M/m_t$ ratio. For large values of this ratio, typical diamond-shape compression waves appeared when the buckling stress was reached and for small values of this ratio diagonal shear waves appeared. Intermediate values led to wave patterns which were combinations of these two types. Failure of the cylinders occurred across the nose (minimum radius section) of the specimen for the cases when the torsional shearing moment was high and in the cover plates when the bending moment was high. This fact explains the reason for the relatively large scatter in the experimental data for the larger values of the $M/m_t$ ratios. The higher values of the experimental stresses correspond to specimens in which the cover plates were strong enough to permit the development of the full torsional shearing strength of the section so that failure finally occurred across the nose section.

Comparison between measured and calculated stresses in the regions below buckling are shown in the second curve in figure 15 and also in the upper curve of figure 30. It is seen that the scatter is random in nature and is of the order of magnitude that would be expected when measuring thin sheet stresses with mechanical extensometers.

The last four lines of tables IX, X, and XI are for specimens with lengths shorter than the standard length of 12.5 inches, which was held throughout the other tests. It can be seen that the test data for these specimens plot satisfactorily on the curves for the other specimens, indicating that there is no new length effect which appears for this combined loading.

## Bending-Plus-Shear Tests

The bending-plus-shear tests were conducted on the testing machine shown in figure 6. Two lengths of specimens were tested, 6.5 and 16.0 inches, and the usual three skin thicknesses and three ellipticity ratios were covered. The moment-to-shear ratio was varied by the position of the jack on the extended loading arm. As previously described, the weight of the extended loading arm is separately balanced out and no tare readings entered the loading force.

The data for these specimens are tabulated in tables XII, XIII, and XIV. The equations used in reducing the data were:

$$\sigma_b = \frac{mb}{I_t} = \frac{Flb}{I_t} \tag{15}$$

$$\tau_{s_b} = \frac{F}{A_s} \tag{16}$$

$$\frac{M}{Fb} = \frac{l}{b}\frac{I_s}{I_t} = \frac{m\frac{I_s}{I_t}}{Fb} \tag{17}$$

Only the buckling data have been recorded and reduced, since ultimate failure was, in nearly every case, caused by cover-plate failure. Thus, ultimate failure could be delayed indefinitely by increasing the cover-plate size (corresponding to an increase in spar-cap size). A few cases in which the $M_b/Fb$ ratio was very low (small moment but large shear) actually failed across the nose section, but the number of these specimens was not sufficiently great to allow the drawing of any general conclusions.

The value of $\sigma_{b_o}$ in the tables was obtained, using the mean curve of figure 18. The resulting values of $\sigma_b/\sigma_{b_o}$ show a scatter which is generally no more than that shown in figure 18, which indicates that very little additional scatter has been put into the points by the addition of direct

shear to the pure bending load. Scatter was particularly bad for the ellipticity ratio of 3. However, this was to be expected, since these specimens were very hard to make without initial deformations near the ends of the minor axis. Also, loads for these specimens were quite light and the accuracy of measuring these light loads had a tendency to decrease.

The data in tables XII, XIII, and XIV have all been plotted in figures 31 to 45. Figures 31, 36, and 41 give the variation of $\sigma_b/\sigma_{b_o}$ as a function of the $M_b/Fb$ ratio and, as mentioned before, the scatter tends to increase as the ellipticity ratio increases.

The results for the shear stress at buckling are plotted in the remaining curves. This shear stress is taken as the average shearing stress distribution. Each set of curves for a given ellipticity ratio has been collected and replotted in figures 35, 40, and 45. The scatter on these curves is not so high as that indicated for the bending stresses, which would tend to indicate that the distribution of the bending stress between the cylindrical sheet and the cover plates may not have been accurately given by the $I_s/I_t$ ratio, as was assumed.

No attempt was made to determine a $\tau_{s_b}/\tau_{s_{b_o}}$ ratio, since it was impossible to obtain a value for $\tau_{s_{b_o}}$. Therefore the value of $\tau_{s_b}$ has been presented simply as a function of the $M_b/Fb$ ratio.

Again, extensometer readings were taken below buckling to check the calculated value of the bending stresses, and the results are shown in figures 15 and 30. The scatter shown is random and is of the order of magnitude expected when using mechanical extensometers to measure stresses in thin sheet structures.

## CONCLUSIONS

The data contained in this report are intended to serve as a guide to the possible buckling and ultimate load-carrying abilities of wing nose sections. In most cases these

nose sections can be approximated by ellipses, and for this reason the elliptical section has been used for test purposes. The data and curves presented should give the designer a considerable insight into the behavior of such sections under pure loading conditions as well as conditions of combined bending and shear and combined bending and torsion. The problem of combined bending, torsion, and shear has not been studied in this investigation and future investigations should study the effect of all three loading conditions and should, if possible, make an attempt actually to measure skin stress distributions by means of electric strain gages in order to obtain a more complete stress distribution pattern.

A summary of the design equations and curves for the conditions studied is given as follows:

1. Pure Torsion

a. Buckling

$$\frac{\tau_b L^2}{Et^2} = 1.60 + \sqrt{14.80 + 1.13\left(\frac{L^2}{2ta\ \epsilon^{2/3}}\right)^{1.6}}$$

(See fig. 12.)

b. Ultimate

$$\frac{\tau_u L^2}{Et^2} = 1.60 + \sqrt{14.80 + 1.13\left(\frac{L^2\ \epsilon^{1/3}}{2ta}\right)^{1.6}}$$

(See fig. 13.)

2. Pure Bending

a. Buckling

$$\frac{\sigma_b}{E} = 1.70\left(\frac{t}{a}\right)^{1.5} + 0.15\left(\frac{t}{L}\right)^{1.5}$$

(See fig. 19.)

b. Ultimate

No ultimate curve since ultimate load is a function of the cover-plate strength.

3. Bending Plus Torsion

a. Buckling

$$\frac{\sigma_b}{\sigma_{b_o}} + \left(\frac{\tau_b}{\tau_{b_o}}\right)^2 = 1$$

(See figs. 26 and 27.)

b. Ultimate

$$\frac{1}{\epsilon}\frac{\sigma_u}{\sigma_{b_o}} + \left(\frac{\tau_u}{\tau_{u_o}}\right)^2 = 1$$

(See figs. 28 and 29.)

4. Bending Plus Direct Shear

a. Buckling

Bending stresses - Figures 31, 36, and 41 for ellipticities 1, 2, and 3, respectively.

Shear stresses - Figures 35, 40, and 45 for ellipticities 1, 2, and 3, respectively.

b. Ultimate

No ultimate values, since the ultimate stress is largely dependent upon cover-plate strength.

Guggenheim Aeronautical Laboratory,
California Institute of Technology,
Pasadena, Calif., July 17, 1944.

## REFERENCES

1. Anon.: ANC-5, Strength of Aircraft Elements. U. S. Government Printing Office, 1942.

2. Anon.: Alcoa Aluminum and Its Alloys. Aluminum Co. of Am., 1941.

3. Donnell, L. H.: Stability of Thin-Walled Tubes under Torsion. NACA Rep. No. 479, 1933.

4. Lundquist, Eugene E.: Strength Tests on Thin-Walled Duralumin Cylinders in Torsion. NACA TN No. 427, 1932.

5. Lundquist, Eugene E., and Burke, Walter F.: Strength Tests on Thin-Walled Duralumin Cylinders of Elliptical Section. NACA TN No. 527, 1935.

6. Flügge, Wilhelm: Statik und Dynamik Der Schalen. Julius Springer (Berlin), 1934.

7. Lundquist, Eugene E.: Strength Tests of Thin-Walled Duralumin Cylinders in Pure Bending. NACA TN No. 479, 1933.

8. Timoshenko, S.: Theory of Elastic Stability. McGraw-Hill Book Co., Inc. (New York), 1936.

9. von Kármán, Theodore, and Tsien, Hsue-Shen: The Buckling of Thin Cylindrical Shells under Axial Compression. Jour. Aero. Sci., vol 8, no. 8, June 1941, pp. 303-312.

## BIBLIOGRAPHY

Cox, H. L.: Stress Analysis of Thin Metal Construction. Jour. R.A.S., vol. 44, no. 3, March 1940, pp. 231-272.

Kanemitsu, Sunao, and Nojima, Noble M.: Axial Compression Tests of Thin Circular Cylinders. Thesis, C.I.T., 1939. (unpublished)

Lundquist, Eugene E.: Strength Tests of Thin-Walled Duralumin Cylinders in Compression. NACA Rep. No. 473, 1933.

TABLE I

Tensile Properties of 24S-T Aluminum Alloy

Sheet Used in Specimens Tested

| Specimen No. | t (in.) | Loading direction relative to grain | $E \times 10^{-6}$ (lb./in.$^2$) | $\sigma_{yp}$ (lb./in.$^2$) | $\sigma_u$ (lb./in.$^2$) |
|---|---|---|---|---|---|
| MT-1 | 0.0101 | With | 10.85 | — | 69100 |
| MT-2 | 0.0102 | " | 10.71 | 51000 | 66300 |
| MT-3 | 0.0099 | Across | 9.94 | 44600 | 65500 |
| MT-4 | 0.0098 | " | 10.05 | 45500 | 66100 |
| MT-5 | 0.0175 | With | 10.46 | 52800 | 68700 |
| MT-6 | 0.0174 | " | 10.49 | 51200 | 69800 |
| MT-7 | 0.0174 | Across | 10.44 | 44900 | 68100 |
| MT-8 | 0.0175 | " | 10.43 | 44800 | 66900 |
| MT-9 | 0.0209 | With | 9.44 | 49500 | 69300 |
| MT-10 | 0.0205 | " | 10.02 | 52500 | 70300 |
| MT-11 | 0.0204 | Across | 9.76 | 45800 | 67600 |
| MT-12 | 0.0204 | " | 10.24 | 44800 | 66900 |
| MT-13 | 0.0319 | With | 11.18 | 55500 | 72800 |
| MT-14 | 0.0320 | " | 10.50 | 56300 | 72100 |
| MT-15 | 0.0315 | Across | 11.20 | 47100 | 71200 |
| MT-16 | 0.0315 | " | 10.51 | 47500 | 70300 |
| MT-17 | 0.0383 | With | 10.65 | 52300 | 70600 |
| MT-19 | 0.0387 | Across | 10.47 | 45800 | 69400 |
| MT-20 | 0.0386 | " | 10.01 | 43800 | 69900 |
| MT-A | 0.0210 | With | 10.00 | 54000 | -- |
| MT-B | 0.0210 | Across | 10.00 | 46300 | -- |
| MT-C | 0.0165 | " | 9.80 | 45500 | -- |
| MT-D | 0.0165 | " | 10.00 | 45100 | -- |

TABLE II

Torsional Strength of Semi-Circular Cylinders, $\varepsilon = 1.0$

24S-T $\mu = 0.3$ $E = 10.3 \times 10^6$ lb./in.$^2$ b = 3.01 in.

| Spec. No. | t (in.) | L (in.) | $Mt_b$ (in.-lb.) | $Mt_u$ (in.-lb.) | $\tau_b$ (in./in.$^2$) | $\tau_u$ (lb./in$^2$) | $\frac{\tau_b L^2}{Et^2}$ | $\frac{\tau_u L^2}{Et^2}$ | $\frac{L^2}{2ta}$ | $\frac{L^2 \varepsilon^{2/3}}{2t\rho_o}$ | $\frac{L^2 \varepsilon^{1/3}}{2ta}$ |
|---|---|---|---|---|---|---|---|---|---|---|---|
| PT-9 | 0.0190 | 34.0 | 8840 | 9090 | 5740 | 5910 | 1790 | 1840 | 10110 | 10110 | 10110 |
| PT-10 | " | " | 8850 | 8850 | 5750 | 5750 | 1790 | 1790 | " | " | " |
| PT-11 | " | " | 8830 | 9000 | 5740 | 5850 | 1780 | 1820 | " | " | " |
| PT-12 | " | " | 8220 | 8220 | 5340 | 5340 | 1660 | 1660 | " | " | " |
| PT-13 | " | " | 8230 | 8290 | 5350 | 5390 | 1660 | 1660 | " | " | " |
| PT-14 | 0.0160 | " | 6060 | 6060 | 4680 | 4680 | 2050 | 2050 | 12010 | 12010 | 12010 |
| PT-15 | " | " | 5430 | 5720 | 4190 | 4410 | 1840 | 1940 | " | " | " |
| PT-26 | 0.0200 | 16.0 | 12380 | 12380 | 7640 | 7640 | 475 | 475 | 2130 | 2130 | 2130 |
| PT-27 | " | " | 13240 | 13240 | 8170 | 8170 | 508 | 508 | " | " | " |
| PT-28 | 0.0160 | " | 7900 | 7900 | 6100 | 6100 | 593 | 593 | 2660 | 2660 | 2660 |
| PT-29 | " | " | 7830 | 7830 | 6050 | 6050 | 587 | 587 | " | " | " |
| PT-73 | 0.0104 | " | 2980 | 2980 | 3540 | 3540 | 814 | 814 | 4100 | 4100 | 4100 |
| PT-74 | 0.0102 | " | 2800 | 2900 | 3400 | 3520 | 812 | 841 | 4180 | 4180 | 4180 |
| PT-20 | 0.0200 | 6.5 | 18040 | 18040 | 11140 | 11140 | 114 | 114 | 351 | 351 | 351 |
| PT-21 | 0.0200 | " | 19450 | 19450 | 12010 | 12010 | 123 | 123 | " | " | " |
| PT-23 | 0.0160 | " | 12840 | 12840 | 9920 | 9920 | 159 | 159 | 439 | 439 | 439 |
| PT-24 | 0.0160 | " | 11930 | 12160 | 9210 | 9390 | 147 | 150 | " | " | " |
| PT-58 | 0.0108 | " | 4000 | 4500 | 4690 | 5160 | 162 | 182 | 651 | 651 | 651 |
| PT-32 | 0.0200 | 2.5 | 23760 | 23760 | 14660 | 14660 | 22.2 | 22.2 | 51.9 | 51.9 | 51.9 |
| PT-33 | 0.0200 | " | 24700 | 24700 | 15250 | 15250 | 23.2 | 23.2 | " | " | " |
| PT-30 | 0.0160 | " | 15000 | 17140 | 11580 | 13230 | 27.3 | 31.3 | 64.9 | 64.9 | 64.9 |
| PT-31 | " | " | 18390 | 18390 | 14200 | 14200 | 33.3 | 33.3 | " | " | " |

TABLE III

Torsional Strength of Semi-Elliptical Cylinders, $\mathcal{E} = 2.0$

24S-T $\mu = 0.3$ $E = 10.3 \times 10^6$ lb./in.$^2$ $b = 3.01$ in.

| Spec. No. | t (in.) | L (in.) | $M_{t_b}$ (in.-lb.) | $M_{t_u}$ (in.-lb.) | $\tau_p$ (lb./in.$^2$) | $\tau_u$ (lb./in.$^2$) | $\frac{\tau_p L^2}{Et^2}$ | $\frac{\tau_u L^2}{Et^2}$ | $\frac{L^2}{2ta}$ | $\frac{L^2 \mathcal{E}^{1/3}}{2t\rho_o}$ | $\frac{L^2 \mathcal{E}^{1/3}}{2ta}$ |
|---|---|---|---|---|---|---|---|---|---|---|---|
| PT-16 | 0210 | 34.0 | 9260 | 10500 | 3190 | 3620 | 812 | 920 | 4570 | 2880 | 5750 |
| PT-48 | 0.0200 | 16.0 | 10390 | 13580 | 3760 | 4920 | 234 | 306 | 1110 | 700 | 1400 |
| PT-49 | " | " | 10240 | 13850 | 3710 | 5020 | 231 | 312 | " | " | " |
| PT-65 | 0.0170 | " | 5400 | 9850 | 2300 | 4200 | 198 | 362 | 1250 | 788 | 1570 |
| PT-71 | 0.0167 | " | 5500 | 10490 | 2390 | 4560 | 213 | 406 | 1280 | 806 | 1610 |
| PT-72 | 0.0106 | " | 2000 | 4240 | 1370 | 2900 | 254 | 536 | 2010 | 1270 | 2530 |
| PT-66 | 0.0104 | " | 1800 | 3670 | 1260 | 2570 | 280 | 590 | 2050 | 1290 | 2580 |
| PT-22 | 0.0200 | 6.5 | 18000 | 23500 | 6530 | 8520 | 67.0 | 87.4 | 183 | 115 | 230 |
| PT-47 | " | " | 16550 | 19650 | 6000 | 7125 | 61.5 | 73.1 | " | " | " |
| PT-59 | 0.0177 | " | 10400 | 14100 | 4260 | 5780 | 55.7 | 75.5 | 198 | 125 | 250 |
| PT-25 | 0.0160 | " | 10500 | 14000 | 4760 | 6350 | 76.4 | 102 | 219 | 138 | 276 |
| PT-60 | 0.0104 | " | 3000 | 4750 | 2100 | 3330 | 79.7 | 126 | 338 | 213 | 426 |
| PT-62 | 0.0101 | " | 2800 | 5060 | 2020 | 3640 | 81.2 | 146 | 348 | 220 | 439 |
| PT-35 | 0.0200 | 2.5 | 25650 | 28760 | 8570 | 10430 | 13.0 | 15.8 | 27.1 | 17.1 | 34.2 |
| PT-36 | 0.0200 | " | 24380 | 35640 | 8830 | 12930 | 13.4 | 19.6 | " | " | " |
| PT-34 | 0.0160 | " | 13930 | 24640 | 6320 | 11180 | 15.0 | 26.5 | 32.5 | 20.5 | 41.0 |
| PT-37 | " | " | 16270 | 23090 | 7370 | 10480 | 17.5 | 24.8 | " | " | " |
| PT-51 | 0.0103 | " | 4000 | 6790 | 2820 | 4790 | 16.2 | 27.4 | 50.5 | 31.8 | 63.6 |
| PT-54 | 0.0101 | " | -- | 6450 | -- | 4640 | -- | 26.6 | 51.5 | 32.5 | 65.0 |

TABLE IV

Torsional Strength of Semi-Elliptical Cylinders, $\varepsilon = 3.0$

24S-T $\mu = 0.3$ $E = 10.3 \times 10^6$ lb./in.$^2$ $b = 3.01$ in.

| Spec. No. | t (in.) | L (in.) | $M_{t_b}$ (in.-lb.) | $M_{t_u}$ (in.-lb.) | $\tau_b$ (lb./in.$^2$) | $\tau_u$ (lb./in.$^2$) | $\frac{\tau_b L^2}{Et^2}$ | $\frac{\tau_u L^2}{Et^2}$ | $\frac{L^2}{2ta}$ | $\frac{L^2 \varepsilon^{1/3}}{2t\rho_o}$ | $\frac{L^2 \varepsilon^{1/3}}{2ta}$ |
|---|---|---|---|---|---|---|---|---|---|---|---|
| PT-17 | 0.0200 | 34.0 | 6060 | 12240 | 1560 | 3140 | 459 | 883 | 3200 | 1540 | 4610 |
| PT-18 | " | 16.0 | 7000 | 17640 | 1800 | 4520 | 112 | 281 | 709 | 340 | 1020 |
| PT-19 | " | " | 6800 | 15960 | 1750 | 4080 | 109 | 254 | " | " | " |
| PT-44 | " | " | 6800 | 15400 | 1750 | 3950 | " | 246 | " | " | " |
| PT-68 | 0.0176 | " | 5500 | 12160 | 1610 | 3550 | 129 | 284 | 806 | 387 | 1160 |
| PT-69 | 0.0174 | " | -- | 12300 | -- | 3630 | -- | 298 | 816 | 392 | 1180 |
| PT-70 | 0.0103 | " | -- | 4600 | -- | 2300 | -- | 539 | 1380 | 663 | 1990 |
| PT-45 | 0.0200 | 6.5 | 14420 | 20030 | 3700 | 5140 | 38.0 | 52.8 | 117 | 56.2 | 169 |
| PT-46 | " | " | 9200 | 17850 | 2360 | 4680 | 24.2 | 47.0 | " | " | " |
| PT-50 | " | " | 13000 | 25200 | 3330 | 6460 | 34.2 | 66.4 | " | " | " |
| PT-63 | 0.0175 | " | 7000 | 17310 | 2050 | 5080 | 27.5 | 68.2 | 134 | 64.4 | 193 |
| PT-61 | 0.0173 | " | 5500 | 15390 | 1630 | 4570 | 22.4 | 62.8 | 135 | 64.9 | 195 |
| PT-67 | 0.0103 | " | 2600 | 6020 | 1300 | 3010 | 50.3 | 116 | 228 | 110 | 329 |
| PT-64 | 0.0102 | " | 3000 | 6630 | 1510 | 3340 | 59.8 | 132 | 240 | 115 | 346 |
| PT-40 | 0.0200 | 2.5 | 25900 | 45800 | 6550 | 11750 | 9.95 | 17.8 | 17.3 | 8.31 | 25.0 |
| PT-41 | " | " | 26000 | -- | 6670 | -- | 10.1 | -- | " | " | " |
| PT-42 | " | " | 24400 | 41000 | 6260 | 10510 | 9.50 | 15.9 | " | " | " |
| PT-38 | 0.0160 | " | 12880 | 22900 | 4140 | 7360 | 9.81 | 17.5 | 21.8 | 10.5 | 31.4 |
| PT-39 | " | " | 11580 | 23550 | 3620 | 7570 | 8.59 | 18.0 | " | " | " |
| PT-56 | 0.0103 | " | 3500 | 7900 | 1750 | 3950 | 10.0 | 22.6 | 33.7 | 16.2 | 48.6 |
| PT-55 | 0.0099 | " | 4000 | 8920 | 2080 | 4640 | 13.1 | 29.2 | 35.0 | 16.8 | 50.5 |

TABLE V

Bending Strength of Circular Cylinders

$a = 3.0$ in. $L = 6.5$ in. $L/a = 2.16$

24S-T $\mu = 0.3$ $E = 10.3 \times 10^6$ lb./in.$^2$

| Spec No. | t (in.) | a/t | $M_b$ (in.-lb.) | $\sigma_b$ (lb./in.$^2$) | $\frac{\sigma_b a}{Et}$ | $\frac{\sigma'_b a}{Et}$ | Remarks |
|---|---|---|---|---|---|---|---|
| PB-103 | 0.0206 | 146 | 18050 | 30800 | 0.436 | 0.250 | Seam on N.A. |
| PB-104 | 0.0205 | 147 | 16200 | 27800 | 0.396 | 0.214 | " " " |
| PB-102 | 0.0162 | 186 | 11600 | 25200 | 0.454 | 0.240 | " " " |
| PB-101 | 0.0160 | 188 | 11820 | 26000 | 0.475 | 0.286 | " " " |
| PB-110 | 0.0102 | 295 | 5000 | 17300 | 0.494 | 0.279 | " " " |
| PB-109 | 0.0094 | 320 | 3060 | 11500 | 0.356 | 0.264 | " " " |
| PB-106 | 0.0199 | 151 | 16190 | 28600 | 0.420 | 0.219 | " " T. side |
| PB-105 | " | " | 15530 | 27400 | 0.403 | 0.262 | " " C. side |
| PB-112 | 0.0194 | 155 | 13410 | 24300 | 0.365 | 0.251 | " " " " |
| PB-107 | 0.0205 | 147 | 13470 | 23100 | 0.329 | 0.220 | " " T. and C. Sides |
| PB-108 | 0.0203 | 148 | 13480 | 23300 | 0.335 | 0.261 | " " " " " " |
| PB-115 | 0.0160 | 188 | 9310 | 20500 | 0.374 | 0.262 | " " " " " " |
| PB-117 | 0.0155 | 194 | 9460 | 21500 | 0.405 | 0.310 | " " " " " " |
| PB-119 | 0.0104 | 289 | 3370 | 11400 | 0.324 | 0.284 | " " " " " " |
| PB-121 | 0.0100 | 300 | 3600 | 12700 | 0.369 | 0.287 | " " " " " " |

TABLE VI

Bending Strength of Semi-Circular Cylinders, $\mathcal{E} = 1.0$
24S-T $\mu = 0.3$ $E = 10.3 \times 10^6$ lb./in.$^2$ $b = 3.01$ in.

| Spec. No. | t (in.) | L (in.) | $I_s$ (in.$^4$) | $I_t$ (in.$^4$) | $\rho_o/t$ | $L/\rho_o$ | $M_b$ (in.-lb.) | $\sigma_b$ (lb./in.$^2$) | $\frac{\sigma_b}{E}\left(\frac{\rho_o}{\mathcal{E}t}\right)^{1.5}$ | $\frac{L}{\rho_o}$ |
|---|---|---|---|---|---|---|---|---|---|---|
| PB-33 | 0.0212 | 34.0 | 1.818 | 4.785 | 142.0 | 11.30 | 19450 | 12250 | 2.01 | 11.30 |
| PB-33B | " | " | " | " | " | " | 19475 | 12270 | 2.01 | " |
| PB-14 | 0.0203 | 16.0 | 1.739 | 4.620 | 148.2 | 5.31 | 19950 | 13000 | 2.28 | 5.31 |
| PB-14B | " | " | " | " | " | " | 18200 | 11860 | 2.08 | " |
| PB-56 | 0.0160 | " | 1.369 | 4.168 | 188.1 | " | 15750 | 11370 | 2.85 | " |
| PB-56B | " | " | " | " | " | " | 15800 | 11440 | 2.87 | " |
| PB-58 | 0.0098 | " | 0.835 | 2.545 | 307.0 | " | 5330 | 6290 | 3.29 | " |
| PB-58B | " | " | " | " | " | " | 4800 | 5660 | 2.96 | " |
| PB-24 | 0.0204 | 12.5 | 1.749 | 4.712 | 147.5 | 4.15 | 23300 | 14880 | 2.58 | 4.15 |
| PB-24B | " | " | " | " | " | " | 22650 | 14470 | 2.51 | " |
| PB-37 | 0.0164 | " | 1.402 | 4.201 | 183.4 | " | 16430 | 11770 | 2.84 | " |
| PB-37B | " | " | " | " | " | " | 16700 | 11960 | 2.88 | " |
| PB-39 | 0.0095 | " | 0.810 | 2.509 | 316.2 | " | 5850 | 7010 | 3.83 | " |
| PB-39B | " | " | " | " | " | " | 5775 | 6920 | 3.78 | " |
| PB-5 | 0.0200 | 6.5 | 1.714 | 4.550 | 150.5 | 2.16 | 24000 | 15900 | 2.85 | 2.16 |
| PB-5B | " | " | " | " | " | " | 23000 | 15200 | 2.73 | " |
| PB-6 | " | " | " | " | " | " | 21800 | 14400 | 2.58 | " |
| PB-6B | " | " | " | " | " | " | 23000 | 15200 | 2.73 | " |
| PB-18 | 0.0207 | " | 1.773 | 4.693 | 145.3 | " | 26150 | 16800 | 2.85 | " |
| PB-18B | " | " | " | " | " | " | 24200 | 15500 | 2.63 | " |
| PB-11 | 0.0175 | " | 1.498 | 4.331 | 172.0 | " | 17870 | 12400 | 2.72 | " |
| PB-11B | " | " | " | " | " | " | 20500 | 14200 | 3.11 | " |
| PB-17 | 0.0106 | " | 0.904 | 2.667 | 283.7 | " | 7000 | 7890 | 3.66 | " |
| PB-17B | " | " | " | " | " | " | 7250 | 8170 | 3.79 | " |
| PB-21 | " | " | " | 2.716 | " | " | 8370 | 9280 | 4.31 | " |
| PB-21B | " | " | " | " | " | " | 7250 | 8040 | 3.73 | " |
| PB-9 | 0.0198 | 2.5 | 1.969 | 4.591 | 152.0 | 0.83 | 16600 | 10900 | 1.99 | 0.83 |
| PB-27 | 0.0200 | " | 1.714 | 4.649 | 150.5 | " | 18750 | 12130 | 2.17 | " |
| PB-52 | 0.0161 | 2.5 | 1.378 | 4.163 | 187.0 | " | 16360 | 11800 | 2.93 | " |
| PB-49 | 0.0095 | " | 0.810 | 2.497 | 316.1 | " | 4110 | 4950 | 2.70 | " |
| PB-34 | 0.0205 | 1.0 | 1.758 | 4.705 | 146.9 | 0.33 | 22550 | 14420 | 2.49 | 0.33 |
| PB-34B | " | " | " | " | " | " | 22750 | 14550 | 2.52 | " |
| PB-43 | 0.0163 | " | 1.395 | 4.176 | 184.6 | " | 18260 | 13140 | 3.20 | " |
| PB-46 | 0.0096 | " | 0.818 | 2.508 | 313.0 | " | 4250 | 5090 | 2.74 | " |

## TABLE VII

Bending Strength of Semi-Elliptical Cylinders, $\varepsilon = 2.0$

24S-T $\mu = 0.3$ $E = 10.5 \times 10^6$ lb/in$^2$ $b = 3.01$ in.

| Spec. No. | $t$ (in.) | $L$ (in.) | $I_s$ (in.$^4$) | $I_t$ (in.$^4$) | $\rho_o/t$ | $L/\rho_o$ | $L/a$ | $t/a$ | $M_b$ (in.-lb.) | $\sigma_b$ (lb./in.$^2$) | $\frac{\sigma_b}{E}\left(\frac{\rho_o}{\varepsilon t}\right)^{1.5}$ | $\frac{L}{\rho_o}$ |
|---|---|---|---|---|---|---|---|---|---|---|---|---|
| PB-16 | 0.0208 | 16.0 | 3.119 | 6.029 | 579 | 1.33 | 2.66 | 0.00346 | 8000 | 3990 | 1.91 | 2.66 |
| PB-16B | " | " | " | " | " | " | " | " | 10000 | 4990 | 2.38 | " |
| PB-59 | 0.0165 | " | 2.468 | 5.249 | 730 | " | " | 0.00274 | 5940 | 3400 | 2.30 | " |
| PB-59B | " | " | " | " | " | " | " | " | 5820 | 3340 | 2.26 | " |
| PB-25 | 0.0198 | 12.5 | 2.967 | 5.902 | 609 | 1.04 | 2.08 | 0.00328 | 9900 | 5050 | 2.60 | 2.08 |
| PB-25B | " | " | " | " | " | " | " | " | 10500 | 5350 | 2.75 | " |
| PB-40 | 0.0165 | " | 2.460 | 5.261 | 729 | " | " | 0.00274 | 7300 | 4160 | 2.80 | " |
| PB-40B | " | " | " | " | " | " | " | " | 6680 | 3820 | 2.58 | " |
| PB-38 | 0.0095 | " | 1.418 | 3.112 | 1266 | " | " | 0.00158 | 1500 | 1450 | 2.24 | " |
| PB-38B | " | " | " | " | " | " | " | " | 1410 | 1360 | 2.10 | " |
| PB-3 | 0.0210 | 6.5 | 3.152 | 6.019 | 573 | 0.540 | 1.08 | 0.00350 | 17700 | 8850 | 4.15 | 1.08 |
| PB-3B | " | " | " | " | " | " | " | " | 15700 | 7850 | 3.69 | " |
| PB-19 | 0.0205 | " | 3.070 | 6.047 | 587 | " | " | 0.00340 | 13050 | 6500 | 3.17 | " |
| PB-19B | " | " | " | " | " | " | " | " | 15300 | 7630 | 3.72 | " |
| PB-10 | 0.0173 | " | 2.591 | 5.367 | 696 | " | " | 0.00287 | 10700 | 6000 | 3.77 | " |
| PB-15 | 0.0106 | " | 1.581 | 3.359 | 1133 | " | " | 0.00176 | 2000 | 1790 | 2.34 | " |
| PB-15B | " | " | " | " | " | " | " | " | 2350 | 2100 | 2.74 | " |
| PB-7 | 0.0205 | 2.5 | 3.074 | 6.040 | 588 | 0.208 | 0.42 | 0.00340 | 9800 | 4880 | 2.38 | 0.42 |
| PB-7B | " | " | " | " | " | " | " | " | 12400 | 6190 | 3.02 | " |
| PB-28 | " | " | " | 6.007 | " | " | " | " | 10250 | 5140 | 2.51 | " |
| PB-28B | " | " | " | " | " | " | " | " | 9400 | 4710 | 2.30 | " |
| PB-53 | 0.0166 | " | 2.474 | 5.276 | 725 | " | " | 0.00276 | 8840 | 5040 | 3.37 | " |
| PB-53B | " | " | " | " | " | " | " | " | 8410 | 4800 | 3.21 | " |
| PB-54 | 0.0100 | " | 1.492 | 3.230 | 1202 | " | " | 0.00169 | 1410 | 1310 | 1.87 | " |
| PB-54B | " | " | " | " | " | " | " | " | 1340 | 1250 | 1.79 | " |
| PB-35 | 0.0210 | 1.0 | 3.155 | 6.117 | 574 | 0.083 | 0.17 | 0.00349 | 19750 | 9760 | 4.60 | 0.17 |
| PB-35B | " | " | " | " | " | " | " | " | 21300 | 10520 | 4.96 | " |
| PB-44 | 0.0165 | " | 2.468 | 5.288 | 729 | " | " | 0.00274 | 14000 | 7950 | 5.36 | " |
| PB-48 | 0.0094 | " | 1.402 | 3.078 | 1280 | " | " | 0.00156 | 3140 | 3080 | 4.83 | " |

## TABLE VIII

Bending Strength of Semi-Elliptical Cylinders, $\varepsilon = 3.0$
24S-T $\mu = 0.3$ $E = 10.3 \times 10^6$ lbs/in.$^2$ b = 3.01 in.

| Spec. No. | t (in.) | L (in.) | $I_s$ (in.$^4$) | $I_t$ (in.$^4$) | $\rho_o/t$ | $L/\rho_o$ | L/a | t/a | $M_b$ (in.-lb.) | $\sigma_b$ (lb./in.$^2$) | $\frac{\sigma_b}{E}\left(\frac{\rho_o}{\varepsilon t}\right)^{1.5}$ | $\frac{L}{\rho_o}$ |
|---|---|---|---|---|---|---|---|---|---|---|---|---|
| PB-26 | 0.0199 | 16.0 | 4.256 | 7.169 | 1361 | 0.590 | 1.77 | 0.00220 | 5400 | 2270 | 2.13 | 1.77 |
| PB-57B | 0.0158 | " | 3.375 | 6.177 | 1715 | " | " | 0.00175 | 2430 | 1180 | 1.57 | " |
| PB-55B | 0.0098 | " | 2.089 | 3.812 | 2760 | " | " | 0.00109 | 910 | 718 | 1.95 | " |
| PB-23 | 0.0206 | 12.5 | 4.410 | 7.285 | 1315 | 0.461 | 1.38 | 0.00231 | 6000 | 2480 | 2.21 | 1.38 |
| PB-23B | " | " | " | " | " | " | " | " | 4570 | 1890 | 1.69 | " |
| PB-42 | 0.0166 | " | 3.541 | 6.343 | 1632 | " | " | 0.00184 | 5390 | 2560 | 3.16 | " |
| PB-42B | " | " | " | " | " | " | " | " | 5000 | 3280 | 2.94 | " |
| PB-41 | 0.0093 | " | 1.982 | 3.675 | 2910 | " | " | 0.00103 | 1000 | 818 | 2.40 | " |
| PB-41B | " | " | " | " | " | " | " | " | " | " | 2.40 | " |
| PB-2 | 0.0200 | 6.5 | 4.284 | 7.120 | 1354 | 0.240 | 0.72 | 0.00221 | 7630 | 3230 | 3.01 | 0.72 |
| PB-2B | " | " | " | " | " | " | " | " | 8000 | 3480 | 3.24 | " |
| PB-20 | 0.0207 | " | 4.430 | 7.370 | 1309 | " | " | 0.00229 | 8800 | 3600 | 3.19 | " |
| PB-20B | " | " | " | " | " | " | " | " | 10400 | 4250 | 3.76 | " |
| PB-13 | 0.0175 | " | 3.745 | 6.549 | 1549 | " | " | 0.00194 | 3900 | 1750 | 2.00 | " |
| PB-13B | " | " | " | " | " | " | " | " | 4800 | 2210 | 2.52 | " |
| PB-22 | 0.0179 | " | 3.830 | 6.724 | 1513 | " | " | 0.00198 | 3800 | 1700 | 1.87 | " |
| PB-22B | " | " | " | " | " | " | " | " | 5900 | 2640 | 2.91 | " |
| PB-12 | 0.0103 | " | 2.195 | 3.978 | 2625 | " | " | 0.00114 | 1350 | 1020 | 2.57 | " |
| PB-12B | " | " | " | " | " | " | " | " | 1200 | 907 | 2.29 | " |
| PB-8 | 0.0199 | 2.5 | 4.262 | 7.298 | 1361 | 0.092 | 0.28 | 0.00220 | 7400 | 3050 | 2.87 | 0.28 |
| PB-8B | " | " | " | " | " | " | " | " | 8450 | 3480 | 3.27 | " |
| PB-29 | 0.0200 | " | 4.284 | 7.200 | 1355 | " | " | 0.00221 | 7650 | 3210 | 2.99 | " |
| PB-29B | " | " | " | " | " | " | " | " | 7250 | 3040 | 2.83 | " |
| PB-51 | 0.0158 | " | 3.375 | 6.154 | 1714 | " | " | 0.00175 | 3110 | 1520 | 2.02 | " |
| PB-51B | " | " | " | " | " | " | " | " | 2890 | 1410 | 1.87 | " |
| PB-50 | 0.0095 | 2.5 | 2.025 | 3.733 | 2848 | 0.092 | 0.28 | 0.00105 | 2170 | 1750 | 4.97 | " |
| PB-50B | " | " | " | " | " | " | " | " | 1430 | 1150 | 3.27 | " |
| PB-36 | 0.0212 | 1.0 | 4.544 | 7.532 | 1279 | 0.037 | 0.11 | 0.00235 | 16550 | 6620 | 5.66 | 0.11 |
| PB-36B | " | " | " | " | " | " | " | " | 16880 | 6750 | 5.78 | " |
| PB-45 | 0.0159 | " | 3.395 | 6.295 | 1703 | " | " | 0.00176 | 13000 | 6220 | 8.18 | " |
| PB-47 | 0.0092 | " | 1.961 | 3.661 | 2940 | " | " | 0.00102 | 2700 | 2220 | 6.63 | " |

TABLE IX

Bending Plus Torsion Tests
$\mathcal{E} = 1.0$  $E = 10.3 \times 10^6$ psi
$A = 40.5$ sq.in., $L = 12.5$ in.

| Spec. No. | $t_s$ in. | $t_c$ in. | $I_s$ in.$^4$ | $I_t$ in.$^4$ | $m_b$ in.lb. | $m_{t_b}$ in.lb. | $m_u$ in.lb. | $m_{t_u}$ in.lb. | $\sigma_b$ psi. | $\tau_b$ psi. | $\sigma_u$ psi. | $\tau_u$ psi. | $\sigma_{b_o}$ psi. | $\sigma_b/\sigma_{b_o}$ | $\sigma_u/\sigma_{u_o}$ | $\tau_{b_o}$ psi. | $\tau_{u_o}$ psi. | $\tau_b/\tau_{b_o}$ | $\tau_u/\tau_{u_o}$ | $M_b$ in.lb. | $M_u$ in.lb. | $M_b/m_{t_b}$ | $M_u/m_{t_u}$ |
|---|---|---|---|---|---|---|---|---|---|---|---|---|---|---|---|---|---|---|---|---|---|---|---|
| BT-1 | 0.0196 | 0.0322 | 1.679 | 4.590 | 10800 | 11100 | 10800 | 11100 | 7080 | 6990 | 7080 | 6990 | 14030 | 0.504 | 0.504 | 8360 | 8360 | 0.836 | 0.836 | 3960 | 3960 | 0.332 | 0.332 |
| -3 | 0.0193 | 0.0321 | 1.654 | 4.548 | 9600 | 9850 | 10600 | 10100 | 6350 | 6300 | 7020 | 6460 | 13750 | 0.462 | 0.462 | 8100 | 8100 | 0.778 | 0.798 | 3490 | 3860 | 0.354 | 0.382 |
| -5 | 0.0193 | 0.0321 | 1.653 | 4.548 | 18000 | 9000 | 19350 | 9850 | 11920 | 6760 | 12800 | 6290 | 13750 | 0.866 | 0.931 | 8100 | 8100 | 0.711 | 0.777 | 6540 | 7030 | 0.727 | 0.714 |
| -7 | 0.0174 | 0.0319 | 1.489 | 4.312 | 9200 | 9200 | 9200 | 9200 | 6420 | 6520 | 6420 | 6520 | 11700 | 0.549 | 0.549 | 7580 | 7580 | 0.855 | 0.855 | 3170 | 3170 | 0.345 | 0.345 |
| -9 | 0.0173 | 0.0317 | 1.481 | 4.286 | 9000 | 9000 | 9850 | 9800 | 6320 | 6420 | 6920 | 7000 | 11650 | 0.542 | 0.594 | 7490 | 7490 | 0.857 | 0.934 | 3100 | 3410 | 01346 | 0.348 |
| -9B | 0.0172 | 0.0316 | 1.472 | 4.267 | 8600 | 8850 | 10000 | 10000 | 6060 | 6210 | 7050 | 7180 | 11600 | 0.522 | 0.608 | 7410 | 7410 | 0.838 | 0.969 | 2970 | 3450 | 0.344 | 0.345 |
| -26 | 0.0206 | 0.0321 | 1.765 | 4.698 | 18000 | 9000 | 18000 | 9000 | 11540 | 5390 | 11540 | 5390 | 15230 | 0.757 | 0.757 | 8940 | 8940 | 0.603 | 0.603 | 6760 | 6760 | 0.753 | 0.753 |
| -28 | 0.0205 | 0.0321 | 1.756 | 4.686 | 6800 | 13300 | 6800 | 13300 | 4370 | 8000 | 4370 | 8000 | 14970 | 0.292 | 0.292 | 8860 | 8860 | 0.903 | 0.903 | 2550 | 2550 | 0.192 | 0.192 |
| -28B | 0.0200 | 0.0320 | 1.714 | 4.622 | 6100 | 12300 | 6100 | 12300 | 3980 | 7560 | 3980 | 7550 | 14570 | 0.273 | 0.273 | 8430 | 8430 | 0.897 | 0.897 | 2260 | 2260 | 0.184 | 0.184 |
| -30 | 0.0206 | 0.0320 | 1.765 | 4.691 | 6600 | 13200 | 6600 | 13200 | 4250 | 7850 | 4250 | 7850 | 15230 | 0.279 | 0.279 | 8940 | 8940 | 0.931 | 0.931 | 2480 | 2480 | 0.188 | 0.188 |
| -32 | 0.0165 | 0.0321 | 1.411 | 4.219 | 4000 | 7600 | 5000 | 10000 | 2850 | 5720 | 3550 | 7540 | 10900 | 0.261 | 0.327 | 7180 | 7180 | 0.797 | 1.050 | 1340 | 1670 | 0.176 | 0.167 |
| -34 | 0.0168 | 0.0317 | 1.436 | 4.225 | 4400 | 8500 | 4600 | 9200 | 3140 | 6250 | 3280 | 6780 | 11160 | 0.281 | 0.294 | 7440 | 7440 | 0.840 | 0.911 | 1500 | 1500 | 0.176 | 0.169 |
| -36 | 0.0169 | 0.0318 | 1.445 | 4.244 | 13000 | 6400 | 13900 | 6850 | 9210 | 4670 | 9900 | 5000 | 11240 | 0.820 | 0.881 | 7520 | 7520 | 0.622 | 0.666 | 4430 | 4730 | 0.693 | 0.690 |
| -37 | 0.0166 | 0.0318 | 1.419 | 4.209 | 14300 | 7200 | 16450 | 8400 | 10280 | 5360 | 11750 | 6260 | 11060 | 0.929 | 1.061 | 7260 | 7260 | 0.738 | 0.862 | 4820 | 5550 | 0.669 | 0.661 |
| -38 | 0.0100 | 0.0196 | 0.852 | 2.562 | 1100 | 2270 | 1600 | 3200 | 1290 | 2810 | 1880 | 3960 | 5120 | 0.252 | 0.367 | 3950 | 3950 | 0.712 | 1.001 | 336 | 532 | 0.161 | 0.166 |
| -40 | 0.0099 | 0.0206 | 0.844 | 2.623 | 2800 | 2730 | 3000 | 3000 | 3210 | 3410 | 3450 | 3750 | 5060 | 0.635 | 0.682 | 3870 | 3870 | 0.882 | 0.969 | 900 | 965 | 0.330 | 0.321 |
| -42 | 0.0099 | 0.0208 | 0.844 | 2.637 | 2400 | 1200 | 4590 | 2300 | 2740 | 1500 | 5240 | 2880 | 5060 | 0.542 | 1.035 | 3870 | 3870 | 0.388 | 0.744 | 768 | 1470 | 0.640 | 0.640 |
| -49 | 0.0212 | 0.0329 | 1.819 | 4.859 | 2800 | 13500 | 2800 | 13500 | 1740 | 7850 | 1740 | 7850 | 15840 | 0.110 | 0.110 | 8880 | 8880 | 0.884 | 0.884 | 1040 | 1040 | 0.077 | 0.077 |
| -51 | 0.0210 | 0.0322 | 1.801 | 4.761 | 21600 | 5500 | 22850 | 5900 | 13660 | 3220 | 14400 | 3490 | 15850 | 0.873 | 0.920 | 8710 | 8710 | 0.370 | 0.401 | 8180 | 8640 | 1.487 | 1.465 |
| -53 | 0.0210 | 0.0326 | 1.801 | 4.782 | 21000 | 3500 | 28900 | 4960 | 13230 | 2050 | 18110 | 2910 | 15850 | 0.844 | 1.158 | 8710 | 8710 | 0.235 | 0.334 | 7910 | 10690 | 2.260 | 2.198 |
| -55 | 0.0204 | 0.0324 | 1.750 | 4.703 | 18000 | 1800 | 27700 | 2780 | 11520 | 1080 | 17750 | 1660 | 14880 | 0.774 | 1.192 | 8780 | 8780 | 0.123 | 0.189 | 6690 | 10300 | 3.715 | 3.708 |
| -57 | 0.0170 | 0.0320 | 1.458 | 4.278 | 1885 | 9400 | 1895 | 9400 | 1330 | 6830 | 1375 | 6830 | 11290 | 0.118 | 0.122 | 7620 | 7620 | 0.896 | 0.896 | 646 | 649 | 0.069 | 0.069 |
| -59 | 0.0169 | 0.0316 | 1.448 | 4.243 | 14000 | 3500 | 14980 | 3620 | 9940 | 2550 | 10640 | 2640 | 11200 | 0.887 | 0.949 | 7530 | 7530 | 0.340 | 0.351 | 4780 | 5110 | 1.366 | 1.411 |
| -72 | 0.0168 | 0.0314 | 1.438 | 4.205 | 13000 | 2240 | 19460 | 3050 | 9300 | 1650 | 13850 | 2240 | 11200 | 0.831 | 1.240 | 7440 | 7440 | 0.222 | 0.301 | 4440 | 6550 | 1.982 | 2.180 |
| -74 | 0.0167 | 0.0310 | 1.429 | 4.164 | 15190 | 3550 | 17850 | 4800 | 10980 | 2630 | 12930 | 3550 | 11120 | 0.986 | 1.161 | 7350 | 7350 | 0.358 | 0.483 | 5200 | 6120 | 1.465 | 1.275 |
| -76 | 0.0104 | 0.0195 | 0.887 | 2.599 | 4800 | 1460 | 6510 | 1670 | 5550 | 1740 | 7550 | 2010 | 5470 | 1.016 | 1.380 | 4210 | 4210 | 0.413 | 0.477 | 1640 | 2220 | 1.124 | 1.328 |
| -78 | 0.0099 | 0.0196 | 0.845 | 2.554 | 500 | 2500 | 900 | 4800 | 590 | 3130 | 1060 | 5930 | 5210 | 0.113 | 0.204 | 3880 | 3880 | 0.806 | 1.450 | 165 | 296 | 0.066 | 0.066 |
| -80 | 0.0105 | 0.0202 | 0.895 | 2.663 | 4800 | 800 | 6320 | 1170 | 5420 | 940 | 7130 | 1380 | 5530 | 0.980 | 1.290 | 4290 | 4290 | 0.219 | 0.322 | 1610 | 2120 | 2.013 | 1.810 |
| -82 | 0.0106 | 0.0206 | 0.904 | 2.704 | 4800 | 510 | 6290 | 600 | 5330 | 600 | 6990 | 700 | 5510 | 0.950 | 1.245 | 4370 | 4370 | 0.137 | 0.160 | 1600 | 2100 | 3.16 | 3.50 |
| -84 | 0.0193 | 0.0316 | 1.653 | 4.513 | 13550 | 14000 | 13550 | 14000 | 9040 | 8950 | 9040 | 8950 | 13750 | 0.658 | 0.658 | 6820 | 6820 | 1.311 | 1.311 | 4960 | 4960 | 0.354 | 0.354 * |
| -84B | 0.0193 | 0.0316 | 1.653 | 4.513 | 10670 | 10700 | 10910 | 10000 | 7140 | 6840 | 7310 | 6840 | 13750 | 0.519 | 0.532 | 6820 | 6820 | 1.004 | 1.004 | 3910 | 3910 | 0.399 | 0.399 * |
| -87 | 0.0195 | 0.0315 | 1.672 | 4.532 | 15470 | 15550 | 15470 | 15550 | 10290 | 9840 | 10290 | 9840 | 14040 | 0.733 | 0.733 | 6580 | 6580 | 1.495 | 2.131 | 5710 | 5710 | 0.367 | 0.367 ** |
| -87B | 0.0195 | 0.0315 | 1.672 | 4.532 | 14180 | 14400 | 14180 | 14400 | 9920 | 9160 | 9420 | 9100 | 14040 | 0.671 | 0.671 | 6580 | 6580 | 1.382 | 1.382 | 5230 | 5230 | 0.363 | 0.363 ** |

* L = 6.5"
** L = 2.5"

TABLE X

Bending Plus Torsion Tests
$\mathcal{E}$ = 2.0 E = 10.3 x $10^6$ psi
A = 68.9 L = 12.5 in.

| Spec. No. | $t_s$ in. | $t_c$ in. | $I_s$ $in^4$ | $I_t$ $in^4$ | $m_b$ in. lb. | $m_{t_b}$ in. lb. | $m_u$ in. lb. | $m_{t_u}$ in. lb. | $\sigma_b$ psi | $\tau_b$ psi | $\sigma_u$ psi | $\tau_u$ psi | $\sigma_{b_0}$ psi | $\tau_{b_0}$ psi | $\tau_{u_0}$ psi | $\sigma_b/\sigma_{b_0}$ | $\sigma_u/\sigma_{b_0}$ | $\tau_b/\tau_{b_0}$ | $\tau_u/\tau_{u_0}$ | $M_b$ in. lb. | $M_u$ in. lb. | $M_b/m_{t_b}$ | $M_u/m_{t_u}$ | $\frac{1}{\mathcal{E}}\frac{\sigma_u}{\sigma_{b_0}}$ |
|---|---|---|---|---|---|---|---|---|---|---|---|---|---|---|---|---|---|---|---|---|---|---|---|---|
| BT-2 | 0.0196 | 0.0321 | 2.939 | 5.842 | 6400 | 6500 | 13000 | 13000 | 3300 | 2420 | 6890 | 4840 | 5300 | 3540 | 5550 | 0.622 | 1.300 | 0.684 | 0.869 | 3220 | 6530 | 0.495 | 0.502 | 0.650 |
| -4 | 0.0195 | 0.0319 | 2.924 | 5.810 | 6000 | 6000 | 12000 | 11820 | 3100 | 2120 | 6250 | 4250 | 5290 | 3510 | 5510 | 0.586 | 1.181 | 0.604 | 0.772 | 3020 | 6040 | 0.504 | 0.590 | 0.590 |
| -6 | 0.0194 | 0.0319 | 2.909 | 5.792 | 7200 | 3700 | 15700 | 8000 | 3740 | 1380 | 8160 | 3000 | 5250 | 3470 | 5460 | 0.712 | 1.554 | 0.398 | 0.549 | 3620 | 7880 | 0.979 | 0.984 | 0.777 |
| -8 | 0.0175 | 0.0320 | 2.621 | 5.454 | 6800 | 6700 | 10500 | 10450 | 3750 | 2780 | 5680 | 4340 | 4270 | 2930 | 5040 | 0.878 | 1.330 | 0.950 | 0.862 | 3270 | 4960 | 0.488 | 0.478 | 0.665 |
| -10 | 0.0178 | 0.0319 | 2.666 | 5.501 | 6600 | 7000 | 11000 | 11000 | 3610 | 2860 | 6020 | 4460 | 4400 | 3030 | 5220 | 0.820 | 1.367 | 0.945 | 0.854 | 3190 | 5330 | 0.456 | 0.484 | 0.684 |
| -12 | 0.0209 | 0.0320 | 3.134 | 6.068 | 6000 | 5000 | 19800 | 9700 | 2980 | 1740 | 9850 | 3390 | 5590 | 3900 | 6040 | 0.533 | 1.761 | 0.446 | 0.561 | 3100 | 10230 | 0.620 | 1.054 | 0.880 |
| -14 | 0.0206 | 0.0321 | 3.119 | 6.057 | 4000 | 8000 | 7400 | 15400 | 1990 | 2800 | 3680 | 5400 | 5560 | 3850 | 5980 | 0.356 | 0.662 | 0.729 | 0.904 | 2060 | 3810 | 0.258 | 0.333 | 0.331 |
| -16 | 0.0206 | 0.0316 | 3.089 | 5.986 | 4000 | 8000 | 7700 | 15100 | 2010 | 2840 | 3880 | 5320 | 5470 | 3780 | 5860 | 0.367 | 0.709 | 0.751 | 0.909 | 2060 | 3970 | 0.258 | 0.263 | 0.354 |
| -18 | 0.0169 | 0.0317 | 2.531 | 5.325 | 4000 | 2000 | 16000 | 8000 | 2260 | 860 | 9040 | 3440 | 4070 | 2810 | 4890 | 0.555 | 2.220 | 0.305 | 0.704 | 1900 | 7600 | 0.950 | 0.950 | 1.110 |
| -20 | 0.0169 | 0.0319 | 2.531 | 5.339 | 6000 | 3000 | 15500 | 7650 | 3380 | 1300 | 8800 | 3310 | 4070 | 2810 | 4890 | 0.830 | 2.160 | 0.463 | 0.676 | 2850 | 7400 | 0.950 | 0.966 | 1.080 |
| -22 | 0.0167 | 0.0313 | 2.501 | 5.260 | 2800 | 5550 | 5550 | 10950 | 1605 | 2480 | 3240 | 4790 | 4000 | 2750 | 4780 | 0.401 | 0.810 | 0.903 | 1.001 | 1330 | 2690 | 0.235 | 0.246 | 0.405 |
| -24 | 0.0172 | 0.0318 | 2.576 | 5.386 | 3000 | 6000 | 6200 | 12600 | 1680 | 2520 | 3480 | 5320 | 4170 | 2920 | 4880 | 0.405 | 0.835 | 0.862 | 1.090 | 1430 | 2960 | 0.238 | 0.235 | 0.418 |
| -39 | 0.0099 | 0.0209 | 1.477 | 3.278 | 600 | 1200 | 2000 | 3890 | 550 | 880 | 1840 | 2860 | 1680 | 1480 | 2580 | 0.328 | 1.095 | 0.595 | 1.109 | 270 | 900 | 0.225 | 0.231 | 0.547 |
| -43 | 0.0101 | 0.0209 | 1.507 | 3.313 | 1800 | 860 | 5900 | 2860 | 1640 | 610 | 5360 | 2060 | 1870 | 1540 | 2600 | 0.877 | 2.869 | 0.396 | 0.793 | 820 | 2680 | 0.954 | 0.938 | 1.434 |
| -45 | 0.0101 | 0.0204 | 1.507 | 3.277 | 1710 | 860 | 6020 | 3070 | 1580 | 620 | 5540 | 2200 | 1870 | 1540 | 2600 | 0.845 | 2.962 | 0.403 | 0.846 | 790 | 2770 | 0.918 | 0.902 | 1.481 |
| -61 | 0.0207 | 0.0320 | 3.100 | 6.035 | 1600 | 8000 | 3400 | 16250 | 800 | 2800 | 1700 | 5700 | 5480 | 3800 | 6360 | 0.146 | 0.310 | 0.737 | 0.896 | 820 | 1750 | 0.102 | 0.108 | 0.155 |
| -63 | 0.0207 | 0.0321 | 3.100 | 6.058 | 10150 | 2110 | 24000 | 6100 | 5060 | 740 | 12020 | 2140 | 5480 | 3800 | 6360 | 0.924 | 2.193 | 0.194 | 0.336 | 5210 | 12310 | 2.465 | 2.020 | 1.096 |
| -65 | 0.0207 | 0.0322 | 3.100 | 6.042 | 9000 | 1500 | 24950 | 4340 | 4500 | 530 | 12450 | 1520 | 5480 | 3800 | 6360 | 0.821 | 2.271 | 0.139 | 0.239 | 4620 | 12810 | 3.082 | 2.955 | 1.136 |
| -66 | 0.0207 | 0.0323 | 3.100 | 6.058 | 7000 | 700 | 27600 | 2780 | 3480 | 240 | 13700 | 970 | 5480 | 3800 | 6360 | 0.635 | 2.500 | 0.063 | 0.182 | 3580 | 14100 | 5.110 | 5.070 | 1.250 |
| -69 | 0.0169 | 0.0311 | 2.523 | 5.273 | 1600 | 8000 | 2600 | 13200 | 920 | 4310 | 1480 | 5580 | 4070 | 2810 | 4890 | 0.226 | 0.364 | 1.532 | 1.160 | 770 | 1240 | 0.096 | 0.094 | 0.182 |
| -71 | 0.0101 | 0.0205 | 1.509 | 3.288 | 500 | 2500 | 1000 | 4700 | 460 | 1810 | 920 | 3400 | 1870 | 1540 | 2600 | 0.225 | 0.492 | 1.175 | 1.309 | 230 | 460 | 0.092 | 0.098 | 0.246 |
| -73 | 0.0103 | 0.0205 | 1.538 | 3.321 | 1600 | 400 | 7510 | 1670 | 1460 | 280 | 6800 | 1180 | 1920 | 1570 | 2720 | 0.760 | 3.540 | 0.178 | 0.434 | 740 | 3480 | 1.850 | 2.080 | 1.770 |
| -77 | 0.0170 | 0.0315 | 2.543 | 5.325 | 8140 | 1120 | 21000 | 3500 | 4620 | 490 | 11860 | 1490 | 4100 | 2850 | 4760 | 1.126 | 2.892 | 0.172 | 0.313 | 3890 | 10050 | 3.470 | 2.865 | 1.446 |
| -83 | 0.0170 | 0.0312 | 2.543 | 5.306 | 5000 | 500 | 23020 | 2270 | 2850 | 210 | 13100 | 970 | 4110 | 2850 | 4760 | 0.694 | 3.189 | 0.074 | 0.024 | 2400 | 11050 | 4.800 | 4.865 | 1.594 |
| -85 | 0.0196 | 0.0321 | 2.935 | 5.840 | 8000 | 8000 | 12000 | 12000 | 4140 | 2960 | 6200 | 4440 | 5120 | 6560 | 8060 | 0.768 | 1.150 | 0.452 | 0.551 | 4020 | 6030 | 0.503 | 0.502 | 0.575 * |
| -85A | 0.0190 | 0.0321 | 2.935 | 5.840 | 7680 | 8000 | 16100 | 16050 | 3960 | 2960 | 8340 | 5960 | 4890 | 6240 | 7740 | 0.810 | 1.705 | 0.474 | 0.770 | 3860 | 8090 | 0.483 | 0.504 | 0.852 * |
| -88 | 0.0194 | 0.0318 | 2.905 | 5.785 | 10000 | 10000 | 16000 | 16000 | 5220 | 3740 | 8370 | 5950 | 5420 | 7440 | 11150 | 0.963 | 1.555 | 0.503 | 0.534 | 5020 | 8040 | 0.502 | 0.502 | 0.778 ** |
| -88A | 0.0194 | 0.0318 | 2.905 | 5.785 | 8980 | 8850 | 13360 | 19500 | 4640 | 3300 | 10150 | 7250 | 5420 | 8050 | 12390 | 0.856 | 1.873 | 0.411 | 0.585 | 4510 | 9740 | 0.510 | 0.499 | 0.936 ** |

* L = 6.5"
** L = 2.5"

TABLE XI
Bending Plus Torsion Tests
$\varepsilon = 3.0$ $E = 10.3 \times 10^6$ psi
$A = 97.4$ sq.in., $L = 12.5$ in.

| Spec. No. | $t_s$ in. | $t_c$ in. | $I_s$ in.$^4$ | $I_t$ in.$^4$ | $m_b$ in.lb. | $m_{t_b}$ in.lb. | $m_u$ in.lb. | $m_{t_u}$ in.lb. | $\sigma_b$ psi | $\tau_b$ psi | $\sigma_u$ psi | $\tau_u$ psi | $\sigma_{b_0}$ psi | $\sigma_b/\sigma_{b_0}$ | $\sigma_u/\sigma_{u_0}$ | $\tau_{b_0}$ psi | $\tau_{u_0}$ psi | $\tau_b/\tau_{b_0}$ | $\tau_u/\tau_{u_0}$ | $M_b$ in.lb. | $M_u$ in.lb. | $M_b/m_{t_b}$ | $M_u/m_{t_u}$ | $\frac{1}{\varepsilon}\frac{\sigma_u}{\sigma_{b_0}}$ | |
|---|---|---|---|---|---|---|---|---|---|---|---|---|---|---|---|---|---|---|---|---|---|---|---|---|---|
| BT-11 | 0.0197 | 0.0318 | 4.219 | 7.104 | 4650 | 4900 | 15700 | 15600 | 1970 | 1280 | 6650 | 4040 | 2820 | 0.699 | 2.358 | 1920 | 4600 | 0.666 | 0.878 | 2760 | 9330 | 0.564 | 0.598 | 0.786 | |
| -13 | 0.0193 | 0.0318 | 4.134 | 7.007 | 5000 | 4850 | 15700 | 15650 | 2150 | 1280 | 6750 | 4150 | 2730 | 0.788 | 2.472 | 1890 | 4540 | 0.677 | 0.914 | 2940 | 9250 | 0.606 | 0.591 | 0.824 | |
| -15 | 0.0202 | 0.0316 | 4.327 | 7.212 | 5850 | 3000 | 22000 | 11000 | 2450 | 760 | 9190 | 2790 | 2920 | 0.839 | 3.147 | 1960 | 4700 | 0.388 | 0.594 | 3510 | 13200 | 1.170 | 1.200 | 1.049 | |
| -17 | 0.0206 | 0.0317 | 4.412 | 7.316 | 4200 | 2100 | 20000 | 10000 | 1740 | 550 | 8250 | 2480 | 3010 | 0.578 | 2.754 | 2010 | 4750 | 0.264 | 0.522 | 2650 | 12080 | 1.204 | 1.208 | 0.911 | |
| -19 | 0.0206 | 0.0319 | 4.412 | 7.331 | 3600 | 7850 | 9000 | 17700 | 1480 | 1950 | 3700 | 4400 | 3010 | 0.492 | 1.229 | 2010 | 4750 | 0.970 | 0.926 | 2160 | 5450 | 0.276 | 0.307 | 0.410 | |
| -19A | 0.0204 | 0.0322 | 4.369 | 7.304 | 3400 | 7100 | 8650 | 17100 | 1400 | 1780 | 3550 | 4280 | 2960 | 0.473 | 1.199 | 1970 | 4660 | 0.904 | 0.918 | 2030 | 5170 | 0.286 | 0.303 | 0.400 | |
| -21 | 0.0198 | 0.0317 | 4.241 | 7.122 | 3000 | 6000 | 8250 | 16850 | 1270 | 1510 | 3480 | 4260 | 2830 | 0.449 | 1.230 | 1940 | 4650 | 0.778 | 0.916 | 1790 | 4910 | 0.298 | 0.292 | 0.410 | |
| -23 | 0.0178 | 0.0317 | 3.809 | 6.629 | 2500 | 1600 | 13200 | 13200 | 1140 | 460 | 6020 | 3820 | 2420 | 0.471 | 2.488 | 2220 | 5490 | 0.207 | 0.696 | 1440 | 7590 | 0.900 | 0.575 | 0.829 | |
| -25 | 0.0166 | 0.0308 | 3.548 | 8.266 | 2000 | 4000 | 7400 | 15000 | 960 | 1240 | 3560 | 4650 | 2180 | 0.440 | 1.633 | 1560 | 3810 | 0.795 | 1.220 | 1130 | 4180 | 0.283 | 0.279 | 0.544 | |
| -27 | 0.0174 | 0.0318 | 3.725 | 6.539 | 2000 | 4000 | 7650 | 15050 | 920 | 1180 | 3540 | 4450 | 2330 | 0.395 | 1.519 | 1680 | 4090 | 0.702 | 1.088 | 1140 | 4560 | 0.285 | 0.289 | 0.508 | |
| -29 | 0.0173 | 0.0315 | 3.702 | 6.492 | 2800 | 2900 | 12650 | 12600 | 1300 | 860 | 5900 | 3750 | 2310 | 0.563 | 2.554 | 1660 | 4040 | 0.518 | 0.928 | 1600 | 7210 | 0.561 | 0.572 | 0.851 | |
| -31 | 0.0175 | 0.0319 | 3.744 | 6.570 | 4000 | 2000 | 17700 | 8800 | 1840 | 590 | 9120 | 2590 | 2350 | 0.783 | 3.455 | 1700 | 4140 | 0.347 | 0.623 | 2280 | 10090 | 1.140 | 1.146 | 1.152 | |
| -33 | 0.0170 | 0.0321 | 3.638 | 6.463 | 2000 | 1030 | 18400 | 9200 | 930 | 310 | 8510 | 2790 | 2260 | 0.412 | 3.765 | 1620 | 4000 | 0.191 | 0.698 | 1120 | 10340 | 1.089 | 1.126 | 1.256 | |
| -44 | 0.0099 | 0.0206 | 2.110 | 3.890 | 700 | 1400 | 2370 | 4720 | 540 | 730 | 1840 | 2440 | 1000 | 0.540 | 1.840 | 840 | 2070 | 0.869 | 1.179 | 380 | 1290 | 0.272 | 0.273 | 0.613 | |
| -46 | 0.0100 | 0.0202 | 2.131 | 3.884 | 900 | 900 | 3800 | 3800 | 710 | 460 | 2960 | 1960 | 1020 | 0.696 | 2.902 | 860 | 2110 | 0.535 | 0.929 | 490 | 2080 | 0.545 | 0.548 | 0.967 | |
| -47 | 0.0098 | 0.0203 | 2.089 | 3.843 | 1260 | 640 | 4320 | 2220 | 990 | 340 | 3370 | 1150 | 990 | 1.000 | 3.404 | 820 | 2020 | 0.415 | 0.589 | 690 | 2350 | 1.079 | 1.059 | 1.135 | |
| -48 | 0.0212 | 0.0318 | 4.550 | 7.469 | 1700 | 8500 | 3730 | 18100 | 690 | 2050 | 1510 | 4360 | 3140 | 0.220 | 0.481 | 2100 | 5040 | 0.976 | 0.865 | 1040 | 2280 | 0.123 | 0.126 | 0.160 | |
| -50 | 0.0211 | 0.0318 | 4.526 | 7.461 | 4000 | 1000 | 20000 | 5000 | 1620 | 240 | 8110 | 1220 | 3120 | 0.519 | 2.599 | 2080 | 4990 | 0.115 | 0.244 | 2430 | 12130 | 2.430 | 2.430 | 0.866 | |
| -52 | 0.0211 | 0.0326 | 4.526 | 7.509 | 7240 | 1190 | 20500 | 3500 | 2890 | 290 | 8080 | 850 | 3120 | 0.926 | 2.589 | 2080 | 4990 | 0.058 | 0.194 | 4360 | 12350 | 3.661 | 3.530 | 0.863 | |
| -54 | 0.0202 | 0.0327 | 4.330 | 7.295 | 3000 | 300 | 19040 | 2000 | 1240 | 80 | 7900 | 510 | 2920 | 0.426 | 2.705 | 1960 | 4700 | 0.041 | 0.108 | 1780 | 11310 | 5.940 | 5.660 | 0.902 | |
| -54A | 0.0202 | 0.0327 | 4.330 | 7.295 | 8000 | 800 | 24950 | 2500 | 3320 | 200 | 10310 | 640 | 2920 | 1.137 | 3.531 | 1960 | 4700 | 0.102 | 0.136 | 4750 | 14810 | 5.940 | 5.940 | 1.177 | |
| -56 | 0.0171 | 0.0319 | 3.657 | 6.477 | 1100 | 5500 | 2850 | 14200 | 510 | 1580 | 1520 | 4250 | 2270 | 0.225 | 0.581 | 1640 | 4050 | 1.024 | 1.052 | 620 | 1610 | 0.111 | 0.113 | 0.194 | |
| -58 | 0.0170 | 0.0312 | 3.633 | 6.393 | 1540 | 400 | 17800 | 2370 | 730 | 120 | 8410 | 1320 | 2260 | 0.323 | 3.721 | 1620 | 4000 | 0.074 | 0.330 | 870 | 10110 | 2.175 | 2.314 | 1.240 | |
| -60 | 0.0170 | 0.0319 | 3.633 | 6.452 | 3580 | 600 | 18600 | 3260 | 1670 | 180 | 8650 | 990 | 2260 | 0.739 | 3.827 | 1620 | 4000 | 0.111 | 0.248 | 2020 | 10480 | 3.365 | 3.215 | 1.276 | |
| -62 | 0.0168 | 0.0320 | 3.583 | 6.400 | 1340 | 250 | 20900 | 2200 | 630 | 80 | 9850 | 670 | 2210 | 0.285 | 4.457 | 1580 | 3900 | 0.051 | 0.172 | 750 | 11700 | 3.000 | 5.320 | 1.486 | |
| -64 | 0.0100 | 0.0205 | 2.131 | 3.906 | 450 | 2250 | 1000 | 5000 | 350 | 160 | 770 | 2570 | 1020 | 0.343 | 0.755 | 860 | 2110 | 1.345 | 1.218 | 250 | 550 | 0.111 | 0.110 | 0.252 | |
| -67 | 0.0100 | 0.0205 | 2.131 | 3.890 | 1200 | 300 | 6160 | 1750 | 930 | 160 | 4780 | 890 | 1020 | 0.912 | 4.686 | 860 | 2110 | 0.168 | 0.422 | 660 | 3380 | 2.200 | 1.952 | 1.562 | |
| -68 | 0.0099 | 0.0200 | 2.110 | 3.865 | 1500 | 250 | 7240 | 1230 | 1170 | 30 | 5640 | 640 | 1000 | 1.170 | 5.640 | 840 | 2070 | 0.155 | 0.309 | 820 | 3950 | 3.280 | 3.210 | 1.880 | |
| -70 | 0.0100 | 0.0100 | 2.131 | 3.870 | 1500 | 250 | 6690 | 900 | 1160 | 130 | 5180 | 460 | 1020 | 1.137 | 5.078 | 860 | 2110 | 0.151 | 0.218 | 1380 | 3680 | 5.520 | 4.090 | 1.693 | |
| -86 | 0.0193 | 0.0319 | 4.140 | 7.023 | 4000 | 4000 | 12000 | 12000 | 1720 | 1060 | 5180 | 3200 | 2730 | 0.630 | 1.896 | 2540 | 6000 | 0.417 | 0.534 | 2360 | 7070 | 0.590 | 0.589 | 0.632 | * |
| -86A | 0.0193 | 0.0319 | 4.140 | 7.023 | 6000 | 5200 | 17020 | 17300 | 2580 | 1390 | 7300 | 4620 | 2730 | 0.937 | 2.671 | 2540 | 6000 | 0.547 | 0.771 | 3500 | 10050 | 0.679 | 0.580 | 0.890 | * |
| -89 | 0.0195 | 0.0317 | 4.180 | 7.055 | 8000 | 8000 | 18000 | 18000 | 3440 | 2100 | 7750 | 4750 | 3510 | 0.980 | 2.200 | 5330 | 10020 | 0.394 | 0.474 | 4740 | 10660 | 0.593 | 0.593 | 0.733 | ** |
| -89A | 0.0195 | 0.0317 | 4.180 | 7.055 | 7000 | 7000 | 18410 | 24300 | 3000 | 1840 | 7900 | 6420 | 3510 | 0.858 | 2.249 | 5330 | 10020 | 0.346 | 0.640 | 4150 | 10890 | 0.593 | 0.592 | 0.750 | ** |

* L = 6.5"

** L = 2.5"

## TABLE XII

Bending Plus Direct Shear Tests

$\varepsilon = 1.0$ . $E = 10.3 \times 10^6$ psi

b = 3.01" = a, L = 6.5" except where noted

| Spec. No. | $t_s$ in. | $I_s$ $in^4$ | $I_t$ $in^4$ | $A_s$ sq.in. | $\ell$ in. | F lb. | $\frac{M}{Fb}$ | $\tau_b$ psi | $\sigma_b$ psi | $\sigma_{b_o}$ psi | $\frac{\sigma_b}{\sigma_{b_o}}$ |
|---|---|---|---|---|---|---|---|---|---|---|---|
| BS-10 | 0.0215 | 1.844 | 5.161 | 0.407 | 14.6 | 1570 | 1.737 | 3850 | 13390 | 16430 | 0.814 |
| -11 | " | " | " | " | 80.0 | 310 | 9.496 | 760 | 14410 | " | 0.877 |
| -11B | " | " | " | " | 80.0 | 270 | 9.496 | 660 | 12590 | " | 0.760 |
| -12 | " | " | 5.406 | " | 29.1 | 750 | 3.292 | 1840 | 12120 | " | 0.738 |
| -12B | " | " | 5.650 | " | 29.1 | 1170 | 3.150 | 3870 | 18140 | " | 1.104 |
| -13 | " | " | " | " | 38.3 | 640 | 4.153 | 1570 | 13050 | " | 0.784 |
| -13B | " | " | " | " | 38.3 | 820 | 4.153 | 2010 | 16710 | " | 1.019 |
| -15B | " | " | 5.650 | " | 53.1 | 610 | 5.752 | 1500 | 17230 | " | 1.049 |
| -16 | " | " | " | " | 4.9 | 2350 | 0.529 | 5760 | 6140 | " | 0.374 |
| -17 | 0.0165 | 1.411 | 5.089 | 0.312 | 4.9 | 960 | 0.451 | 3080 | 2780 | 11130 | 0.250 |
| -18 | " | " | " | " | 10.1 | 1140 | 0.931 | 3650 | 6810 | " | 0.611 |
| -19 | " | " | " | " | 14.6 | 1040 | 1.346 | 3330 | 8990 | " | 0.807 |
| -20 | 0.0220 | 1.887 | 5.204 | 0.416 | 10.1 | 2620 | 1.210 | 6300 | 15210 | 17050 | 0.891 |
| -21 | 0.0215 | 1.844 | 5.161 | 0.407 | 64.8 | 350 | 7.700 | 860 | 13220 | 16430 | 0.805 |
| -21B | " | " | " | " | 32.5 | 1050 | 3.865 | 2580 | 19900 | 16430 | 1.211 |
| -22 | 0.0165 | 1.411 | 5.089 | 0.312 | 10.1 | 1330 | 0.931 | 4260 | 7950 | 11130 | 0.714 |
| -23 | " | " | " | " | 79.8 | 300 | 7.360 | 960 | 14150 | " | 1.270 |
| -23B | " | " | " | " | 59.2 | 260 | 5.460 | 830 | 9100 | " | 0.816 |
| -24 | " | " | " | " | 38.4 | 380 | 3.540 | 1220 | 8630 | " | 0.774 |
| -24B | " | " | " | " | 38.4 | 340 | 3.540 | 1090 | 7730 | " | 0.694 |
| -25 | " | " | " | " | 36.1 | 690 | 3.330 | 2210 | 14710 | " | 1.320 |
| -64 | 0.0101 | 0.861 | 2.167 | 0.191 | 79.8 | 62 | 10.52 | 320 | 6870 | 5350 | 1.282 |
| -64B | " | " | " | " | " | 64 | 10.52 | 340 | 7100 | " | 1.327 |
| -65 | " | " | 2.624 | " | 59.4 | 98 | 6.47 | 510 | 6690 | " | 1.250 |
| -65B | " | " | " | " | " | 75 | 6.47 | 390 | 5110 | " | 0.955 |
| -66 | 0.0100 | 0.852 | 2.554 | 0.189 | 41.0 | 130 | 4.060 | 690 | 6290 | 5150 | 1.221 |
| -66B | " | " | " | " | " | 114 | " | 600 | 5510 | 5150 | 1.070 |
| -67 | 0.0103 | 0.878 | 2.611 | 0.194 | 29.6 | 200 | 3.250 | 1000 | 6830 | 5750 | 1.187 |
| -67B | " | " | " | " | " | 160 | " | 820 | 5460 | 5750 | 0.950 |
| -68 | 0.0100 | 0.852 | 2.583 | 0.189 | 19.8 | 310 | 2.170 | 1640 | 7150 | 5150 | 1.388 |
| -68B | " | " | " | " | " | 260 | " | 1370 | 5990 | 5150 | 1.162 |
| -69 | " | " | 2.590 | " | 9.9 | 310 | 1.081 | 1640 | 3570 | 5150 | 0.692 |
| -70 | 0.0101 | 0.861 | 2.617 | 0.191 | " | 350 | 1.084 | 1830 | 3990 | 5350 | 0.776 |
| * -57B | 0.0196 | 1.679 | 4.456 | 0.371 | 79.9 | 310 | 9.800 | 840 | 16420 | 14510 | 1.131 |
| * -58B | 0.0205 | 1.756 | 4.607 | 0.388 | 14.2 | 1690 | 1.790 | 4350 | 15650 | 15250 | 1.027 |
| * -59 | 0.0100 | 0.852 | 2.583 | 0.189 | 41.4 | 120 | 4.540 | 630 | 5790 | 5150 | 1.125 |
| * -59B | " | " | " | " | 19.9 | 300 | 2.185 | 1590 | 6950 | 5150 | 1.350 |

* L = 16.0 in.

TABLE XIII

Bending Plus Shear Tests

$\mathcal{E} = 2.0$ $E = 10.3 \times 10^6$ psi

b = 3.01 in. a = 6.02 in.

L = 6.5 in. except where noted

| Spec. No. | $t_s$ in. | $I_s$ $in^4$ | $I_t$ $in^4$ | $A_s$ sq.in. | $\ell$ in. | F lb. | $\frac{M}{Fb}$ | $\tau_b$ psi | $\sigma_b$ psi | $\sigma_{b_o}$ psi | $\frac{\sigma_b}{\sigma_{b_o}}$ |
|---|---|---|---|---|---|---|---|---|---|---|---|
| BS-37 | 0.0200 | 2.999 | 5.835 | 0.583 | 79.8 | 150 | 13.32 | 260 | 6180 | 5260 | 1.172 |
| -37B | " | " | " | " | " | 230 | " | 400 | 9360 | " | 1.780 |
| -38 | 0.0210 | 3.152 | 6.019 | 0.613 | 10.1 | 1510 | 1.76 | 2470 | 7670 | 5670 | 1.355 |
| -39 | " | " | " | " | 23.0 | 590 | 4.00 | 960 | 6710 | " | 1.183 |
| -39B | " | " | " | " | " | 780 | " | 1270 | 8870 | " | 1.565 |
| -40 | " | " | " | " | 35.6 | 400 | 6.18 | 650 | 7120 | " | 1.255 |
| -40B | " | " | " | " | " | 370 | " | 600 | 6590 | " | 1.161 |
| -41 | " | " | " | " | 50.4 | 340 | 8.76 | 560 | 8560 | " | 1.510 |
| -41B | " | " | " | " | 64.8 | 220 | 11.26 | 360 | 7140 | " | 1.529 |
| -41C | " | " | " | " | 4.9 | 1510 | 0.85 | 2460 | 3700 | " | 0.652 |
| -71 | 0.0104 | 1.552 | 3.266 | 0.303 | 8.0 | 370 | 1.26 | 1220 | 2760 | 1970 | 1.401 |
| -71B | " | " | " | " | 8.2 | 280 | 1.30 | 920 | 2140 | " | 1.087 |
| -73 | 0.0103 | 1.537 | 3.262 | 0.300 | 14.4 | 150 | 2.26 | 500 | 1990 | 1950 | 1.020 |
| -73B | " | " | " | " | " | 170 | " | 570 | 2020 | " | 1.035 |
| -74 | 0.0104 | 1.552 | 3.273 | 0.303 | 19.5 | 120 | 3.08 | 400 | 2150 | 1970 | 1.091 |
| -74B | " | " | " | " | " | 140 | " | 460 | 2510 | " | 1.272 |
| -76 | " | " | " | " | 28.9 | 140 | 4.53 | 460 | 3720 | " | 1.889 |
| -76B | " | " | " | " | " | 140 | " | 460 | 3720 | " | 1.889 |
| -78 | 0.0102 | 1.522 | 3.281 | 0.297 | 41.2 | 75 | 6.37 | 250 | 2830 | 1920 | 1.472 |
| -78B | " | " | " | " | " | 75 | " | 250 | 2830 | " | 1.472 |
| -80 | 0.0100 | 1.492 | 3.223 | 0.291 | 59.1 | 32 | 9.10 | 110 | 1770 | 1860 | 0.951 |
| -80B | " | " | " | " | " | 47 | " | 165 | 2590 | " | 1.391 |
| -82 | " | " | " | " | 79.8 | 35 | 12.26 | 120 | 2610 | " | 1.402 |
| -82B | " | " | " | " | " | 38 | " | 130 | 2830 | " | 1.510 |
| -84 | 0.0175 | 2.621 | 5.490 | 0.510 | 79.8 | 170 | 12.65 | 330 | 7440 | 4310 | 1.725 |
| -84B | " | " | " | " | " | 170 | " | 330 | 7440 | " | 1.725 |
| -86 | 0.0174 | 2.606 | 5.472 | 0.507 | 59.4 | 220 | 9.41 | 430 | 7190 | 4270 | 1.681 |
| -86B | " | " | " | " | " | 210 | " | 410 | 6860 | " | 1.605 |
| -87 | 0.0173 | 2.591 | 5.396 | 0.504 | 38.5 | 250 | 6.15 | 500 | 5380 | 4240 | 1.269 |
| -87B | " | " | " | " | " | 320 | " | 640 | 6880 | " | 1.621 |
| -89 | 0.0170 | 2.546 | 5.313 | 0.496 | 23.4 | 390 | 3.73 | 790 | 5160 | 4130 | 1.220 |
| -89B | " | " | " | " | " | 440 | " | 890 | 5830 | " | 1.378 |
| -91 | 0.0172 | 2.576 | 5.356 | 0.501 | 19.5 | 440 | 3.12 | 880 | 4820 | 4200 | 1.148 |
| -91B | " | " | " | " | " | 620 | " | 1240 | 6800 | " | 1.619 |
| -93 | " | " | " | " | 14.4 | 710 | 2.29 | 1420 | 5740 | " | 1.366 |
| -93B | " | " | " | " | " | 770 | " | 1540 | 6240 | " | 1.485 |
| -95 | " | " | " | " | 4.9 | 1080 | 0.77 | 2160 | 2970 | " | 0.707 |
| * -60 | 0.0199 | 2.984 | 5.889 | 0.580 | 24.6 | 620 | 4.14 | 1070 | 7790 | 5220 | 1.491 |
| * -60B | " | " | " | " | 14.5 | 880 | 2.44 | 1520 | 6530 | " | 1.250 |
| * -61 | 0.0099 | 1.477 | 3.205 | 0.288 | 29.0 | 95 | 4.44 | 370 | 2590 | 1830 | 1.415 |
| * -61B | " | " | " | " | 14.5 | 200 | 2.22 | 770 | 2720 | " | 1.486 |

* L = 16.0 in.

TABLE XIV

Bending Plus Direct Shear Tests

$\varepsilon = 3.0$, $E = 10.3 \times 10^6$ psi

b = 3.01 in., a = 9.03 in.

L = 6.5 in. except where noted

| Spec. No. | $t_s$ in. | $I_s$ $in^4$ | $I_t$ $in^4$ | $A_s$ sq.in. | $\ell$ in. | F lb. | $\frac{M}{Fb}$ | $\tau_b$ psi | $\sigma_b$ psi | $\sigma_{b_o}$ psi | $\frac{\sigma_b}{\sigma_{b_o}}$ |
|---|---|---|---|---|---|---|---|---|---|---|---|
| BS-34 | 0.0200 | 4.284 | 7.120 | 0.804 | 19.6 | 480 | 3.294 | 600 | 3970 | 2920 | 1.360 |
| -34B | " | " | " | " | " | 920 | " | 1150 | 7620 | " | 2.605 |
| -35 | " | " | " | " | 35.6 | 260 | 7.122 | 325 | 3920 | " | 1.341 |
| -35B | " | " | " | " | 68.9 | 110 | 13.78 | 135 | 3210 | " | 1.099 |
| -36 | " | " | " | " | 10.1 | 970 | 2.025 | 1210 | 4140 | " | 1.418 |
| -36B | " | " | " | " | " | 1520 | " | 1890 | 6490 | " | 2.220 |
| -56 | 0.0197 | 4.219 | 7.089 | 0.792 | 53.1 | 150 | 10.50 | 190 | 3380 | 2820 | 1.199 |
| -56B | " | " | " | " | 77.5 | 120 | 15.33 | 150 | 3920 | " | 1.390 |
| -72 | 0.0101 | 2.152 | 3.879 | 0.405 | 10.1 | 130 | 1.870 | 320 | 1020 | 1040 | 0.981 |
| -75 | 0.0105 | 2.238 | 3.955 | 0.421 | 19.5 | 110 | 3.670 | 260 | 1630 | 1100 | 1.469 |
| -75B | " | " | " | " | " | 100 | " | 240 | 1480 | " | 1.333 |
| -77 | 0.0104 | 2.216 | 3.952 | 0.417 | 23.4 | 100 | 4.363 | 240 | 1780 | 1090 | 1.631 |
| -77B | " | " | " | " | " | 74 | " | 175 | 1320 | " | 1.211 |
| -79 | " | " | " | " | 29.6 | 120 | 5.505 | 290 | 2710 | " | 2.485 |
| -79B | " | " | " | " | " | 81 | " | 195 | 1830 | " | 1.679 |
| -81 | 0.0101 | 2.152 | 3.886 | 0.405 | 47.4 | 48 | 8.732 | 120 | 1720 | 1040 | 1.652 |
| -81B | " | " | " | " | " | 41 | " | 100 | 1470 | " | 1.413 |
| -83 | 0.0100 | 2.131 | 3.891 | 0.401 | 59.4 | 87 | 10.84 | 215 | 4000 | 1030 | 2.880 |
| -83B | " | " | " | " | " | 53 | " | 130 | 2440 | " | 2.370 |
| -85 | 0.0104 | 2.216 | 3.980 | 0.417 | 79.8 | 97 | 14.79 | 230 | 5850 | 1090 | 5.360 |
| -85B | " | " | " | " | " | 46 | " | 110 | 2780 | " | 2.550 |
| -88 | 0.0178 | 3.809 | 6.636 | 0.715 | 79.8 | 90 | 15.22 | 125 | 3260 | 2480 | 1.312 |
| -88B | " | " | " | " | " | 90 | " | 125 | 3260 | " | 1.312 |
| -90 | 0.0170 | 3.638 | 6.405 | 0.683 | 59.3 | 120 | 11.20 | 175 | 3330 | 2270 | 1.466 |
| -90B | " | " | " | " | " | 100 | " | 145 | 2780 | " | 1.223 |
| -92 | 0.0175 | 3.745 | 6.549 | 0.703 | 38.5 | 145 | 7.315 | 205 | 2570 | 2370 | 1.083 |
| -92B | " | " | " | " | " | 185 | " | 265 | 3270 | " | 1.380 |
| -94 | 0.0179 | 3.830 | 6.660 | 0.719 | 29.6 | 215 | 5.662 | 300 | 2910 | 2460 | 1.181 |
| -94B | " | " | " | " | " | 295 | " | 410 | 3990 | " | 1.621 |
| -96 | 0.0175 | 3.745 | 6.572 | 0.703 | 19.5 | 385 | 3.694 | 550 | 3440 | 3280 | 1.445 |
| -96B | " | " | " | " | " | 370 | " | 530 | 3310 | " | 1.432 |
| -97 | 0.0173 | 3.702 | 6.485 | 0.695 | 14.3 | 470 | 2.715 | 680 | 3130 | 2340 | 1.338 |
| -97B | " | " | " | " | " | 370 | " | 530 | 2440 | " | 1.041 |
| -98 | " | " | " | " | 9.8 | 620 | 1.859 | 890 | 2820 | " | 1.203 |
| -98B | " | " | " | " | " | 680 | " | 980 | 3100 | " | 1.324 |
| * -28 | 0.0200 | 4.284 | 7.120 | 0.804 | 89.4 | 110 | 17.87 | 135 | 4160 | 2850 | 1.459 |
| * -28B | " | " | " | " | " | 95 | " | 120 | 3590 | " | 1.260 |
| * -29 | " | " | " | " | 19.6 | 670 | 3.924 | 840 | 5550 | " | 1.948 |
| * -29B | " | " | " | " | " | 430 | " | 540 | 3570 | " | 1.252 |
| * -30 | " | " | " | " | 35.6 | 330 | 7.122 | 410 | 4960 | " | 1.740 |
| * -30B | " | " | " | " | " | 330 | " | 410 | 4960 | " | 1.740 |
| * -31 | " | " | " | " | 47.9 | 230 | 9.583 | 290 | 4650 | " | 1.631 |
| * -32 | " | " | " | " | 68.9 | 145 | 13.77 | 180 | 4230 | " | 1.482 |
| * -33 | " | " | " | " | 53.8 | 115 | 10.74 | 145 | 2620 | " | 0.912 |
| * -33B | " | " | " | " | " | 195 | " | 245 | 4440 | " | 1.558 |
| * -62 | 0.0197 | 4.219 | 7.133 | 0.792 | 15.4 | 620 | 3.034 | 770 | 4030 | 2790 | 1.443 |
| * -63 | 0.0100 | 2.121 | 3.884 | 0.401 | 24.0 | 85 | 4.376 | 210 | 1580 | 1010 | 1.564 |

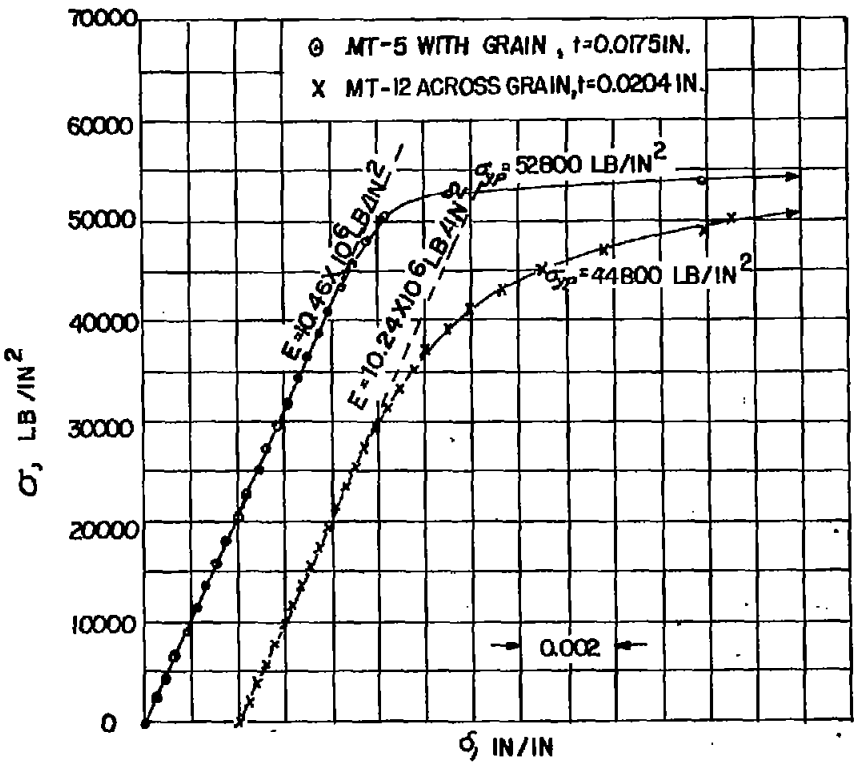


Figure 1.- Typical tensile stress-strain curves for 24S-T aluminum alloy sheet used in specimens.

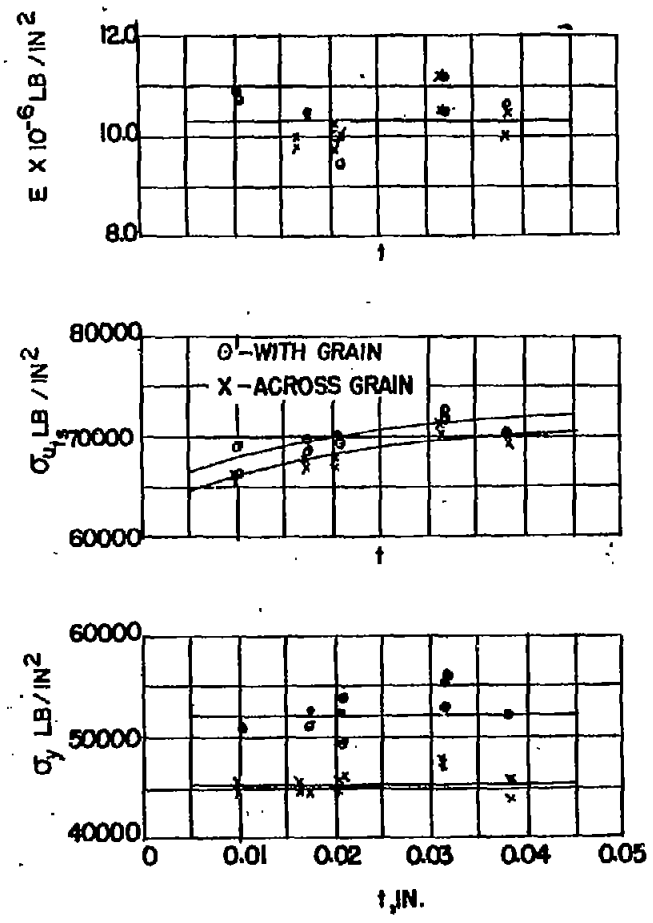


Figure 2.- Tensile properties of 24S-T aluminum alloy sheet used in specimens.

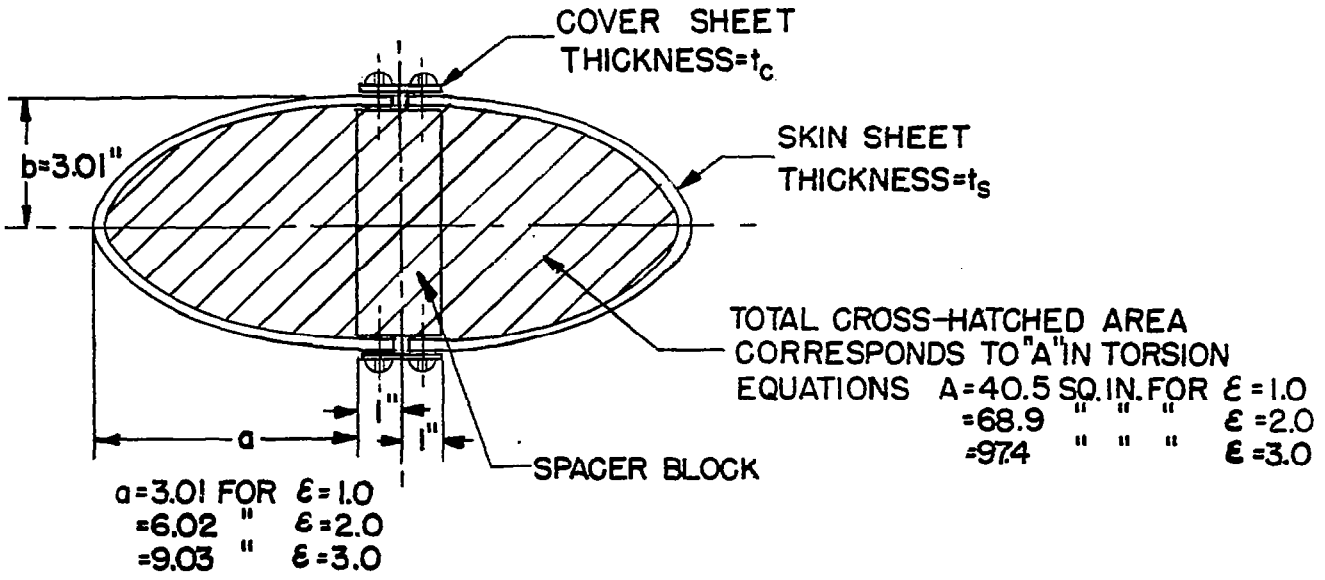


Figure 3a.- Cross section of specimen.

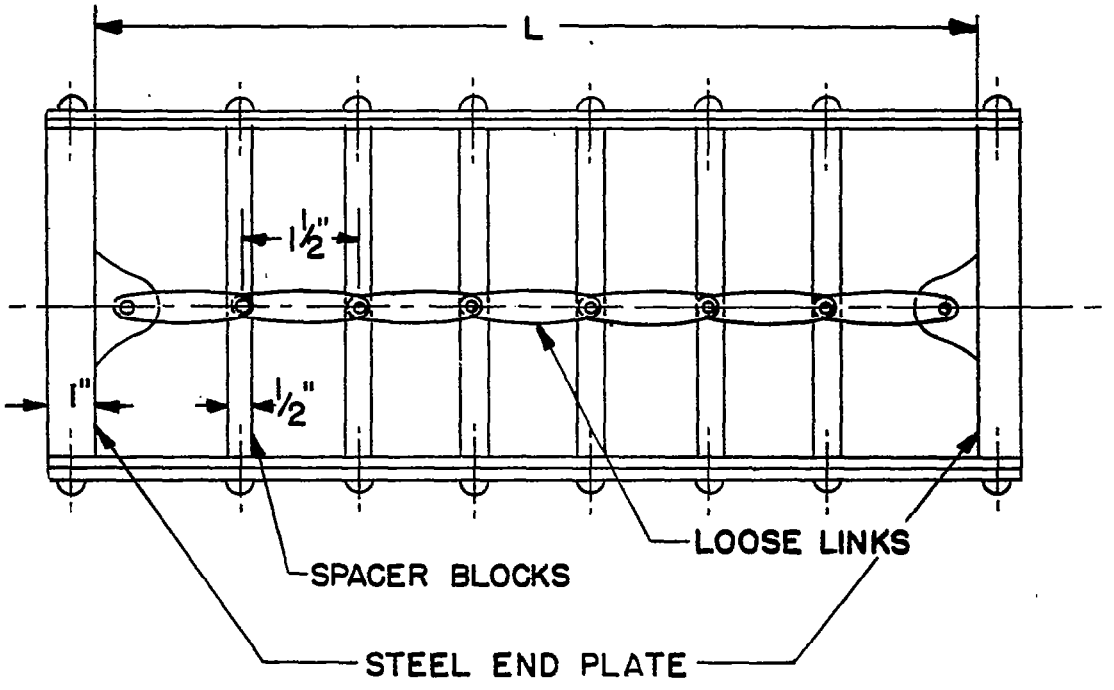


Figure 3b.- Longitudinal section of specimen showing spacer blocks.

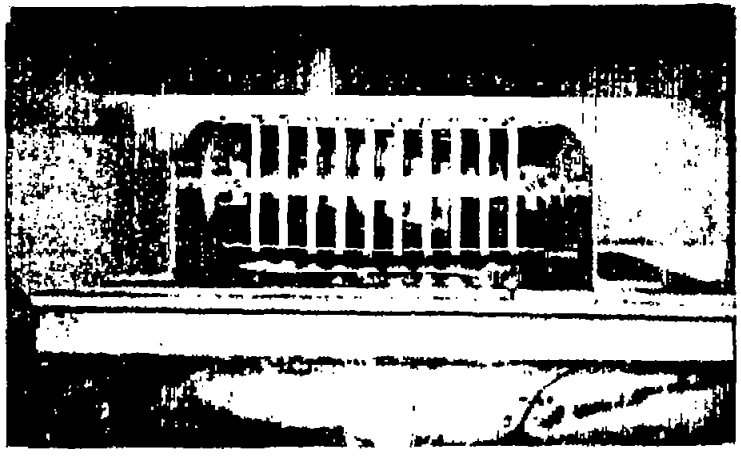

Figure 3c.- Exposed section of test specimen showing details of construction.

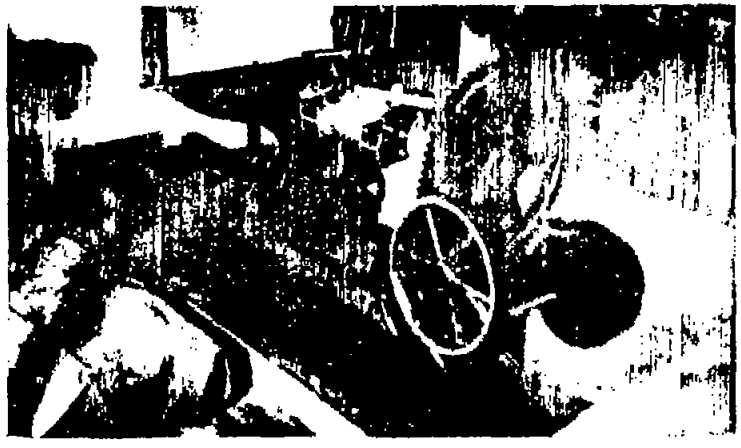

Figure 4.- Testing machine and apparatus used for pure torsion tests.

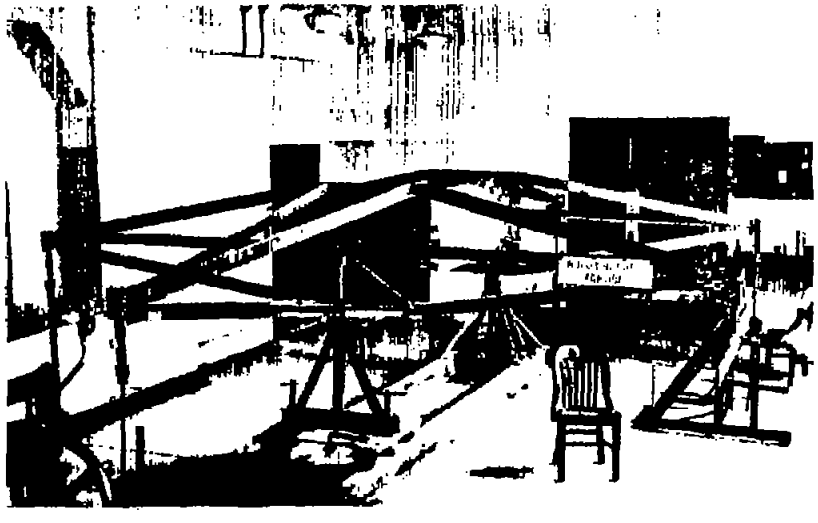

Figure 5.- Testing machine used for pure bending and bending plus torsion tests.

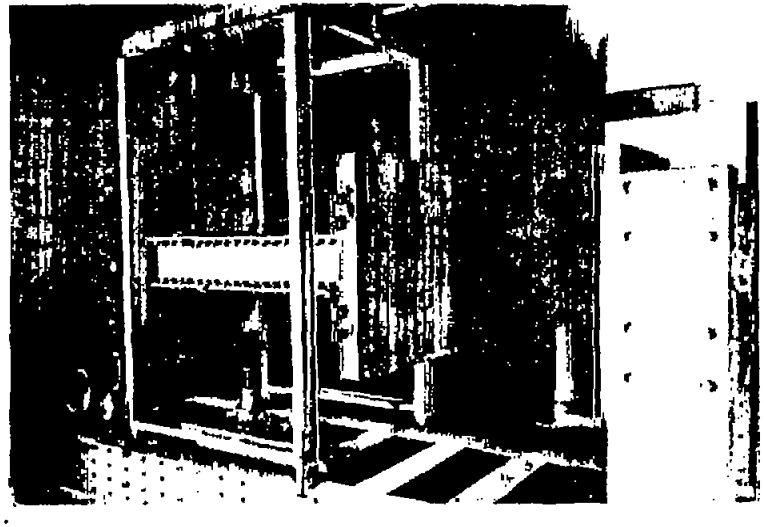

Figure 6.- Testing machine used for bending plus shear tests.

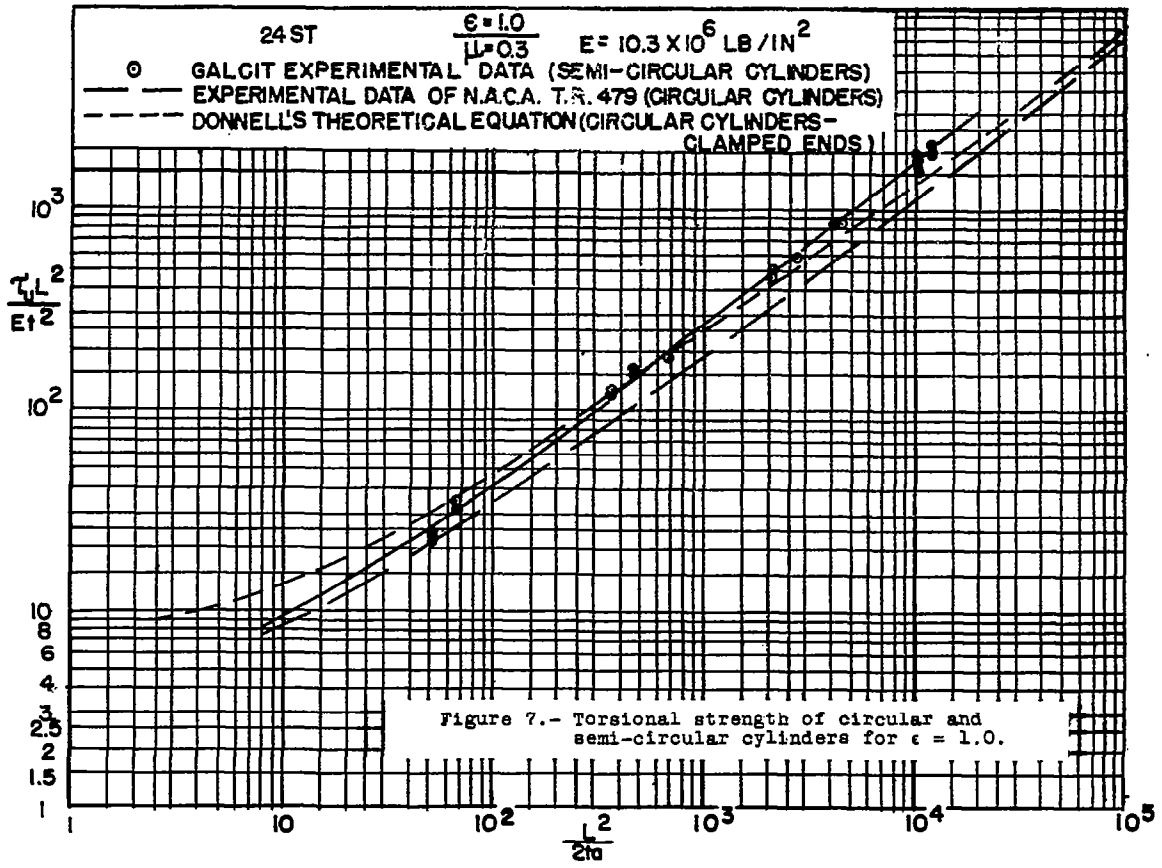


Figure 7.- Torsional strength of circular and semi-circular cylinders for ε = 1.0.

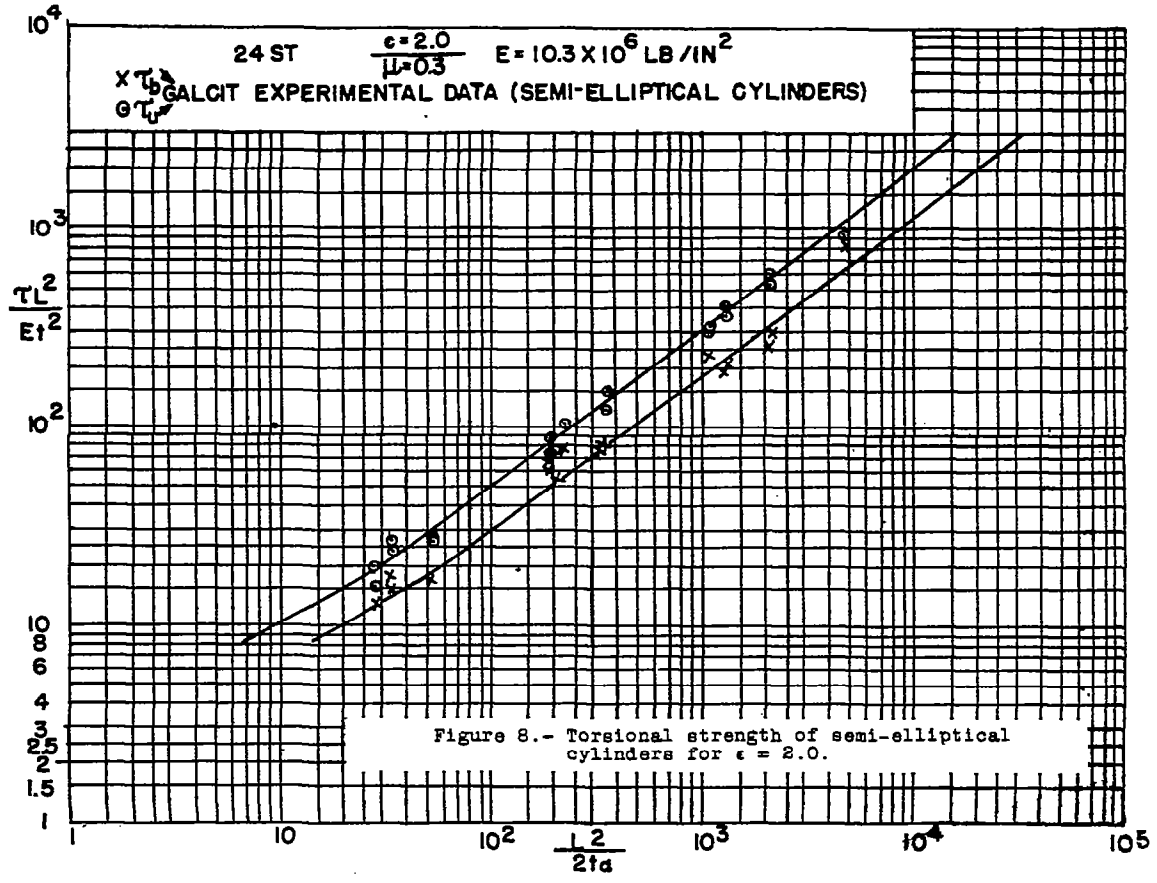


Figure 8.- Torsional strength of semi-elliptical cylinders for ε = 2.0.

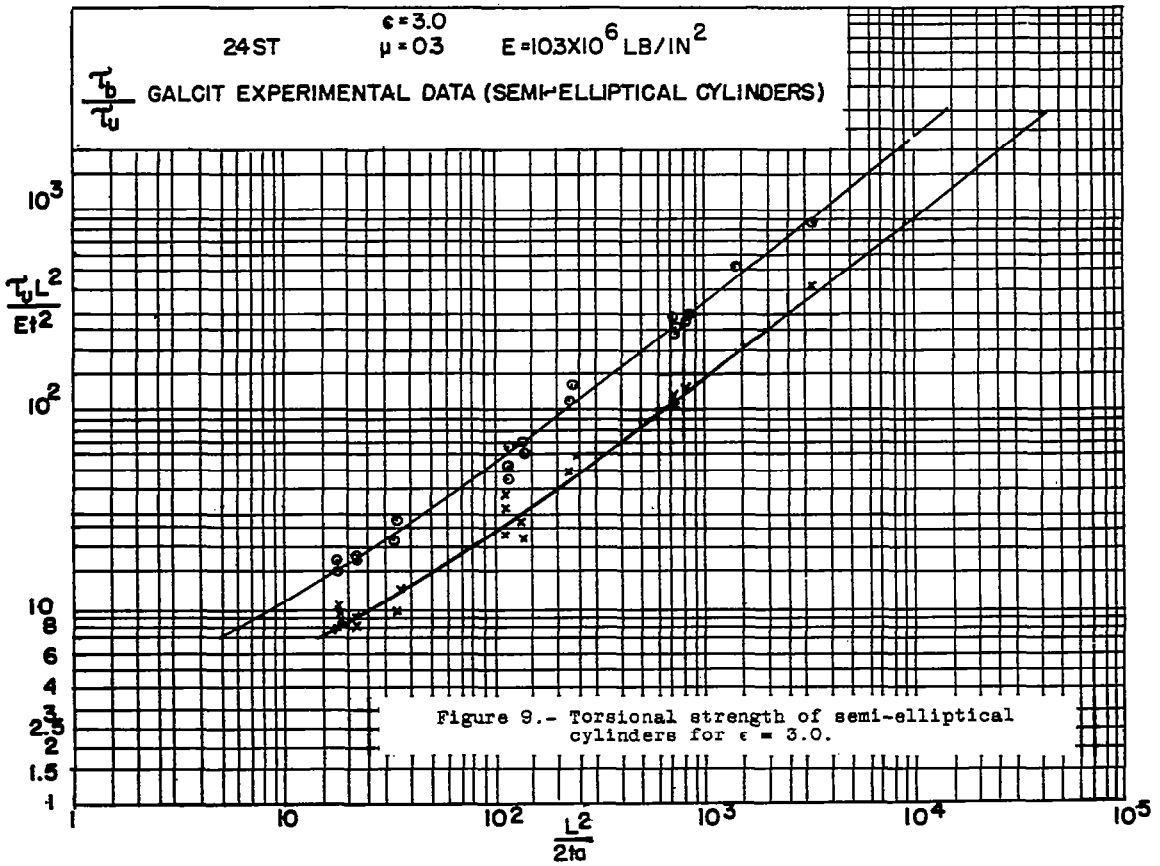


Figure 9.- Torsional strength of semi-elliptical cylinders for ε = 3.0.

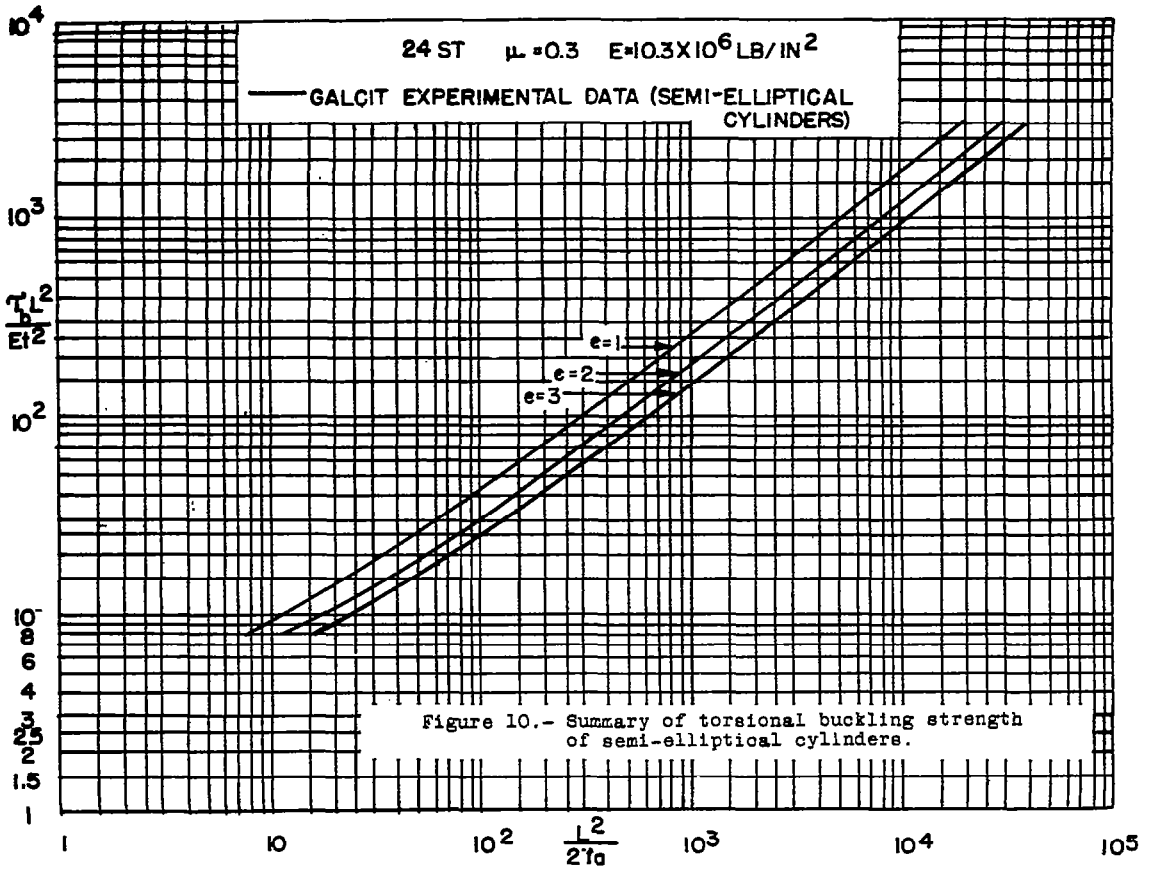


Figure 10.- Summary of torsional buckling strength of semi-elliptical cylinders.

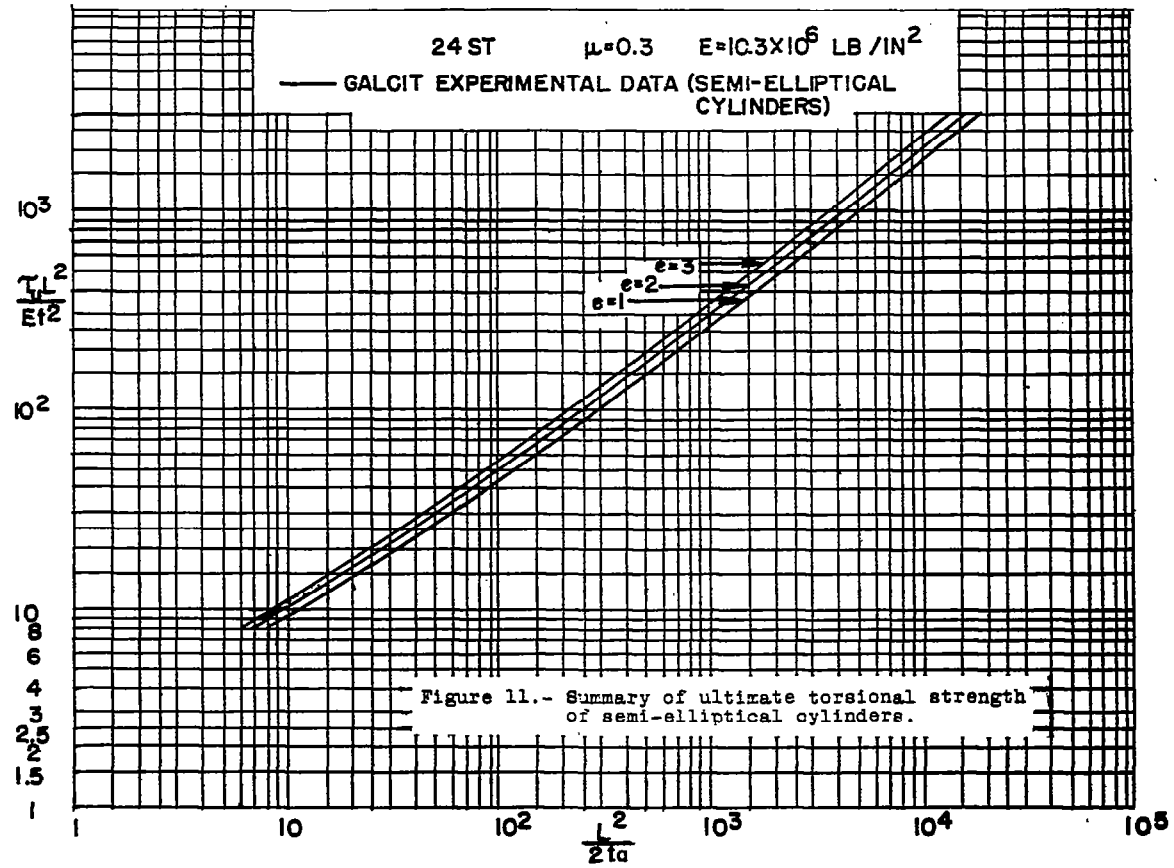


Figure 11.- Summary of ultimate torsional strength of semi-elliptical cylinders.

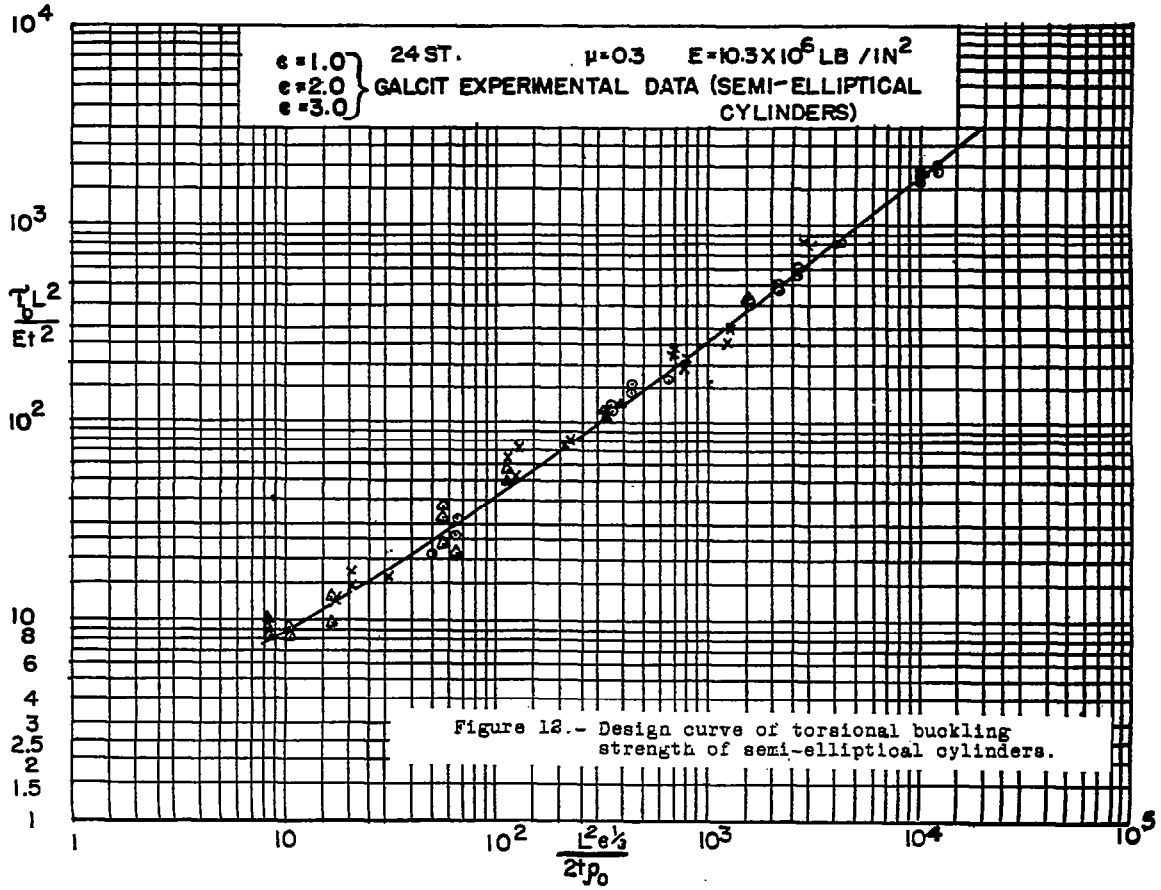


Figure 12.- Design curve of torsional buckling strength of semi-elliptical cylinders.

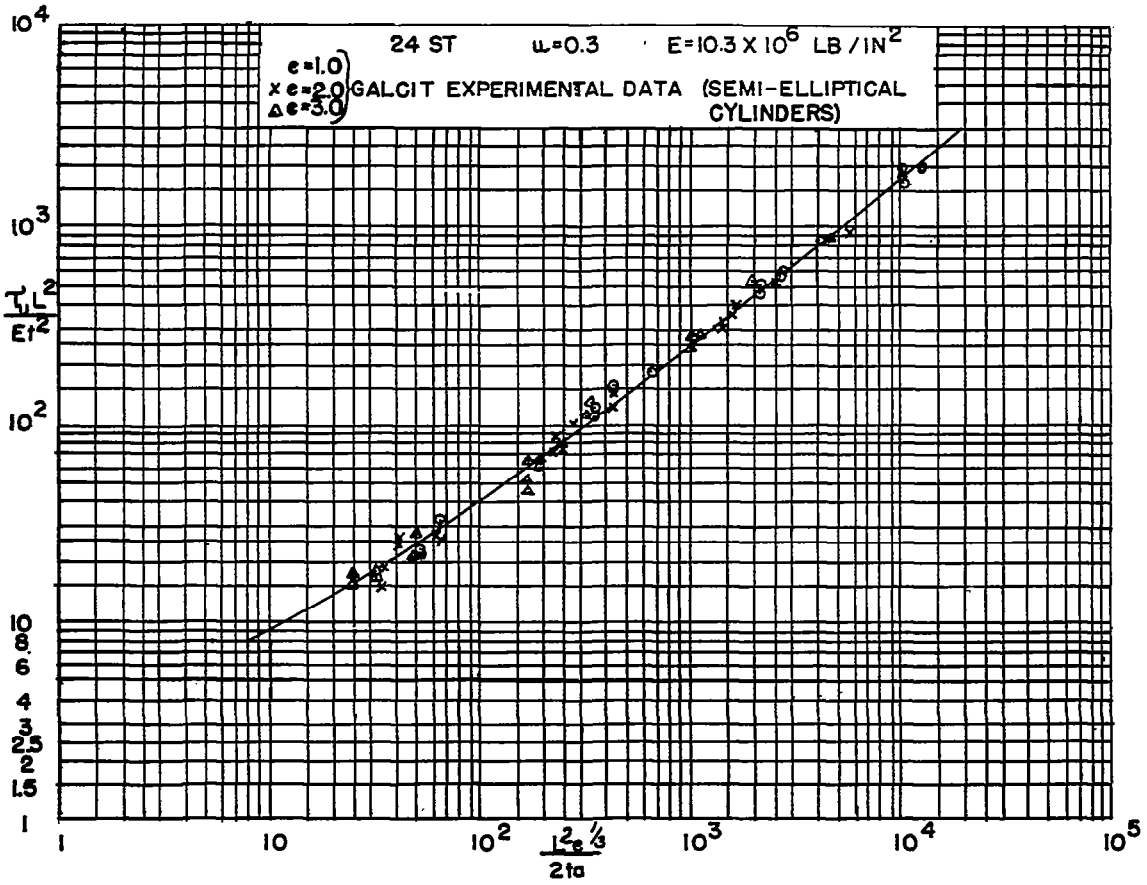


Figure 13.- Design curve of ultimate torsional strength of semi-elliptical cylinders.

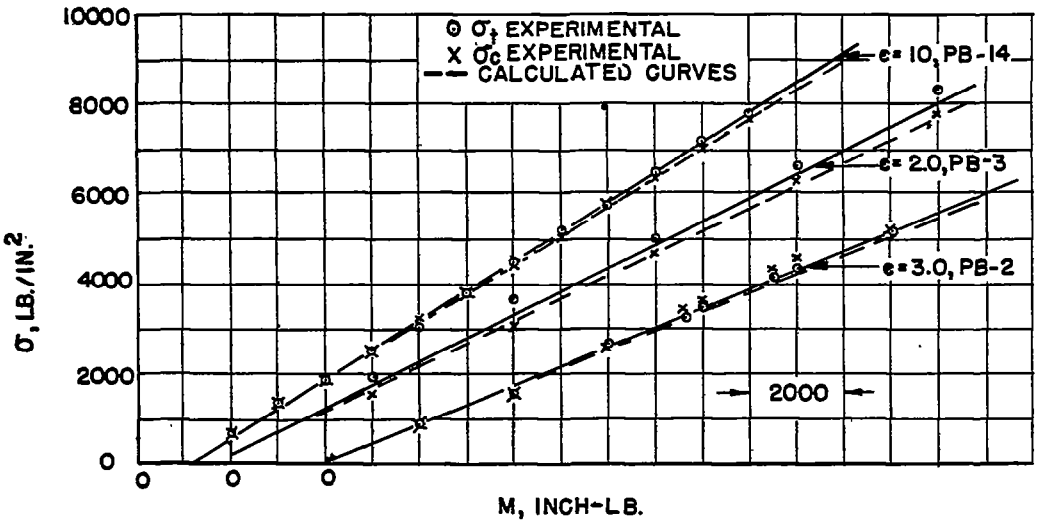


Figure 14.- Comparison of experimental and calculated normal stresses for pure bending (below buckling).

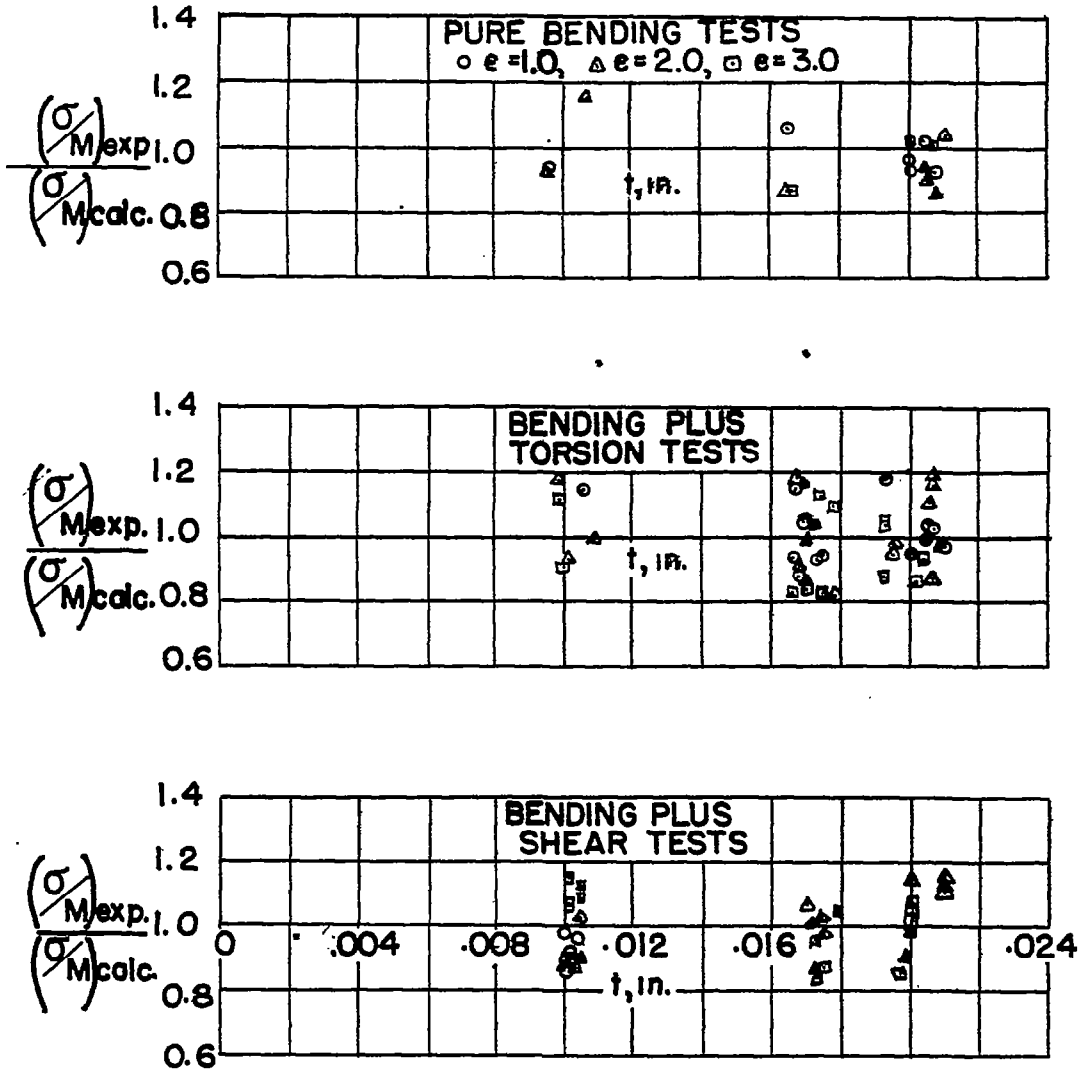


Figure 15.- Comparison of experimental and calculated normal stresses due to bending deformation taken just below the buckling load.

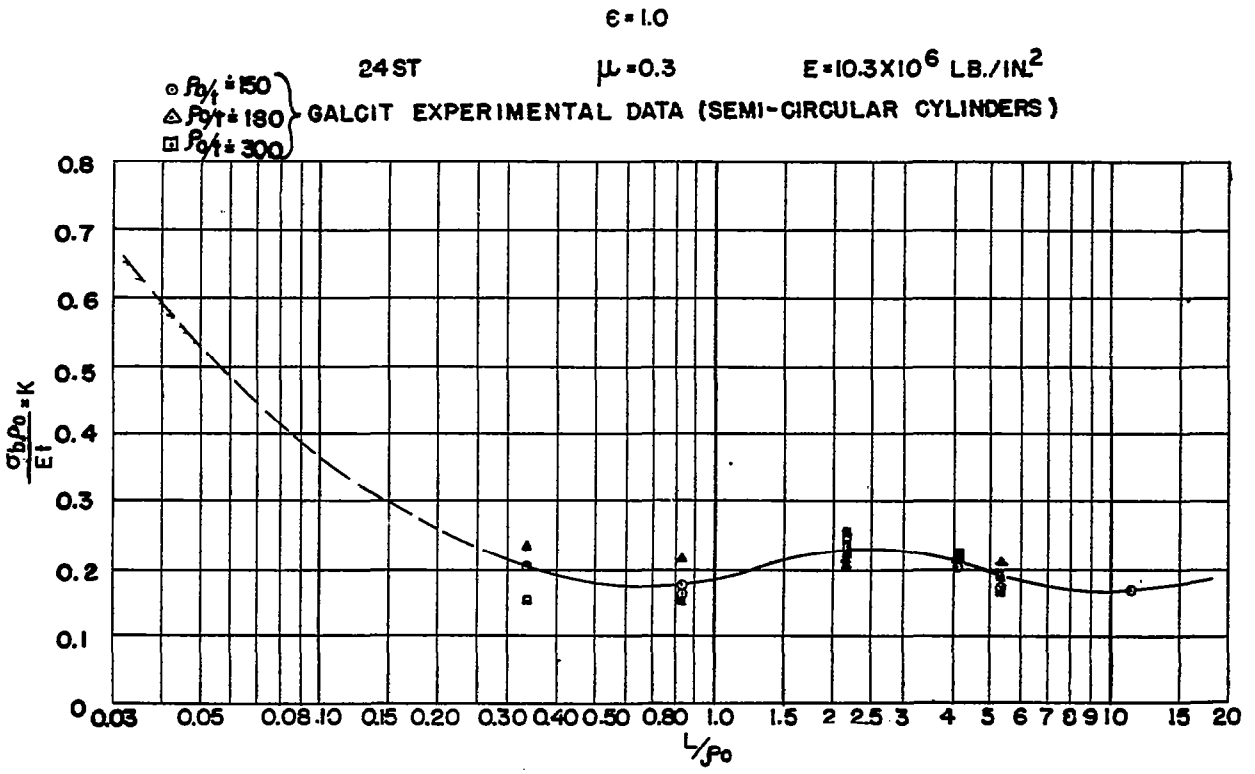


Figure 16.- Design curve of buckling (and ultimate) strength of semi-circular cylinders under pure bending.

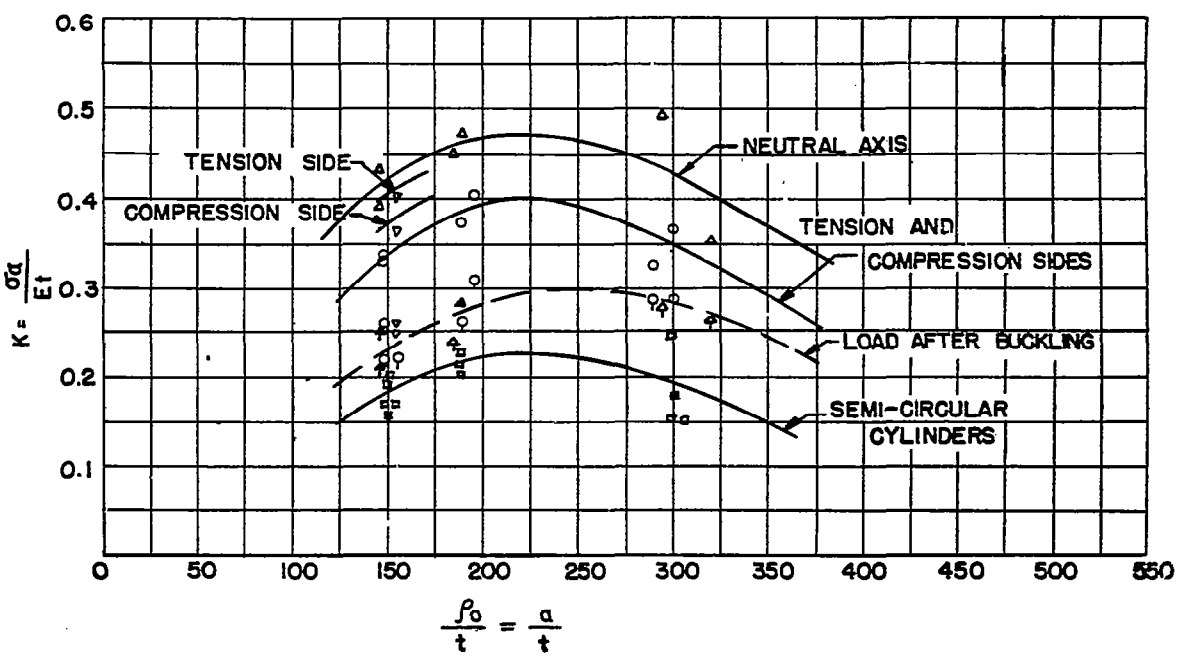


Figure 17.- Effect of seams on buckling strength of circular cylinders.

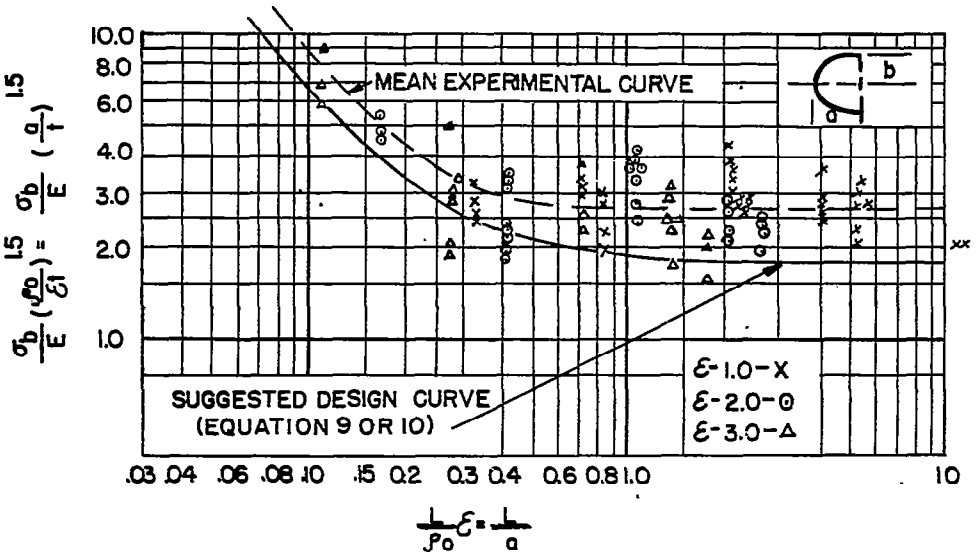


Figure 18.- Bending strength of semi-elliptical and semi-circular cylinders.

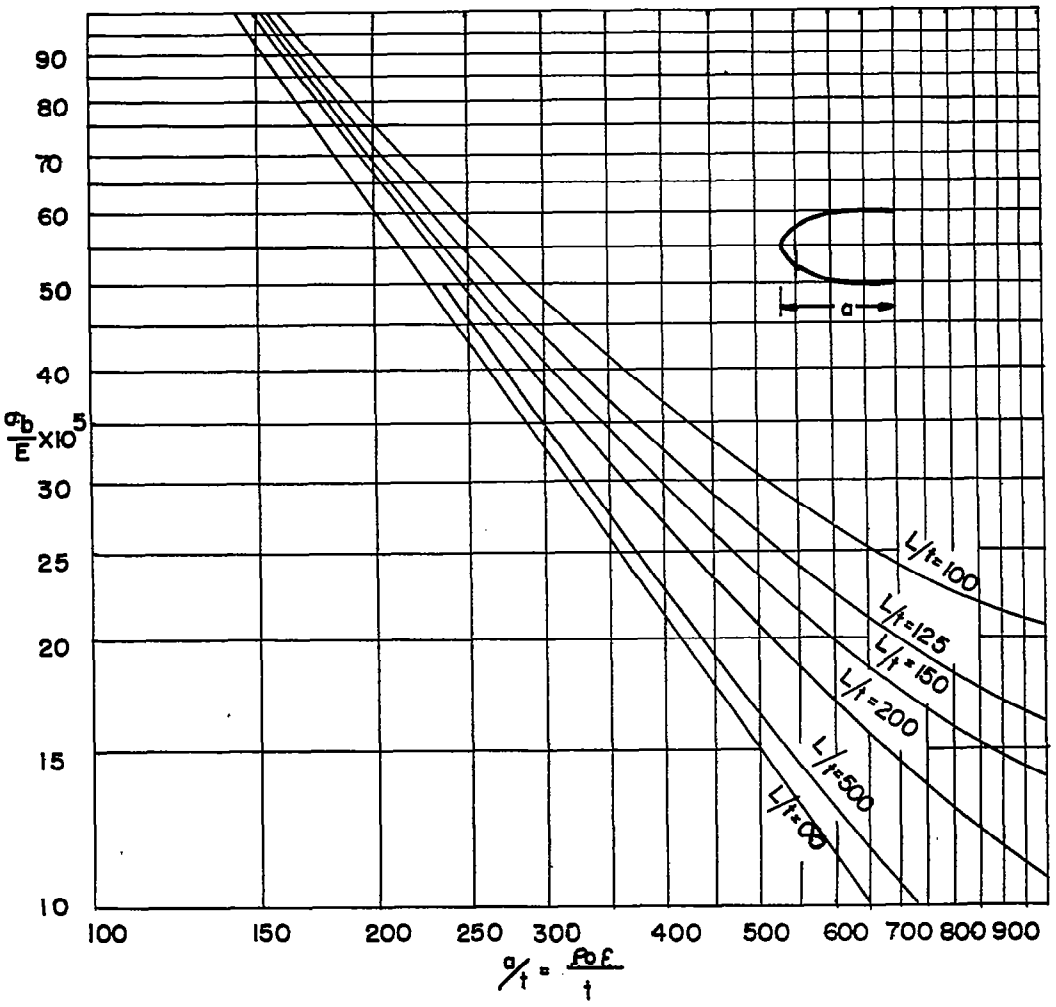


Figure 19.- Buckling stress for semi-elliptical cylinders under pure bending.

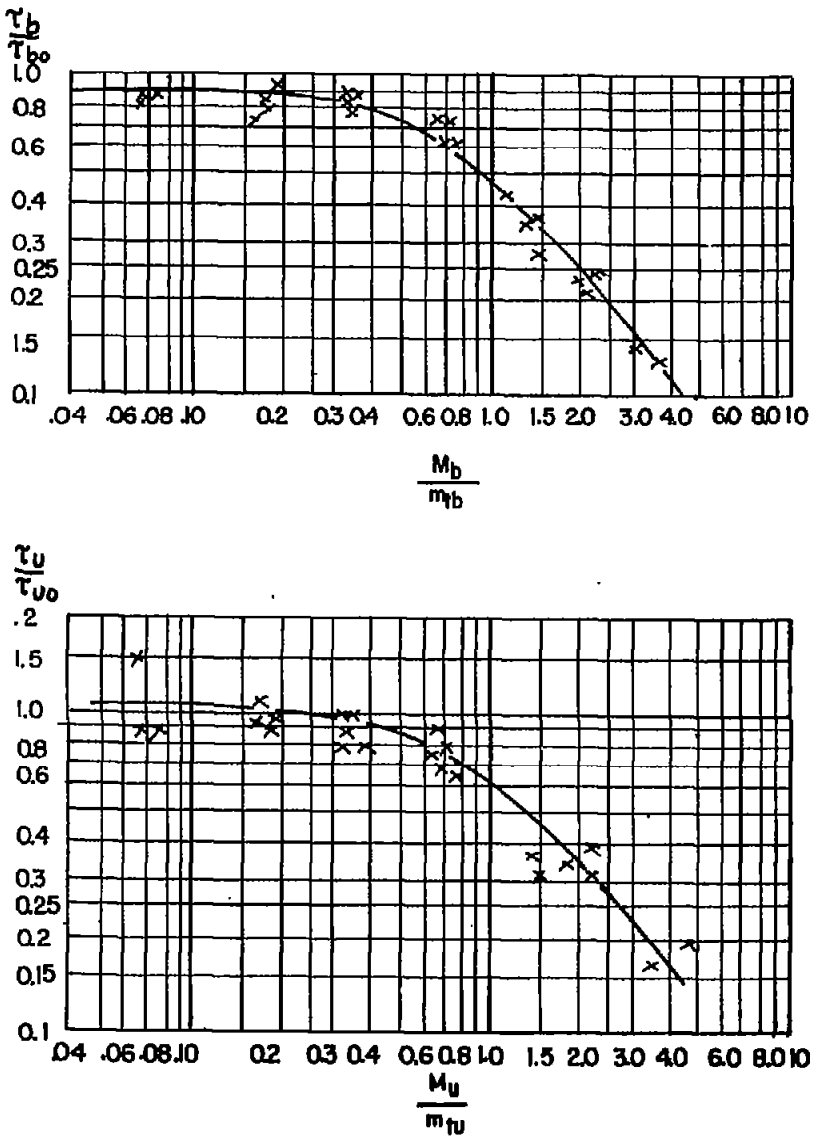


Figure 20.- Torsional stresses in semi-circular cylinders loaded in bending plus torsion for $\epsilon = 1.0$.

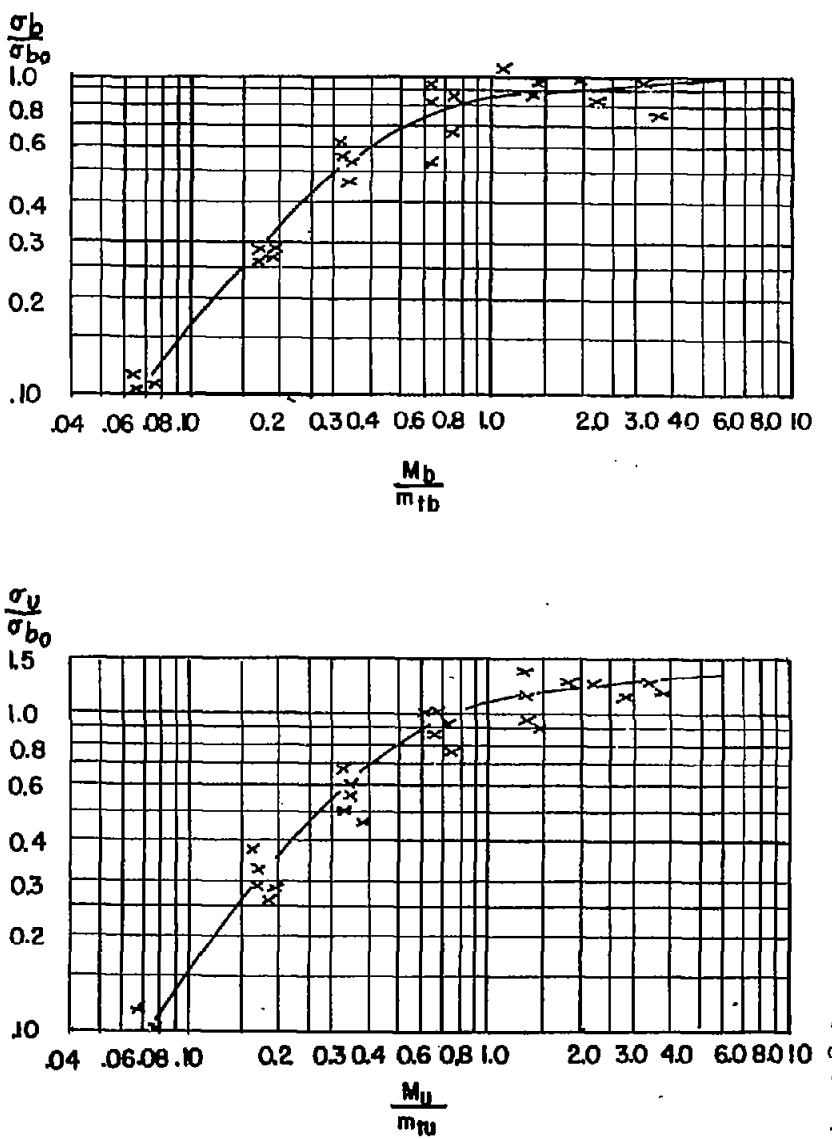


Figure 21.- Bending stresses in semi-circular cylinders loaded in bending plus torsion for $\epsilon = 1.0$.

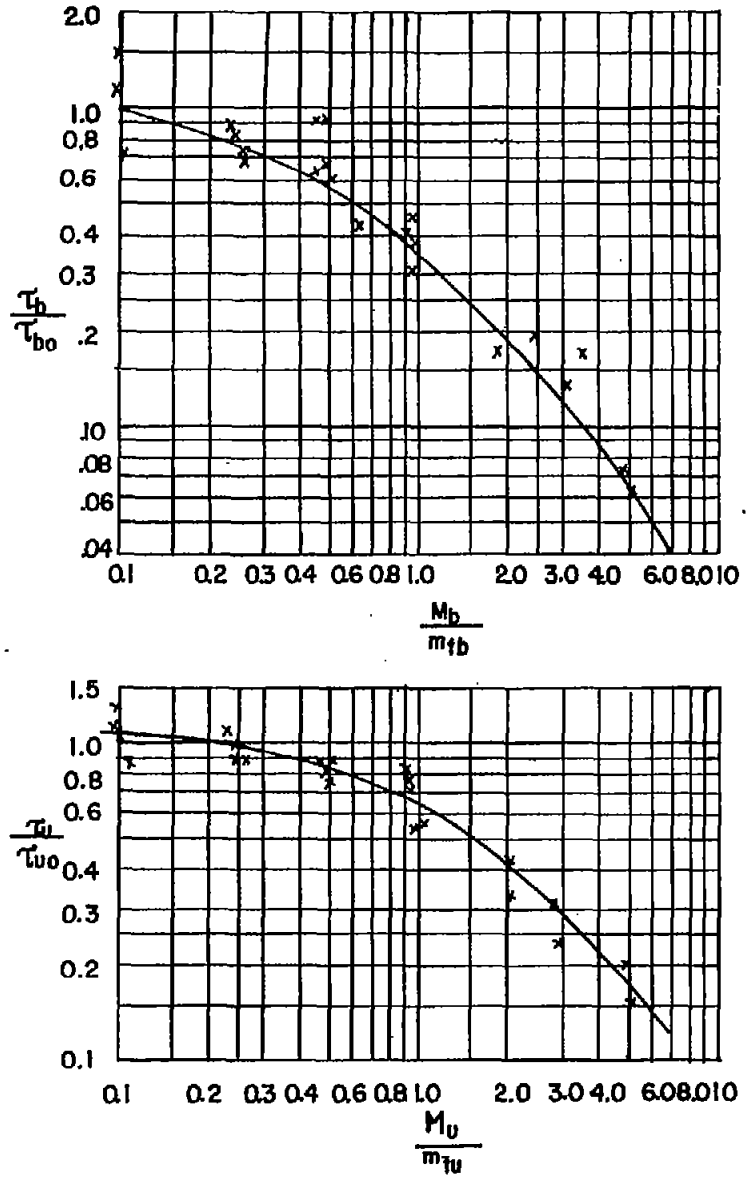


Figure 22.- Torsional stresses in semi-elliptical cylinders loaded in bending plus torsion for $\epsilon = 2.0$.

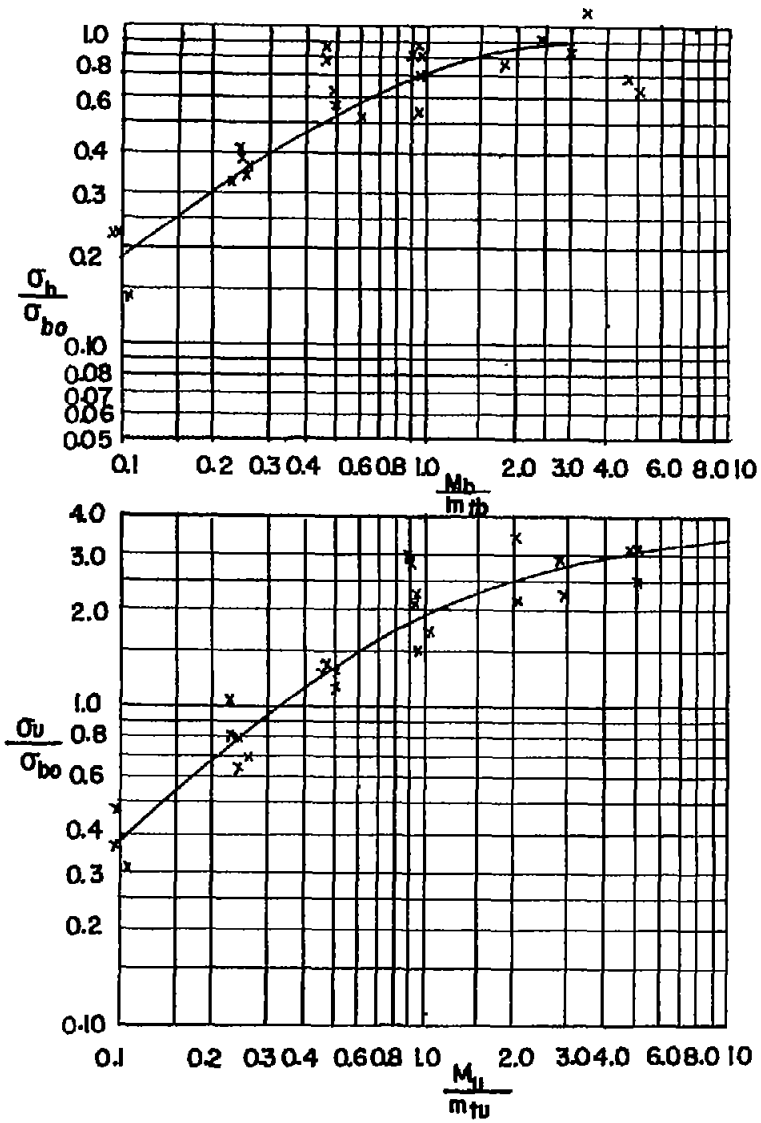


Figure 23.- Bending stresses in semi-elliptical cylinders loaded in bending plus torsion for $\epsilon = 2.0$.

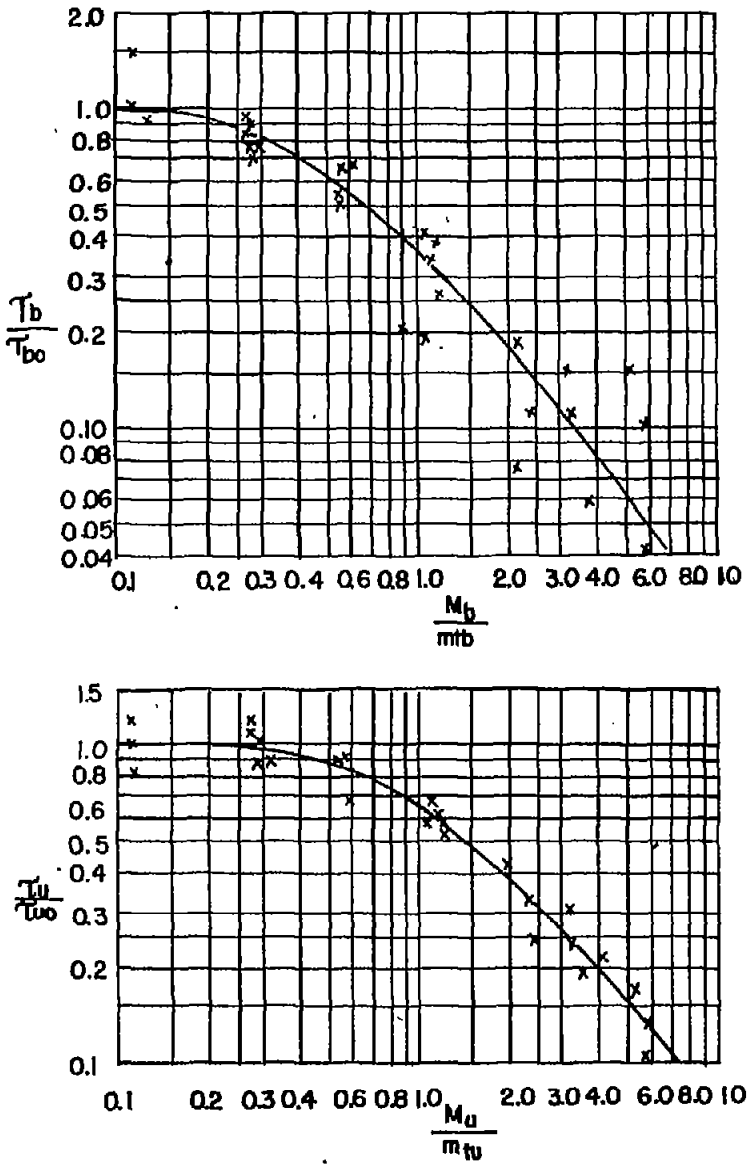


Figure 24.- Torsional stresses in semi-elliptical cylinders loaded in bending plus torsion for $\epsilon = 3.0$.

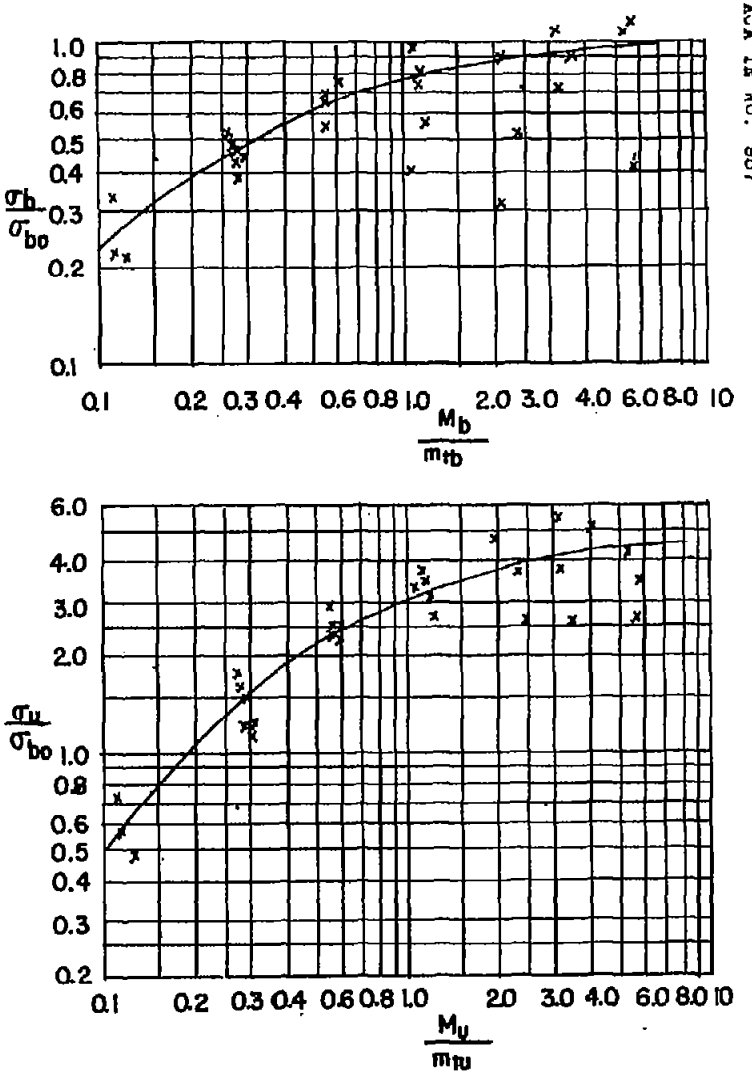


Figure 25.- Bending stresses in semi-circular cylinders loaded in bending plus torsion for $\epsilon = 3.0$.

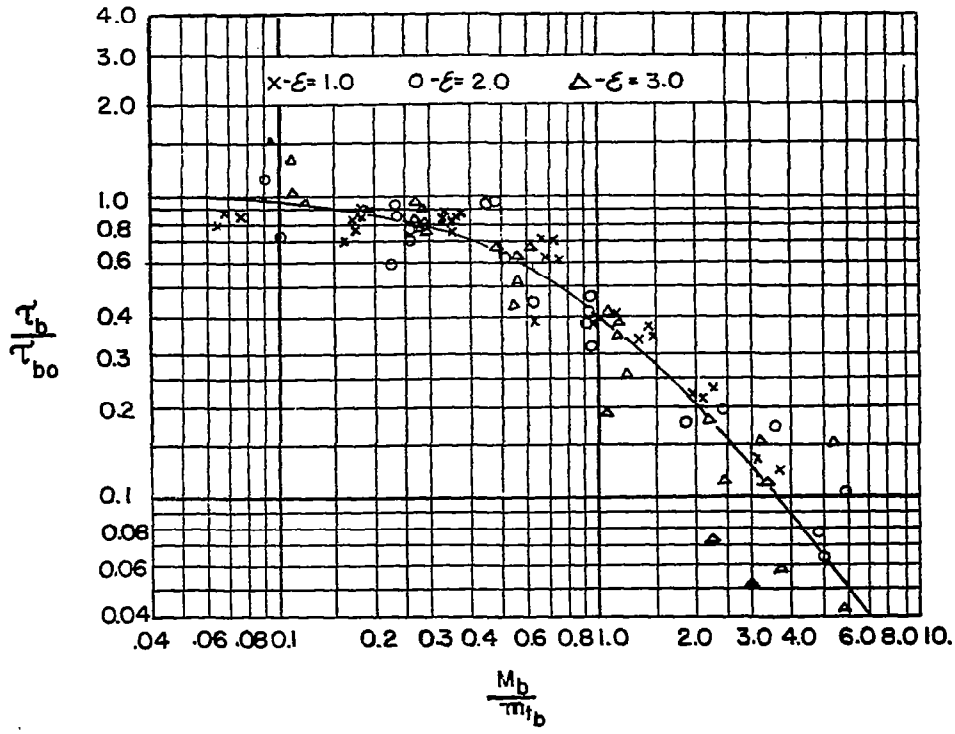


Figure 26.- Torsional buckling stress in semi-elliptical cylinders loaded in bending plus torsion.

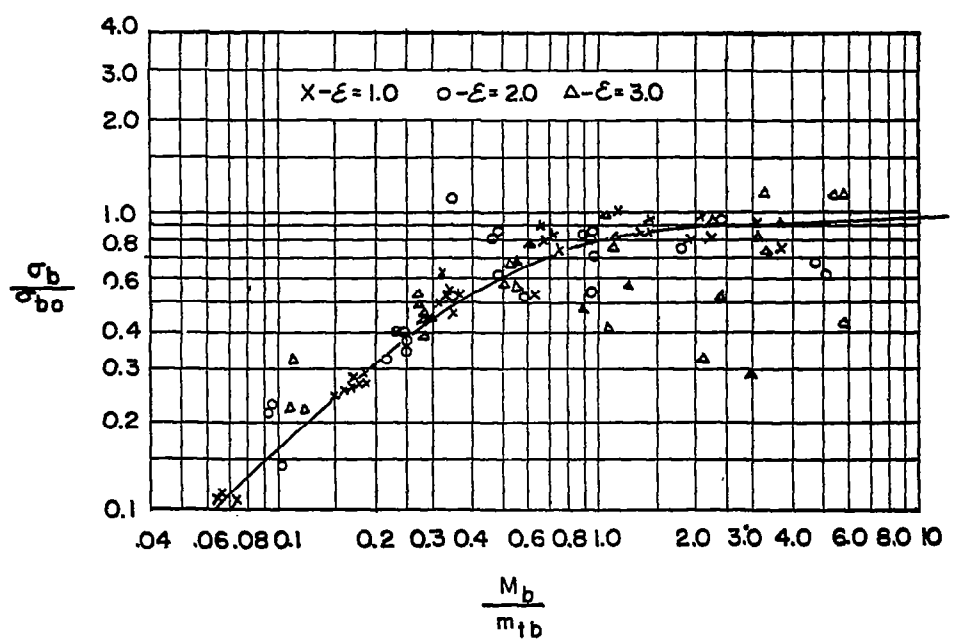


Figure 27.- Compression buckling stress in semi-elliptica cylinders loaded in bending plus torsion.

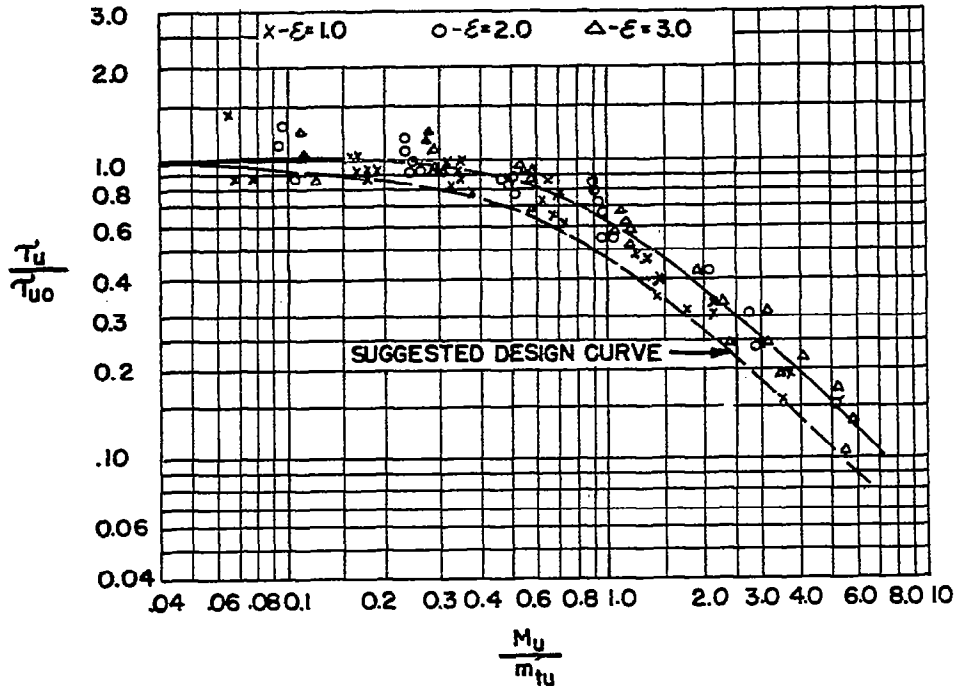


Figure 28.- Ultimate torsional stress in semi-elliptical cylinders loaded in bending plus torsion.

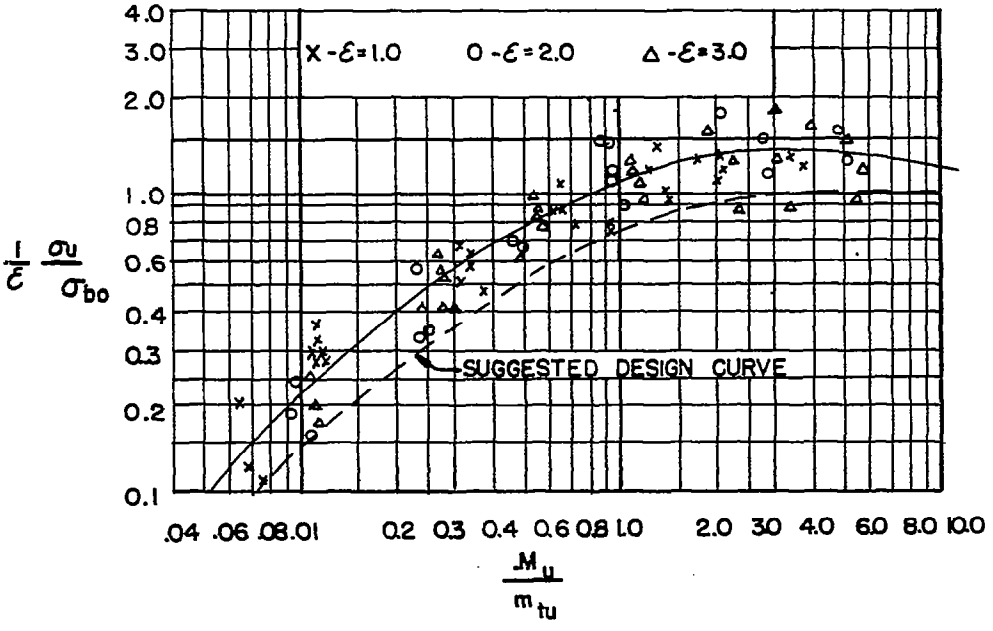


Figure 29.- Ultimate compression stress in semi-elliptical cylinders loaded in bending plus torsion.

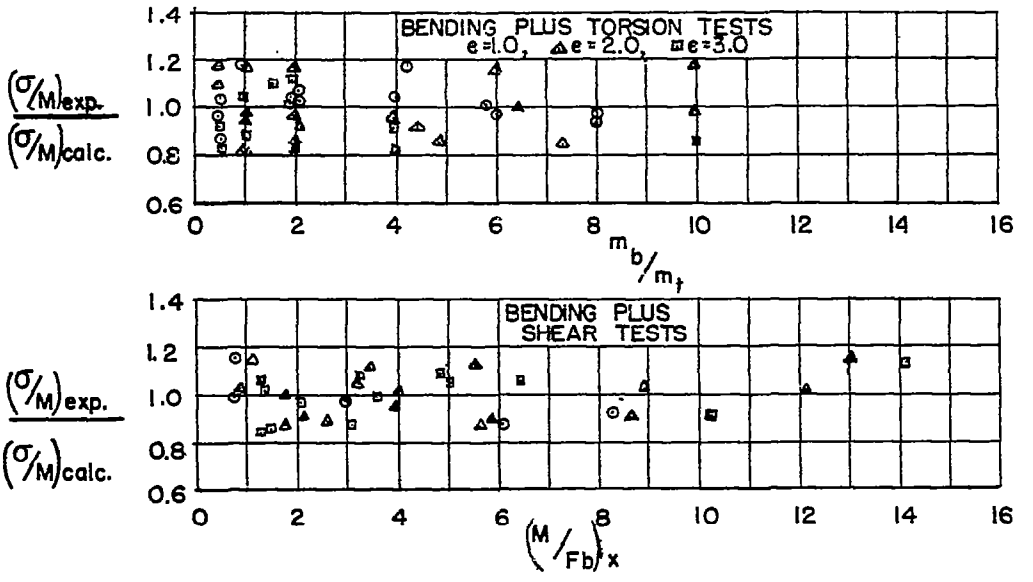


Figure 30.- Comparison of experimental and calculated bending stresses for combined loading conditions taken just below the buckling load.

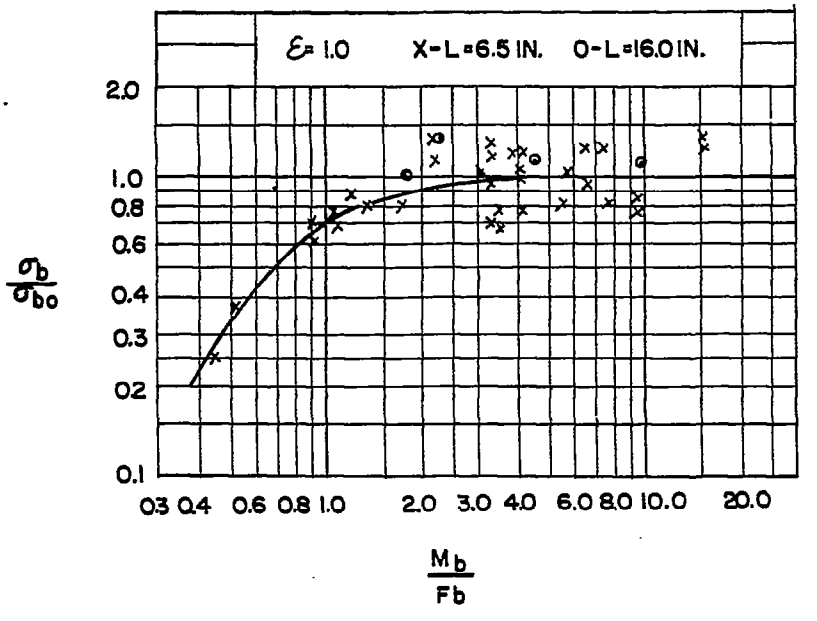


Figure 31.- Buckling stress in compression for bending plus shear tests.

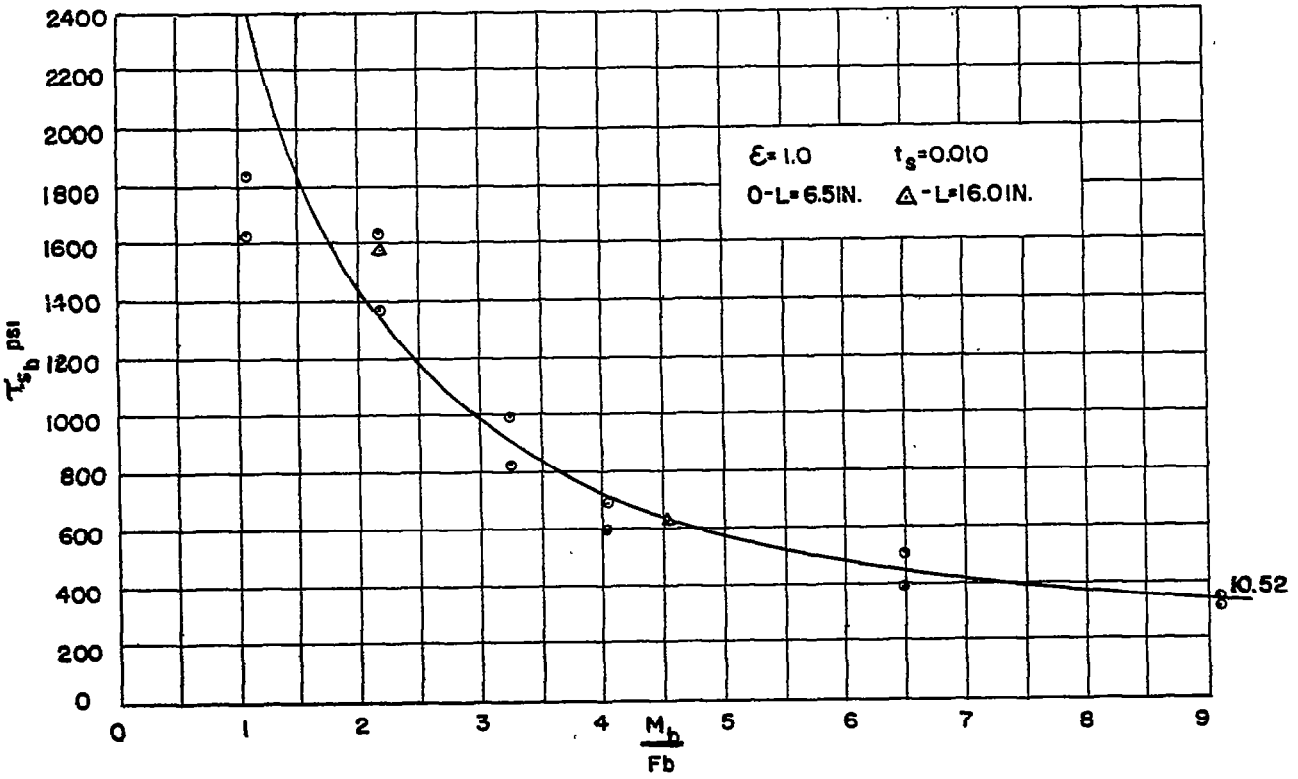


Figure 32.- $\tau_{s_b}$ for bending plus shear tests.

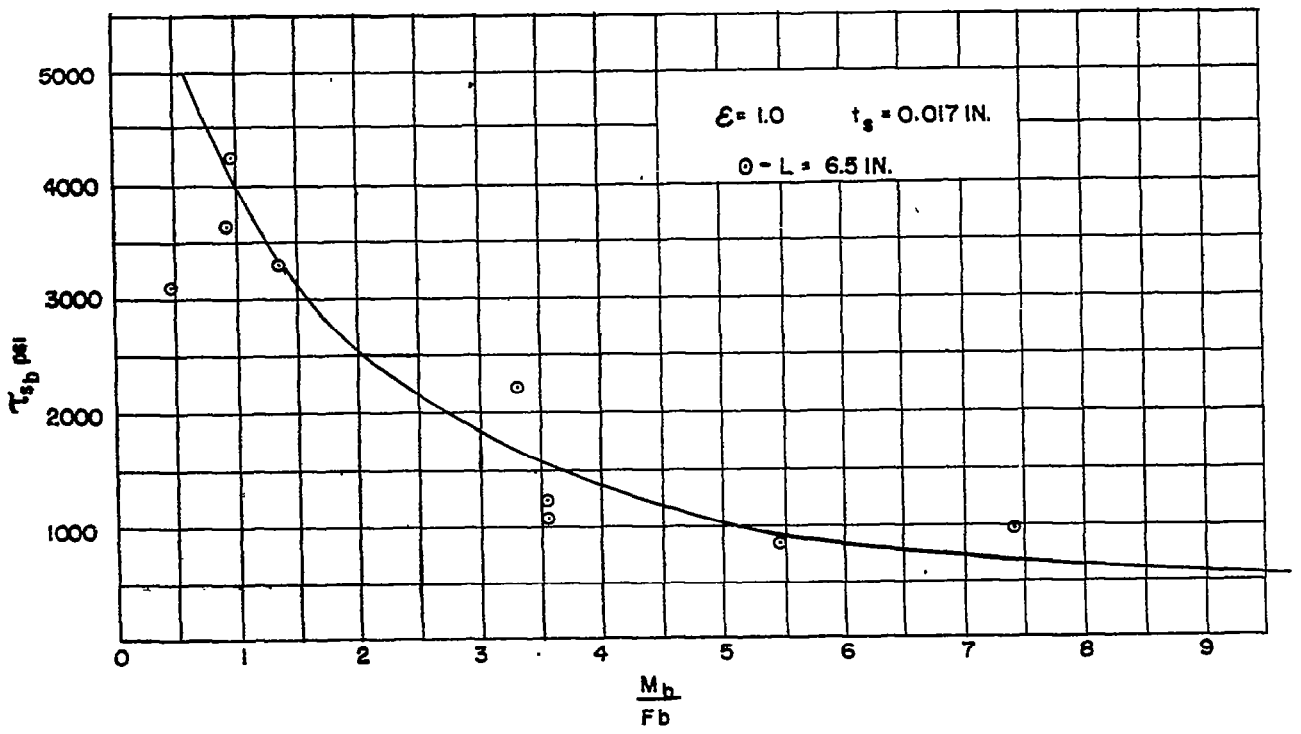


Figure 33 - $\tau_{s_b}$ for bending plus shear tests.

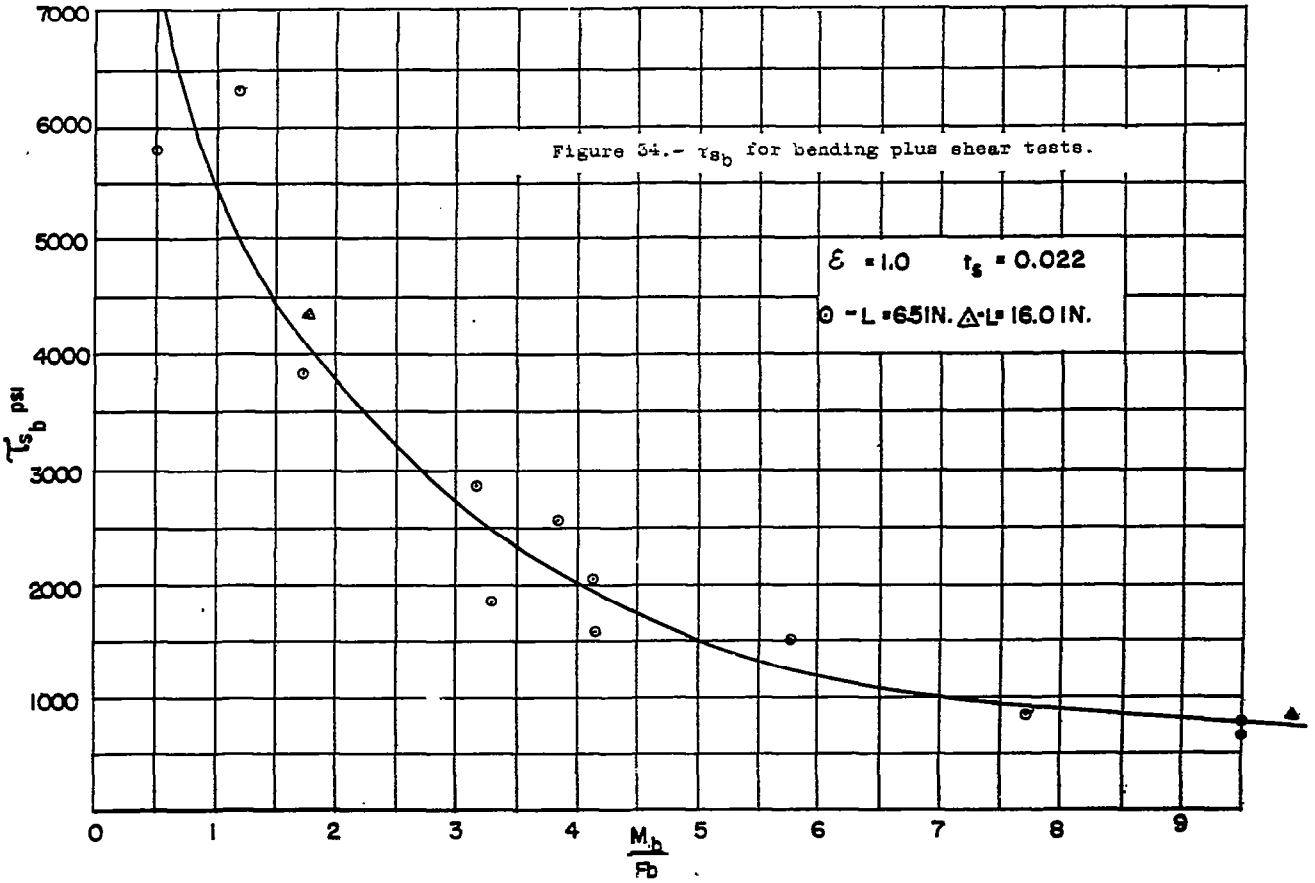


Figure 34.- $\tau_{s_b}$ for bending plus shear tests.

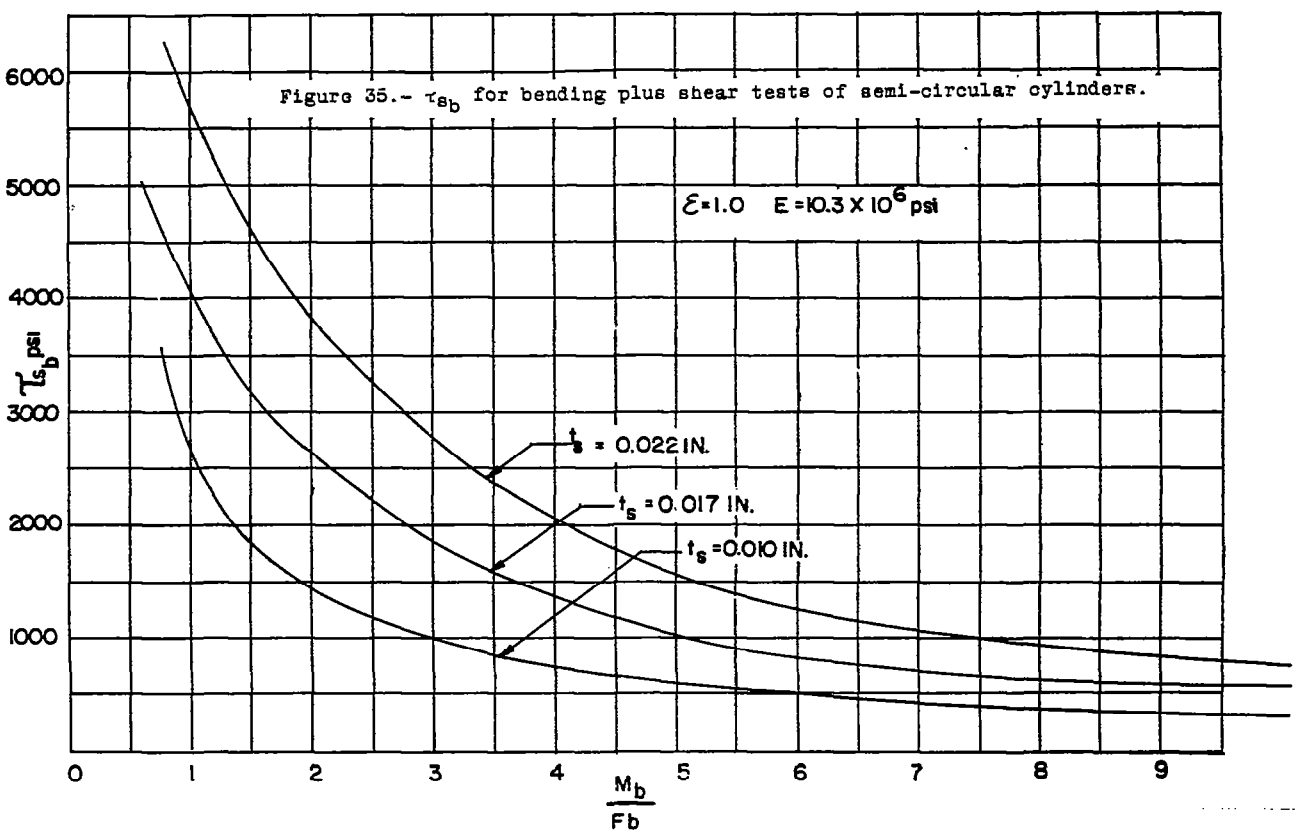


Figure 35.- $\tau_{s_b}$ for bending plus shear tests of semi-circular cylinders.

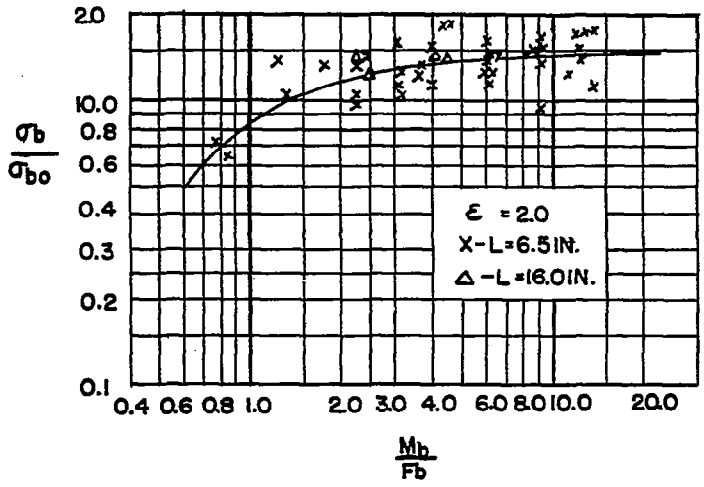


Figure 36.- Buckling stress in compression for bending plus shear tests.

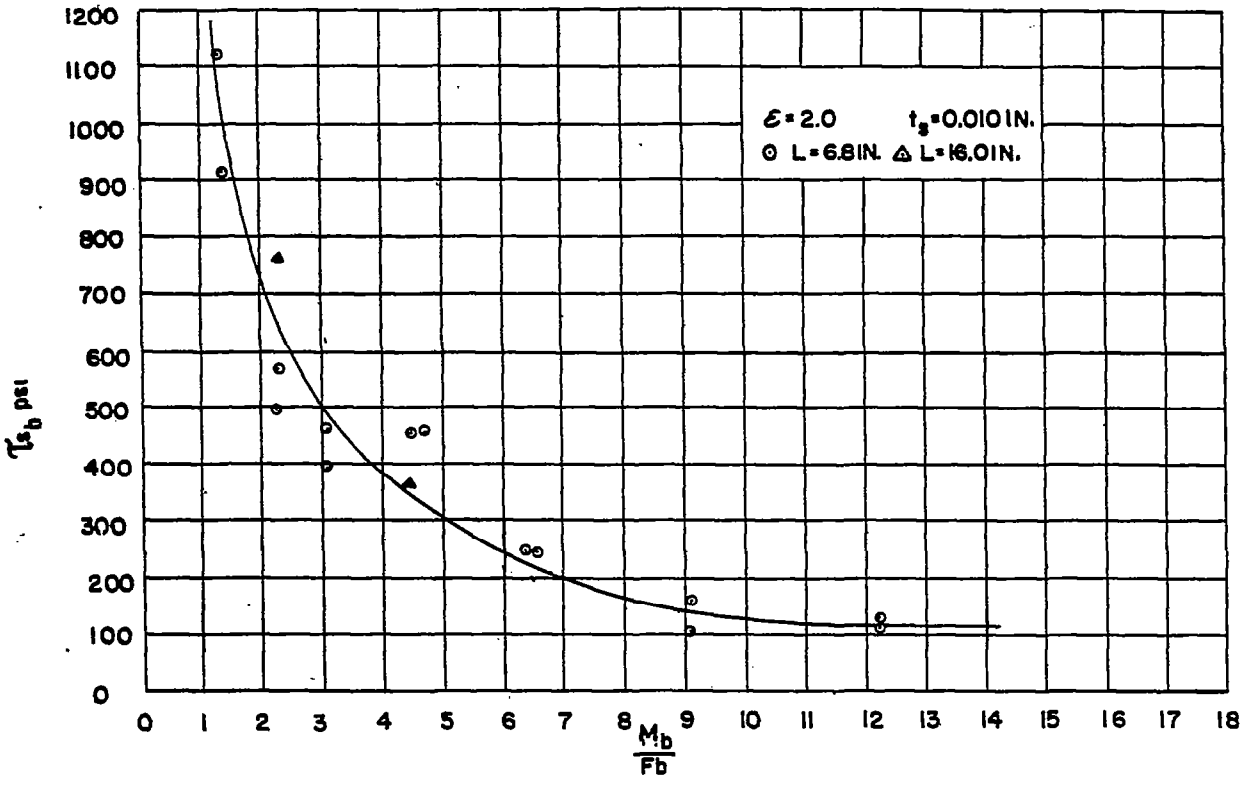


Figure 37.- $\tau_{s_b}$ for bending plus shear tests.

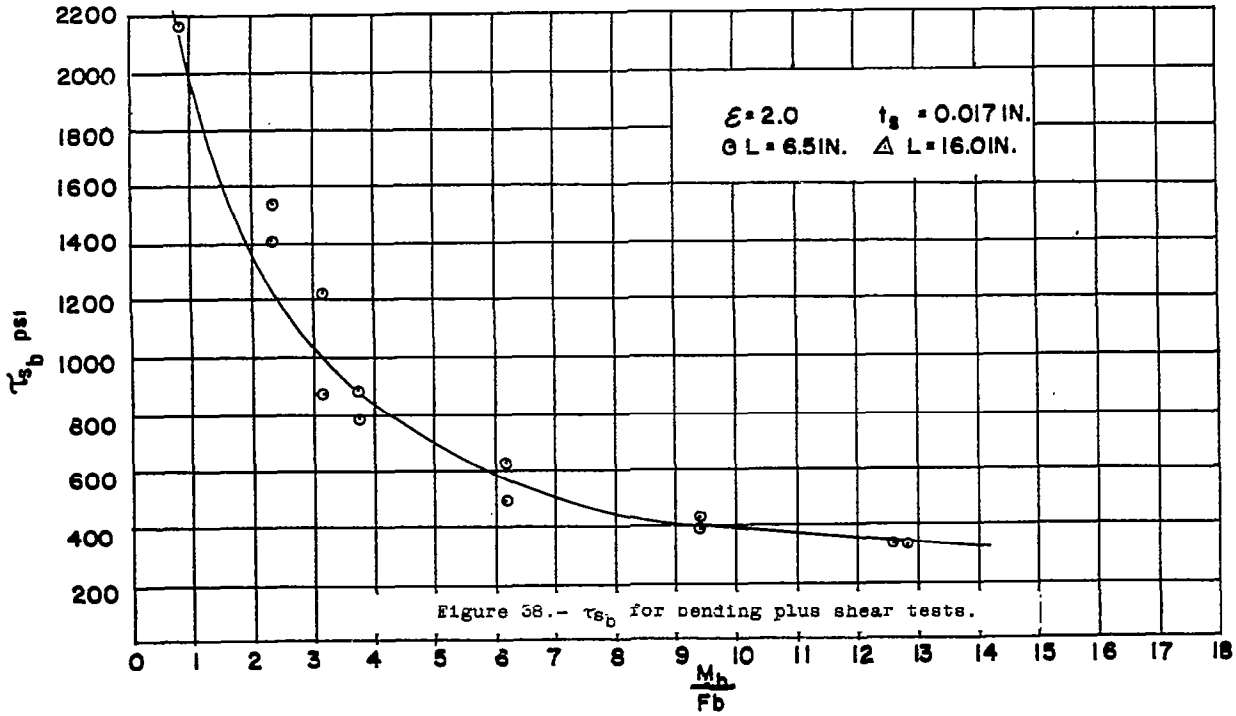


Figure 38.- $\tau_{s_b}$ for bending plus shear tests.

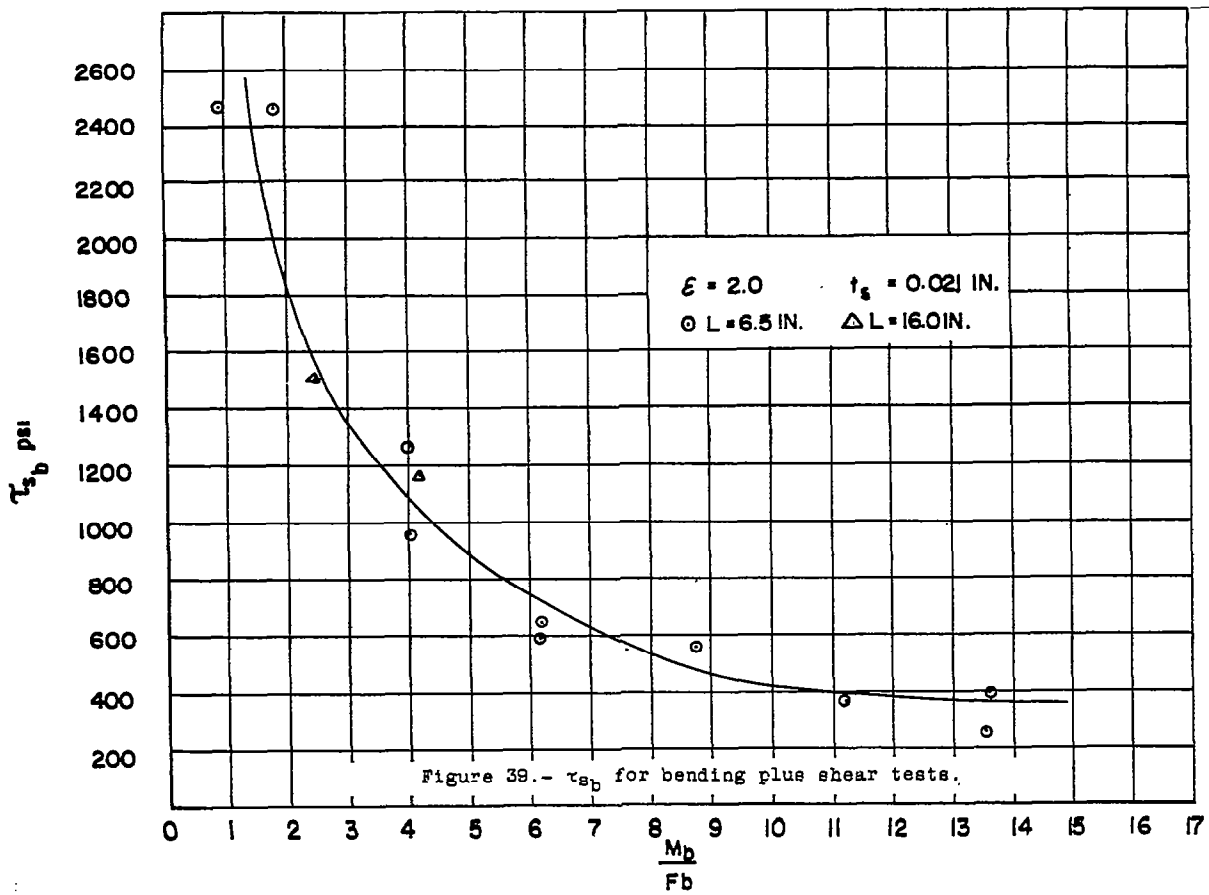


Figure 39.- $\tau_{s_b}$ for bending plus shear tests.

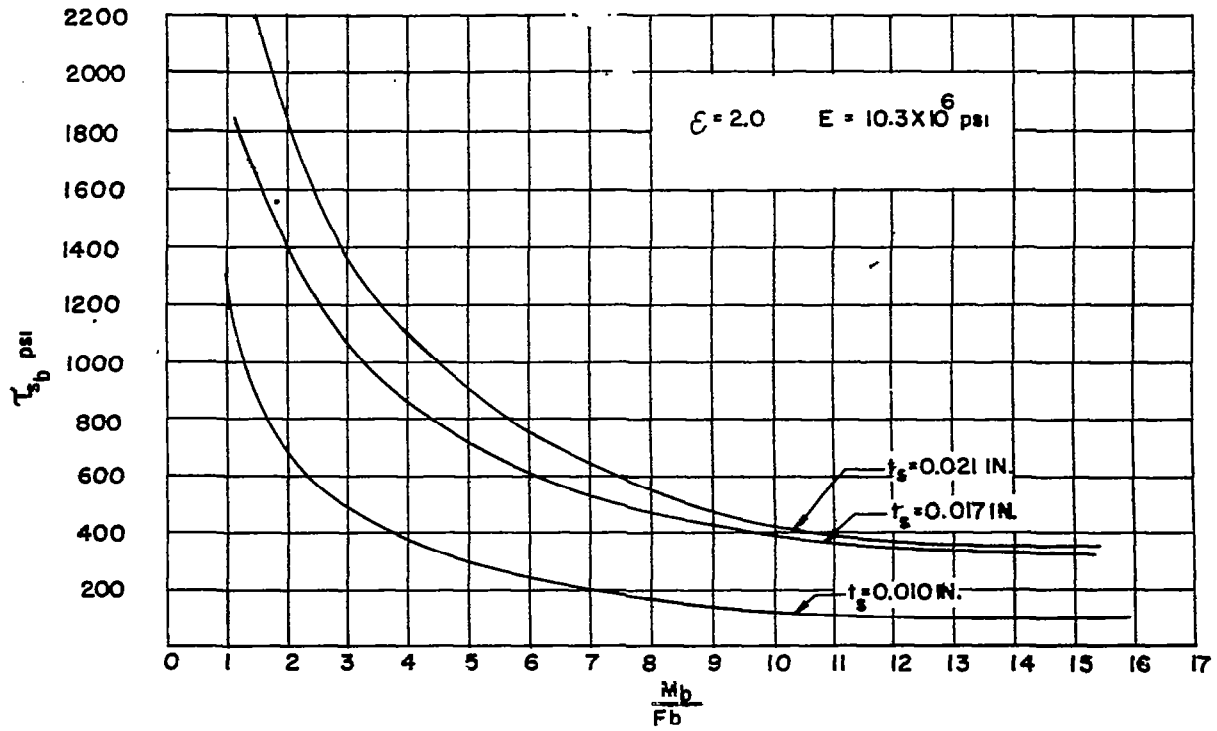


Figure 40.- $\tau_{s_b}$ for bending plus shear tests of semi-elliptical cylinders.

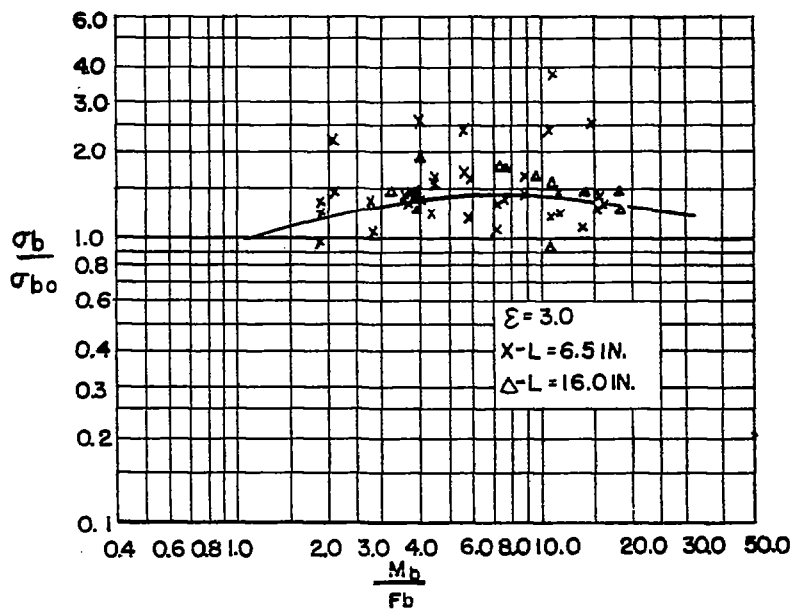


Figure 41.- Buckling stress in compression for bending plus shear tests.

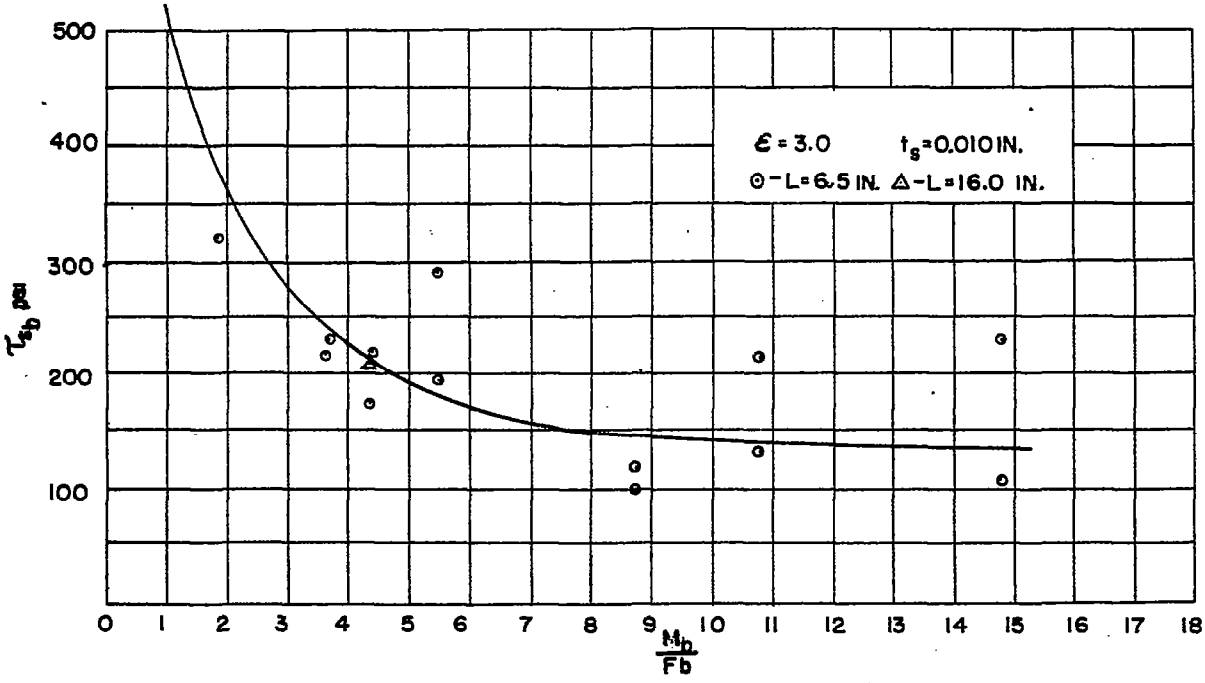


Figure 42.- $\tau_{sb}$ for bending plus shear tests.

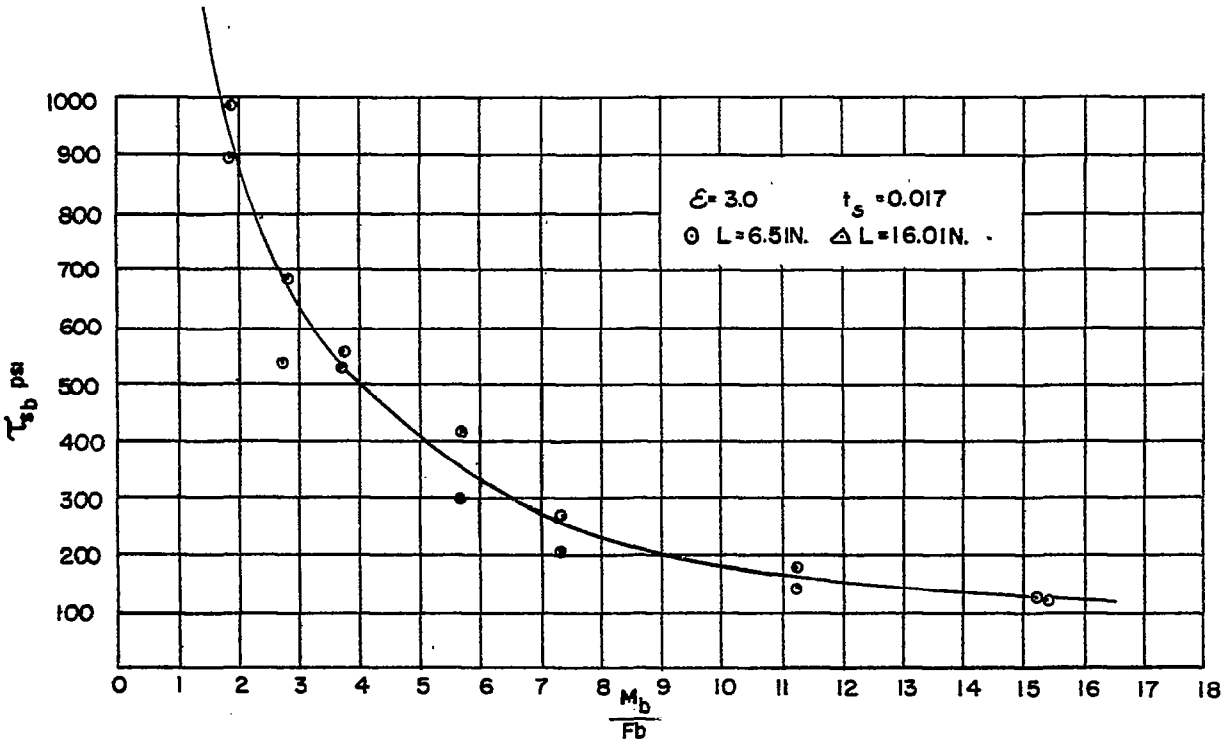


Figure 43.- $\tau_{sb}$ for bending plus shear tests.

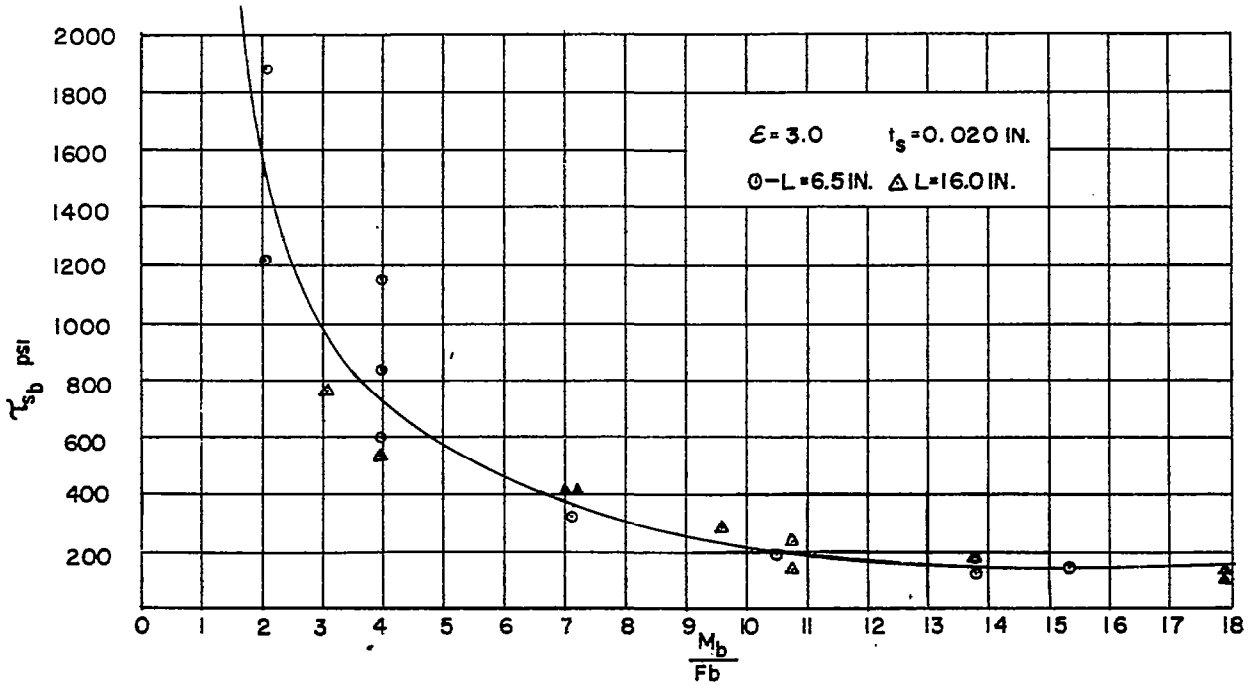


Figure 44 – $\tau_{s_b}$ for bending plus shear tests.

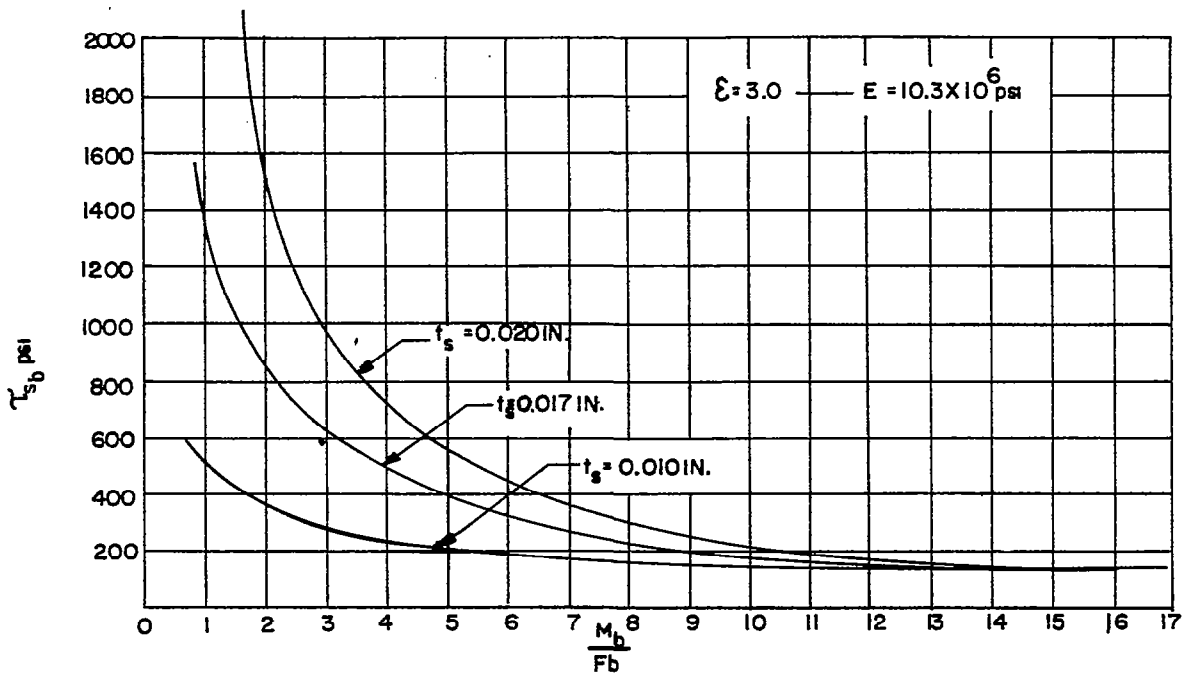


Figure 45.- $\tau_{s_b}$ for bending plus shear tests of semi-elliptical cylinders.

RESTRICTED

TITLE: The Strength of Semielliptical Cylinders Subjected to Combined Loadings

AUTHOR(S): Sechler, E. E.; Frederick, J. L.
ORIGINATING AGENCY: National Advisory Committee for Aeronautics, Washington, D. C.
PUBLISHED BY: (Same)

ATI- 8483
REVISION (None)
ORIG. AGENCY NO. TN-952
PUBLISHING AGENCY NO.

| DATE | DOC. CLASS. | COUNTRY | LANGUAGE | PAGES | ILLUSTRATIONS |
|---|---|---|---|---|---|
| Feb '45 | Restr. | U.S. | Eng. | 63 | photos, tables, graphs |

ABSTRACT: P20 ! !

Tests made on elliptical cylinders with center support yielded series of interaction curves for combined loadings on such cylinders which should be useful in wing nose section analysis. Data and curves presented should give designer considerable insight into behavior of such sections under pure loading conditions as well as conditions of combined bending and shear and combined bending and torsion. In most cases, wing nose sections can be approximated by ellipses and, for this reason, the elliptical section has been used for test purposes.

Stiffened Cylinders

DISTRIBUTION: ~~Request~~ copies of this report only from Originating Agency

DIVISION: Stress Analysis and Structures (7)
SECTION: Structural Theory and Analysis Methods (2)

SUBJECT HEADINGS: Cylinders - Stress analysis (28505)

ATI SHEET NO.: R-7-2-11

Air Documents Division, Intelligence Department
Air Materiel Command

AIR TECHNIC
RESTRIC

AD-B805 296

Classification cancelled
or changed to _____

AUTH:

By _____
Signature and Grade

Date APR 29 1949

Classification cancelled per authority
of List NACA dd. 28 Sept 1945
George R. Jordan, USCO. 29 Apr 1949